

BARC
HIGHLIGHTS

**MATERIALS
SCIENCE
AND
ENGINEERING**



भारत सरकार
Government of India

**भाभा परमाणु अनुसंधान केंद्र
BHABHA ATOMIC RESEARCH CENTRE**

स्वर्ण जयंती वर्ष
GOLDEN JUBILEE YEAR
2006-2007

For further details contact:

Dr. A. K. Suri

Associate Director, Materials Group
Bhabha Atomic Research Centre, Trombay, Mumbai - 400 085, India.

E mail: aksuri@barc.gov.in

Published by :

Dr. Vijai Kumar

Associate Director, Knowledge Management Group and
Head, Scientific Information Resource Division,
Bhabha Atomic Research Centre, Trombay, Mumbai - 400 085, India.

E mail: vijai@barc.gov.in

FOREWORD

Bhabha Atomic Research Centre (BARC) is celebrating its golden jubilee year during 2006-07. On 20th January, 1956, Pandit Jawaharlal Nehru formally inaugurated the Atomic Energy Establishment Trombay (AEE), which is renamed as Bhabha Atomic Research Centre (BARC) on January 22, 1967. As a premier R&D centre of the Department of Atomic Energy (DAE), BARC has a mandate to provide R&D support to the nuclear power programme, to pursue all activities related to nuclear fuel cycle, to operate research reactors for supporting neutron beam research and supplying radioisotopes for various applications, to conduct frontline basic research in physical, chemical, biological and engineering sciences all of which leading towards improving quality of life of our people. The achievements BARC has made over the last 50 years are well known not only to the scientific community in the country but also to our people at large. Scientific achievements made by this premier research centre are well documented in various publications of DAE including a series named "BARC Highlights". During this golden jubilee year, we have made an effort to bring out some glimpses of recent research and development accomplishments in the form of 8 volumes, highlighting the following areas:

1. Nuclear Fuel Cycle
2. Physical Sciences
3. Chemical Science and Engineering
4. Materials Science and Engineering
5. Life Sciences
6. Reactor Technology and Engineering
7. Electronics, Instrumentation and Computers
8. Environmental Science and Engineering

These volumes will showcase the latest work in the aforementioned areas and will demonstrate how each of these is directed towards achieving the overall goal of using nuclear energy for the benefit of our people.

Nuclear energy programme in India has now reached a level of maturity. Today, India is self-sufficient in building nuclear power stations of 540 MWe capacities and has gained mastery over the entire fuel cycle. We are in the threshold of entering the second stage of nuclear power programme, in which a rapid growth in installed capacity is expected through the fast reactor programme. In the area of basic research in science and engineering, BARC has been maintaining a leading position both in national and international scenario. One of the strongest points of basic research in BARC lies in its capability in building sophisticated research facilities in-house. The core competence of the scientists and engineers in our centre covers a very wide range as is reflected in the 8 companion volumes getting released on the occasion of the golden jubilee year.

The present volume on Materials Science and Engineering gives a birds eye view of the multitude of activities being pursued in this field. Materials research programme in BARC encompasses extractive metallurgy of rare and refractory metals, development of alloys and thermodynamical treatments for obtaining desired properties of materials for both structural and functional applications, characterization of materials in different length scales and development of several advanced processing techniques.

In the extractive and process metallurgy area, recent work on standardization of flow sheet for the production of nuclear grade calcium which is exclusively used as a reductant for recovery of actinides, extraction and refinement of refractory metals and their alloys, processing of zirconium alloy scrap for recovery of the valuable metal through a single step iodide refining process merit special mention. Electrodeposition techniques have been used innovatively for production of multilayered metallic structures with individual layers of a few nanometer, fission type neutron sensors and nanocrystalline deposits. Other techniques such as crystallization of metallic glasses, vapour condensation, sol-gel processing and ball milling have also been used for the formation of nanocrystalline materials which have been studied for their novel properties.

The variety of processing techniques, most of which have been developed and built in-house, have given the opportunity to scientists in several disciplines to participate in the development of materials relevant to our departmental programmes. Apart from the conventional pyro, hydro and electro metallurgical techniques, beam processing involving electron, plasma or laser has been exploited to a large extent as is illustrated in this volume.

Research on nuclear structure materials both in-core and out of core remains to be the main thrust area. Work on the present and future generation zirconium alloys on different types of stainless steels and nickel based superalloys for application in reprocessing and waste management operations and on life management of structural components are all linked with detailed investigations on microstructure and properties – mechanical, corrosion and radiation stabilities. Comprehensive facilities for these investigations from atomic scale to macro levels of actual components, set up over the last decade, are well utilized for such studies. The potentials of these sophisticated experimental facilities are also utilized in studying some of the recently discovered phenomena in materials science. Work on metallic glasses, particularly zirconium bearing bulk metallic glasses, quasicrystals, several metastable phases, evolution of ordered structures are some examples.

Consistent with some recently introduced activities, namely, development of high temperature reactor energy conversion, hydrogen production and storage and accelerator driven systems, new avenues for R & D on materials have opened up. This is reflected in new programmes such as work on carbon based material, development of components and systems of solid oxide fuel cell, materials required for liquid metal handling, materials for thermochemical dissociation of water and for storage of hydrogen.

This volume will not only provide an account of the current work and recent accomplishments of materials research community in BARC, but also bring out the linkages between the spectrum of these activities with the primary goals of our centre.

Srikumar Banerjee
Director

PREFACE

Materials Science and Engineering play an important role in all aspects of technological development and the success of any programme incorporating advanced technology is directly linked to the developments in the field of materials science. The country's nuclear energy programme has already matured from conventional Pressurized Heavy Water Reactor (PHWR) to Fast Breeder Reactor (FBR) and this has poised additional challenges to the material scientist. With the future programme on Compact High Temperature Reactor (CHTR) and a concurrent thrust on the Accelerator Driven Sub-critical System (ADSS), it will be a daunting task to meet the challenges with respect to materials with superior properties. Thus, the need to develop cost-effective techniques and develop advanced materials for nuclear and specialised applications indigenously will be of utmost importance due to existence of technology control regimes in respect of strategically important materials.

Activities covering wide areas of research and technology development in materials science and engineering are being pursued at BARC. Development of refractory metals & alloys such as TZM, Mo-30W, niobium and tantalum-based alloys along with development of silicide, aluminide type of protective oxidation-resistant coatings are being carried out for the proposed high temperature reactors. Process flowsheets for high purity refractory metal-based alloys are being developed to produce "clean" alloys with ultra-low impurity levels. A process flowsheet has been developed to recover Cobalt for isotope production, from spent cracker catalyst, in the shape of slugs and pellets. High purity Zirconium from zircaloy and Zr-Nb mill scrap, generated during fabrication of reactor components, is being recovered in a single step by iodide refining. The technology for preparation and purification of nuclear grade calcium required as reductant for preparation of metallic uranium fuel and uranium powder of stringent specifications for specialized applications has been developed.

In the field of nano-technology, development of multi-layer nano-coatings by pulsed electrolysis, carbon nano-tubes and thermal plasma synthesis of nano-crystalline materials are the significant activities being pursued. Amorphous carbon (a-C) composites are being developed as neutron scattering material for AHWR. A novel process involving binderless micro-granulation has been developed to granulate and densify nano-sized carbon fines. High Resolution Transmission Electron Microscopy (HRTEM) and Scanning Probe Microscopy (SPM) are the tools being used by researchers at BARC for characterization of nano-materials. Rapidly solidified and bulk metallic glasses of zirconium-based alloys have been developed with special emphasis on studies of the correlation between microstructure and mechanical properties.

Research activities in Surface Engineering are being pursued to prepare coatings of relevance to DAE programmes. Neutron sensors, as import substitutes, have been successfully developed and used to monitor neutron flux for out-of-core as well as in-core applications. The complete technology for fission type ($^{235}\text{UO}_2$) and absorption type (^{10}B) neutron sensors has been indigenously developed. Electroless nickel (EN) coating has been extensively used for a variety of applications including coated metal optics. Hard and wear-resistant EN-Si₃N₄ composite coatings are being developed for water lubricated bearings for fuel handling machines. Corrosion-resistant nickel coatings have found application on difficult-to-plate uranium shielding components for the first, indigenously built ^{60}Co Teletherapy Unit. The co-operative efforts of various Divisions of BARC have resulted in developing the state-of-the-art Bhabhatron unit for cancer treatment which has been commissioned at the Advanced Centre for Treatment, Research & Education on Cancer, Navi Mumbai. This is an excellent example of the use of expertise and technologies for societal benefits developed in-house. A frontier area of research in surface engineering is the effort initiated in the development of multi-layer coatings on spherical particles leading to TRISO-coated fuel for the compact High Temperature Reactor.

Development of the technologies related to bulk synthesis of conventional and nano-ceramics, sol-gel technique and combustion synthesis have helped extend the frontiers of research in expanding the field of ceramics to realms of technology. Reproducible grade hydroxylapatite bioceramics with applications in the field of prosthetic implants have been developed. $\alpha\text{-CaSO}_4 \cdot 0.5\text{H}_2\text{O}$ ceramic as bone void filler and an indigenous substitute for 'Osteoset' has been synthesized through controlled dehydration process and material has produced excellent results during clinical testing. Other developments being pursued in this field are the materials for high temperature Solid Oxide Fuel Cell (SOFC), and neutron absorbers for high temperature nuclear reactors. Melt-texturing techniques to develop high

Tc superconducting magnetic bearings have made significant progress. Sol-gel technology has been exploited for development of high purity Nd_2O_3 for laser applications and $\text{Bi}_2\text{O}_3 - \text{BeO}$ for rechargeable neutron sources.

The tools and methodologies required for materials science research have also been used to develop important products and processes. Ceramic-to-metal seals, components of sodium leak detector and diffusion bonding of dissimilar materials, are some of the materials developed from the sound foundation of materials science. Many of these products have found applications for joining stainless steel to aluminum and Al-alloy bonded composites which have been used in fabricating neutron and radiation detectors.

Establishing the phase diagrams of materials from the first principles and adopting multi-scale materials modeling for correlating the structure and properties from the nano/micro scale to meso scale is an emerging field. Establishing structure – property correlations and tailoring the properties of structural materials have been a major component of research. Understanding the microstructure of structural materials like stainless steels in sensitized and cold-worked condition has provided an insight to directly correlate the performance of these materials in nuclear power reactors. Modification of the structure at grain boundaries by a thermo-mechanical treatment has resulted in the development of superior resistance to sensitization and corrosion in stainless steels. Loops based on thermosiphon principle have been established for compatibility studies of structural materials in high temperature liquid lead – bismuth eutectic.

Significant work has been carried out in the development of processes and process equipment for crystal technology, high power induction coupled plasma reactor, microwave electron-cyclotron-resonance plasma processing facility for depositing diamond like carbon coatings, plasma CVD, nitriding/carbonitriding, ceramic fabrication etc.

The achievements of scientists at BARC in the field of materials research is quite vast. The work being carried out is to bring synergy to focus both on the fundamental and the applied aspects of various programmes to meet the growing aspirations of nuclear and advanced technology related programmes.

A. K. Suri



MATERIALS SCIENCE AND ENGINEERING

CONTENTS

FOREWORD

PREFACE

1.	PROCESSING OF PRIMARY & SECONDARY RESOURCES	1
1.1	Refractory metals and alloys	2
1.2	Iodide Refining	5
1.3	Processing of zircon sand	6
1.4	Cobalt for radioisotope applications	7
1.5	Synthesis of metal extractants	10
2.	STRATEGIC MATERIALS	12
2.1	Production of calcium	13
2.2	Production of uranium powder	14
2.3	Development of boron and boron-based products	14
2.4	Beryllia Powder ceramics and shape formation	16
3.	NOVEL MATERIALS & TECHNIQUES	17
3.1	Crystal technology	18
3.2	Development of novel carbon material	19
3.3	Development of melt texturing for superconducting magnetic bearing	20
3.4	Aluminium foam	21
3.5	Supercritical fluid (SCF) processing facility	22
4.	AMORPHOUS AND NANOMATERIALS	23
4.1	Metallic Glasses	24
4.2	Nano-materials	24
4.3	Deposition of nanocrystalline Nickel-Copper alloy coatings by pulse electrolysis	26
4.4	Nanostructured Nickel/Copper multilayer coatings by pulse electrolysis	29
4.5	Synthesis of carbon nanotubes by catalytic chemical vapour deposition	31



5.	<i>SURFACE ENGINEERING</i>	32
5.1	Neutron sensors	33
5.2	Hard nitride coatings by magnetron sputtering	34
5.3	Electroless nickel and composite coating	37
5.4	Plating on difficult-to-plate metals: nickel on uranium	38
5.5	High temperature Spouted-bed coating	40
6.0	<i>ADVANCED CERAMICS</i>	41
6.1	Silicon carbide for structural and tribological applications	42
6.2	Sol-gel, solution combustion and nano-material processing	43
6.3	Development of bioceramics for orthopaedic applications	47
6.4	Synthesis of thermal spray-grade yttrium oxide powder	48
6.5	Development of sealing glasses and glass-ceramics	48
6.6	Development of ceramic acoustic emission sensor element	49
7.	<i>MATERIALS FOR FUEL CELLS</i>	50
7.1	Development of cathode material	51
7.2	Development of anode material	53
7.3	Slurry based tape casting of electrodes and support	53
7.4	Interconnect material	54
7.5	Planar solid oxide fuel cell	54
7.6	Polymer electrolyte for PEMFC	55
8.	<i>EQUILIBRIUM PHASE DIAGRAMS</i>	56
8.1	Phase diagrams of Rare earth-refractory metal system	57
8.2	Binary Phase Diagrams	58
8.3	Thermodynamic studies	58
8.4	Equilibrium Studies in Uranate Systems	60
9.	<i>PHASE TRANSFORMATION STUDIES</i>	62
9.1	Cold-worked microstructure of alloy 800	63
9.2	Study of the martensite to austenite transformation in steels by dilatometry	64
9.3	Ageing response of alloy 625	65



9.4	Diffusion in metals & alloys	66
9.5	Sequence of Clustering & ordering in dilute Cu-Ti alloys	67
9.6	Sigma & other TCP Phases in Ni-Mo base alloys	68
10.	MODELLING AND SIMULATION	69
10.1	Discrete dislocation plasticity modelling applied to irradiated materials	70
10.2	Atomistic modelling of materials	71
10.3	Diffusion Paths in ternary systems	72
10.4	First Principles Calculations	73
10.5	Computer simulation of the early stages of ordering transformation	74
11.	BEAM PROCESSING OF MATERIALS	75
11.1	Plasma spray coatings	76
11.2	Laser etching of thoria pellets	80
11.3	Electron beam processes	80
12.	ADVANCED TECHNIQUES OF JOINING OF MATERIALS	83
12.1	Solid state diffusion bonding	84
12.2	Ceramic-metal seals	85
12.3	Transient liquid phase bonding	87
12.4	Electro Magnetic Forming Technique	88
12.5	Friction Stir welding	88
13.	CORROSION AND COMPATIBILITY STUDIES	89
13.1	Grain boundary engineering	90
13.2	Electrochemical potentiokinetic reactivation (EPR) technique	91
13.3	Nodular corrosion in zirconium alloy clad tubes	93
13.4	Thermal buoyancy driven lead-bismuth eutectic loop	94
13.5	Compatibility studies between thoria and zircaloy-2	97
13.6	Metallurgical investigation of aluminium clad of Dhruva fuel	97
14.	MATERIALS ISSUES IN WASTE MANAGEMENT	98
14.1	Nuclear waste	99
14.2	Toxic waste	99
15.	TECHNOLOGY TRANSFERS AND PATENTS	102



1. PROCESSING OF PRIMARY AND SECONDARY RESOURCES

INTRODUCTION

Processing of indigenous resources to meet the growing demand for metals of strategic as well as economic importance has been one of the objectives of the materials programme of the Department. Development of alternative/innovative processing routes for primary resources and recycling of secondary sources is important as far as environmental safeguards are concerned. Recycling of scrap/waste containing metals such as zirconium or cobalt offers benefits with respect to process economics besides improving yield. Iodide refining of zirconium bearing mill scrap provides high purity zirconium in a single step without any effluent discharge. Cobalt bearing spent catalyst, available from the Heavy Water plants, is a readily available, concentrated, low volume secondary source for cobalt and has been processed to yield cobalt slugs and pellets.

1.1 REFRACTORY METALS AND ALLOYS

New generation reactors, viz. accelerator driven sub-critical system (ADSS), compact high temperature reactor (CHTR) and advanced heavy water reactor (AHWR), need structural materials capable of withstanding an environment aggressive with respect to radiation, temperature, corrosion (gaseous and liquid metal) and stress for prolonged period. Refractory metal alloys such as niobium-1wt% zirconium (Nb-1Zr), Nb-1Zr-0.1C, TZM, molybdenum-30wt% tungsten (Mo-30W), tantalum-10wt% tungsten (Ta-10W) etc. are potential candidate materials for such applications. Conventionally refractory metal-based alloys are prepared by direct consumable or non-consumable arc melting of the constituent metals. This requires pure constituent metals and repeated melting for achieving compositional homogeneity. An alternative technique is being developed for the preparation of these alloys, which consists of aluminothermic co-reduction of the mixed oxides in presence of judicious proportion of additives which result in a consolidated alloy product well separated from the slag. The prepared alloy is further subjected to homogenization in an arc melting furnace and finally refined by electron beam melting. The reduction campaigns were carried out in a specially designed water-cooled copper reactor. The product from this stage was homogenized in the arc furnace.

It has been found possible to approach near targeted composition. An optical microstructure of Mo-30W alloy revealing large grains of about 200-300 μm is presented.

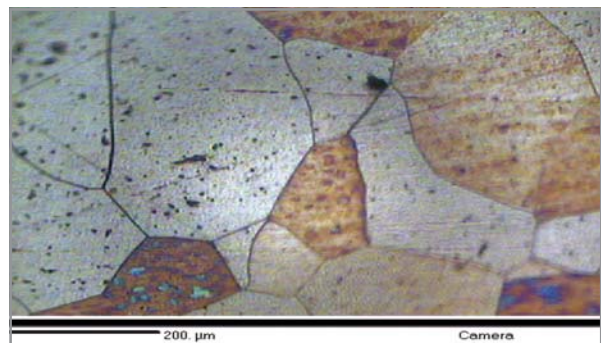
One major drawback of refractory metals and alloys is their low oxidation resistance at elevated temperatures. Proper oxidation resistant coatings need to be developed before application of these alloys.

Silicide, aluminide and/or alumino-silicide type of coatings are reported to be well suited for high temperature applications. Amongst a large number of coating techniques, **in-situ chemical vapor deposition** process has been taken up to form single and multilayer coatings. The process is carried out at high temperatures (900-1200 $^{\circ}\text{C}$) under an inert or reducing atmosphere to avoid oxidation of the substrate and the powdered metal/master alloy. The substrate is embedded in a powder mixture and sealed inside an alumina crucible. A typical pack consists of three components: (i) a master alloy or pure metal powder (pure



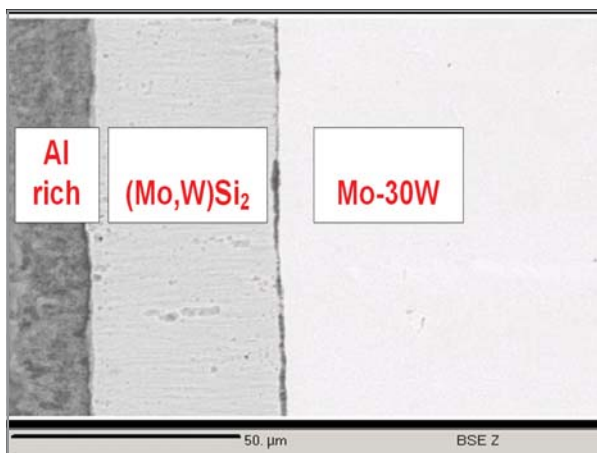
Vacuum arc melting furnace

aluminium and/or silicon powders) containing element(s) to be incorporated into the substrate, (ii) a halide activator salt (NH_4Cl or NH_4F), and (iii) an inert filler (Al_2O_3). Initially the activator reacts with the master alloy or metal powder, producing volatile

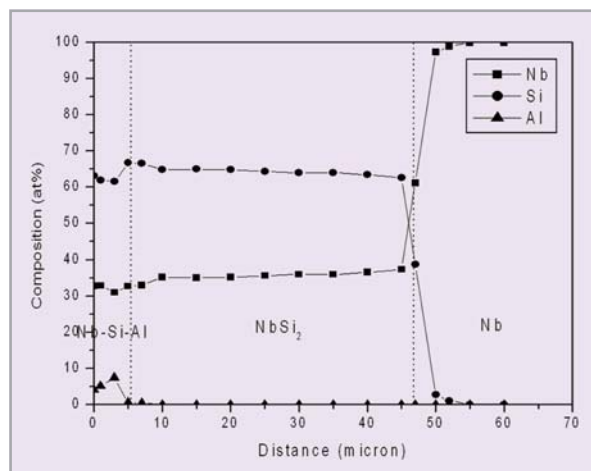


Optical microstructure of Mo-30W alloy.

metal halides. Driven by the chemical-potential gradients for the elemental components between the pack and the substrate, these volatile species diffuse to the substrate surface where a variety of reactions can contribute to the deposition of the coating element(s).

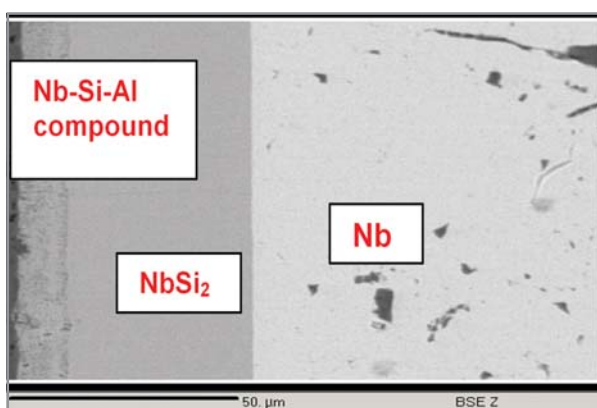


BSE image showing the interface between the coating and Mo-30W matrix



X-ray line scans showing distribution of Nb, Si & Al across the interface

The accompanying figures reveal the composition of various coating layers. Distribution profile of silicon (Si) and aluminium (Al) on niobium substrate is also shown.



BSE image showing the interface between the coating and niobium matrix

handling of halides, respectively. Although recently developed carbothermic processes overcome these limitations, the products of carbothermic processes may, depending upon the operating conditions, contain more residual carbon than permissible. Use of silicon under vacuum for the extraction of niobium and tantalum from their pentoxides, and for removing the residual oxygen from the extracted metals is feasible. Unlike conventional silicothermic processes, where oxygen is removed as SiO_2 , removal of oxygen in these processes occurs as SiO vapour.

Thermodynamic feasibility of the silicothermic reduction of Nb_2O_5 and Ta_2O_5 was evaluated by constructing Pourbaix-Ellingham diagrams for Nb-Si-O and Ta-Si-O systems. Calculations were also performed to evaluate the thermodynamic feasibility of deoxidizing the metals by pyrovacuum treatment with silicon. These calculations also confirmed that, unlike carbon, it would be possible to remove any residual silicon remaining after deoxidation.

S. Majumdar, P. Sengupta, G.B. Kale, S.P. Chakraborty and I.G. Sharma < smajum@barc.gov.in >

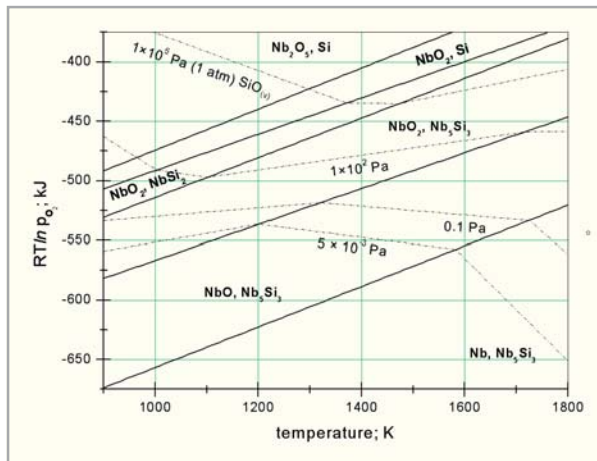
■ A Silicothermic Process for Reduction and Refining of Niobium and Tantalum

The commercial methods for extraction of niobium and tantalum are aluminothermic reduction of Nb_2O_5 , and reduction of K_2TaF_7 by sodium. These methods have limitations of yield and involve

Pourbaix-Ellingham diagram for Nb-Si-O system

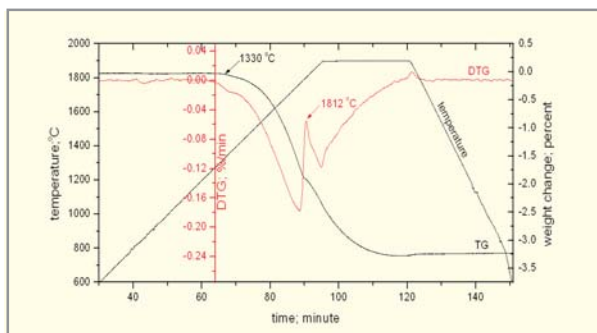
Reduction and deoxidation processes both were studied thermogravimetrically. As compared to carbothermic reduction, the silicothermic process begins at a lower temperature and proceeds to a much greater degree of completion at comparable temperatures, in a shorter time. The product was an Nb-Si-O or Ta-Si-O alloy, which is refineable

to the pure metal by pyrovacuum treatment at a higher temperature.



Thermoanalytical studies on relative extent of reduction by carbothermy and silicothermy of niobium and tantalum pentoxides (1600°C in vacuum) were carried out.

Charge	Start of reduction (°C)	Holding time at 1600°C (minutes)	Extent of reduction (%)
Niobium			
Carbothermy	1300	90	67
Silicothermy	1150	70	96
Tantalum			
Carbothermy	1250	75	40
Silicothermy	1150	70	95



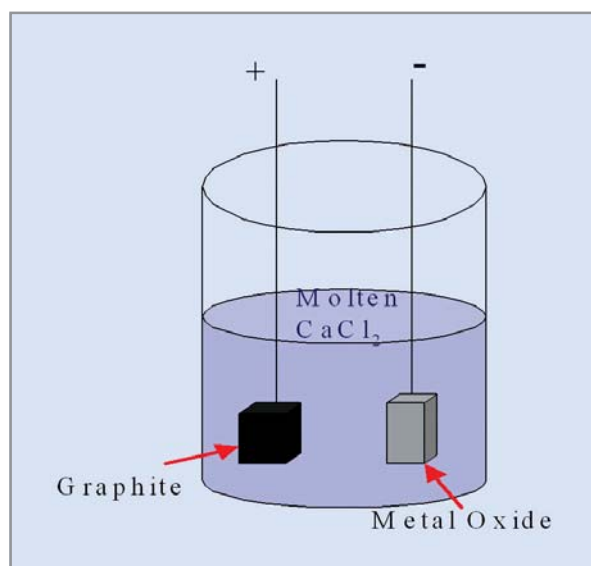
Thermogram obtained during deoxidation of niobium with silicon

The deoxidation process with silicon during the pyrovacuum treatment began around 1350°C, which is a substantially lower temperature for other modes of deoxidation in these metals. It was possible to deoxidize and desilicize the metals to 99.9% purity.

Alok Awasthi, Y.J. Bhatt, N. Krishnamurthy, Y. Ueda and S.P Garg, *J. Alloys Comp.*, 315 (2001) pp.187-192.

■ Preparation of Refractory and Reactive Metals by Direct Electrolysis of Oxides

Many important nuclear and refractory metals are commercially produced using the Kroll's process. In this process, the molten chloride of the metal is reduced by magnesium and the metal is obtained as sponge. Although the process is economical, it is slow and requires handling of corrosive chlorides. Laboratories all over the world are working on technically superior processes. The emphasis has been on electrolytic processes. However, electrolysis of molten halides has not been successful due to dendrite formation and multiple valencies of the anions. Also, electrolysis of oxides dissolved in a halide bath has not been successful due to poor solubility of the oxides.



The possibility of directly electrolyzing the oxides even in solid state has been investigated in the laboratory. In this process, the oxide to be reduced is made the cathode. A reactive graphite anode is preferred to decrease the voltage required. Molten CaCl_2 acts as the electrolyte. On application of sufficient voltage, the overall reaction of many complex processes occurring in the cell is that the oxygen atoms from the cathode travel via the electrolyte and reach anode to react with it.

All the oxygen from the cathode is removed with time and pure metal remains in the end at the cathode. The process has been demonstrated using green Ta_2O_5 pellet as the cathode. No controlled atmosphere was necessary and the molten CaCl_2 was exposed to atmospheric air during the course of electrolysis. The pellet was removed from the cell after the current stopped flowing. XRD studies confirmed that the pellet had converted to tantalum, which was the only phase present.

Further studies are continuing to fully understand the process mechanism. The investigations thus far have indicated that the increased electrical conductivity of the oxides at the temperature of the electrolysis does not explain the large current flowing into the cell.

Sanjay Kumar Singh, Abhishek Mukherjee, Alok Awasthi and N. Krishnamurthy <sanjayk@barc.gov.in>



Macrostructure of a section of crystal bar zirconium

1.2 ZIRCONIUM CRYSTAL BAR FROM Zr-2.5Nb ALLOY SCRAP BY IODIDE REFINING

Zr-2.5Nb alloy is being used as standard coolant tube material in pressurized heavy water reactors owing to its superior mechanical properties as well as lower hydrogen pickup. Light scrap generated during fabrication of coolant tubes, consisting mainly of chips as well as turnings is high in oxygen, nitrogen and carbon necessitating a purification step before it can be recycled. At the



Crystal bar zirconium with the retort cover flange

same time, the storage and subsequent disposal of such scrap poses safety and environmental problems. It is, therefore, attractive to recover a high purity product like crystal bar zirconium from such waste material having low hafnium contamination. With increasingly stringent specifications with respect to impurities such as oxygen and nitrogen for use in advanced reactor applications, crystal bar zirconium offers blending options to maintain close tolerances over impurities in the finished tubes.

Zr-2.5Nb alloy scrap reacts with iodine gas at 300 to 350° C to yield volatile zirconium tetra iodide (ZrI_4), which is then decomposed to yield pure, metallic zirconium at higher temperature, 1200 to 1350° C, on a resistively heated filament,

made of zirconium wire. The iodine, released during the decomposition process, diffuses back to the surface of the scrap to complete the reaction cycle. The requirement of iodine is low owing to recycling in a closed system.

Extent of Purification		
Element	Feed (ppm)	Crystal Bar (ppm)
O	>2000	<300
N	300	<30
C	130	<100
H	100	<25
Fe	80	<50
Al	30	<25
Hf	170	100
Nb	2.5wt%	1000-1200
Zr	Balance	Balance

Impurity Levels in Feed & Crystal Bar Zr

The effective purification of zirconium, by iodide process, takes place since impurities, such as carbon, oxygen and nitrogen, are present in scrap as carbide, oxide and nitride respectively that are more stable with respect to iodides. Owing to difference in thermodynamic and kinetic factors, transfer of metallic impurities to the filament is also restricted.

As the direct monitoring of the temperature of the growing filament is not feasible, an indirect technique involving the adjustment of voltage and current to the filament is successfully adopted. At constant temperature, for a given filament length, regardless of diameter, where L is the filament length in cms :

$$E I^{1/3} = K'L$$

Close control over scrap and filament temperatures allows control over the extent of transfer of metallic impurities to the product. The precise control of the filament voltage and current, and thereby the filament temperature, during the entire refining operation, is carried out by a PLC that monitors the output of the transformer. Investigations with fresh as well as accumulated scrap indicate that fresh scrap need not be subjected to a pretreatment operation in order to activate the scrap surface

for reaction with iodine. Further, recycling of feed scrap allows for improvement in yield.

R.H. Rakhasia, P.K. Tripathy, R.C. Hubli and A.K. Suri, *Proceedings National Symposium on Vacuum Science & Technology and Vacuum Metallurgy, IVSNS-2003, Oct 15-17, (2003), 291-295.*

R.H. Rakhasia, P.K. Tripathy, R.C. Hubli and A.K. Suri, (2005), *BARC Newsletter*, 256.

R.H. Rakhasia, P.K. Tripathy, R.C. Hubli and A.K. Suri, (2005), *Proceedings ICME-2005, Bhubaneswar, June 13-14 (2005), 437-444.*

1.3 RECENT DEVELOPMENTS IN THE PROCESSING OF ZIRCON SAND

Zirconium oxide (ZrO₂) is an important intermediate in the preparation of zirconium alloys, and as such also finds widespread applications in ceramic industry. Commercial production of ZrO₂ is carried out by the alkali fusion of zircon.

Studies have been carried out to evolve alternate route for the opening up of zircon ore which are based on selective reaction either with ZrO₂ or with SiO₂ and therefore may offer some economic advantage over the established caustic fusion process. Three new alternate routes viz. i) carbothermic reduction ii) lime sintering and iii) soda ash sintering have been developed.

■ Carbothermic Reduction of Zircon

The carbothermic reduction of zircon under vacuum involves removal of silica content of zircon as volatile SiO (g) which is pumped out, leaving behind ZrO₂ in a single step as per reaction:



A ZrO₂ product, having monoclinic structure, was obtained at a recovery of 99% when a charge containing 0.95 mol carbon / mol zircon was heated at 1550°C for 1.5 h under a vacuum of < 0.006 Pa. The product was found to contain 98.6% ZrO₂, 0.34% SiO₂, with an average particle size of 22 microns. The stabilised (cubic) variety of ZrO₂ could be prepared by heating a charge

containing 0.95 mol C/ mol zircon doped with 0.11 mol CaO under a vacuum of <0.006 Pa. The ZrC product could also be obtained when a charge, consisting of 4 moles C/ mol zircon, was heated at 1500°C. Thus a variety of finely powdered products such as monoclinic ZrO₂, stabilized ZrO₂ and ZrC can be obtained at high recoveries in a single step. Experimental studies have been carried out on laboratory scale and are required to be scaled up for techno-economic evaluation.

■ Lime Sintering Process

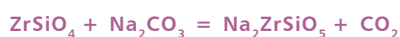
The lime sintering process is based on the selective attack of silica in zircon by lime as per the reaction:



The sinter is leached sequentially with 5% HCl and 2% NaOH solution to remove calcium silicate, leaving behind ZrO₂ product. Almost 100% recovery of ZrO₂ is obtained when a charge containing zircon with lime in the mole ratio 1:1.2 is sintered at 1400°C for 2 hours followed by leaching of sinter. The product thus obtained contains 98.8% ZrO₂, 0.9% SiO₂, 0.5% CaO. The process uses 0.367 ton CaO/ ton zircon as against 1.1 ton NaOH / ton zircon used in the caustic fusion process.

■ Soda Ash Sintering Process

Soda ash sintering process is based on the reaction:



Leaching of sinter with hot concentrated acid solubilises the zirconium values, leaving behind SiO₂ as per the equation:



Zirconium recoveries of 88.8% were obtained when a charge containing Zircon and soda ash in the mol ratio 1:1.1 was heated at 1050°C for 2 hours and the sinter was leached with hot HCl. The process uses 0.63 ton soda ash / ton zircon as against a requirement of 1.1 ton NaOH / ton zircon in the alkali fusion process.

P.K. Tripathy, D.V. Bavbande , R.K. Fotedar and J.M. Juneja, *High Temperature Materials and Processes*, 24 (2005) , 7.

1.4 COBALT FOR RADIOISOTOPE APPLICATIONS

Cobalt metal, in the form of slugs and pellets of right purity and specifications, is required for the preparation of ⁶⁰Co radioisotope, extensively used as gamma-ray source for medical as well as radiography applications. Non availability of Indian primary resources makes it mandatory to exploit indigenously available secondary resources of cobalt such as spent ammonia cracker catalyst, alnico and cemented carbide tool scrap, β-cake, converter slag, ocean nodules, etc.

■ Processing of Secondary Cobalt Source & Solvent Extraction

Spent ammonia cracker catalyst containing about 21% cobalt, generated in heavy water plant has been exploited to recover cobalt values. After leaching with sulfuric acid and oxidizing Fe²⁺ in the leach liquor to Fe³⁺, the liquor was treated with ammonia for the quantitative removal of Fe³⁺ and Al³⁺. In an alternate method, Fe³⁺ and Al³⁺ were removed by extraction with D2EHPA. Cobalt was stabilized in the trivalent oxidation state in ammoniacal medium and nickel was extracted using LIX84I. Nickel free raffinate was obtained with a cobalt purity of >99.85% and cobalt recovery of ~85%.

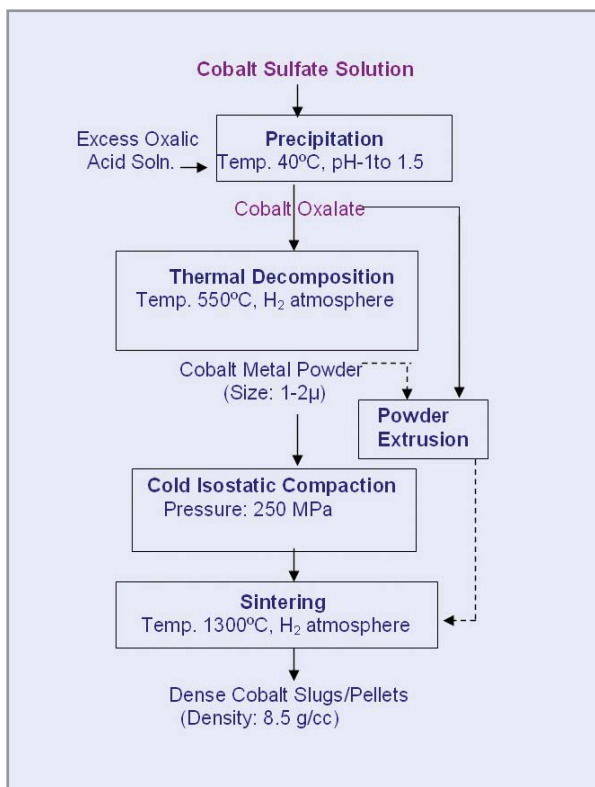
M.V. Rane, V.H. Bafna , R. Sadanandam, A.K. Sharma , K. Ramadevi, N.K. Menon, M.F. Fonseca, S.K. Tangri and A.K. Suri *Hydrometallurgy*, 77, 2005, 247–251.

R. Sadanandam, N.K. Menon, M.V. Rane, A.K. Sharma, M.F. Fonseca, S.K. Tangri & A.K. Suri *Proceedings of International Seminar On Mineral Processing Tech.*, I.I.Sc., Bangalore, January 3-5, 2002.

■ Production of Cobalt Powder & Shapes

Cobalt oxalate is precipitated by adding oxalic acid to cobalt sulfate solution. The process parameters for precipitation as well as thermal decomposition to cobalt powder have been optimized to prepare metal powder of proper size and morphology suitable for making carbide tools as well as slugs and pellets. The cobalt metal powder for the assigned task was produced from oxalate by thermal decomposition at 550°C under reducing atmosphere.

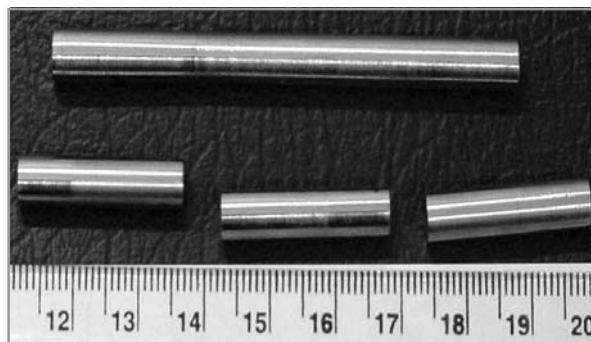
Conventionally, cobalt slugs/pellets are fabricated through the



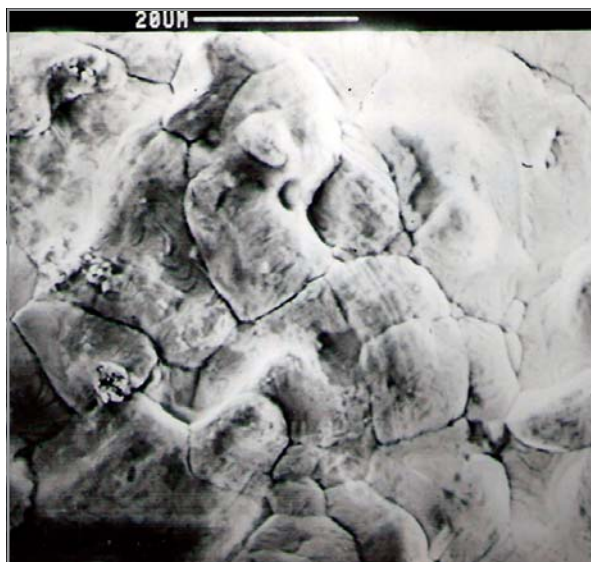
Flow sheet for the preparation of cobalt Slugs and Pellets

powder processing route involving appropriate combination of expensive and laborious hot working techniques, such as hot extrusion, hot swaging under reducing atmosphere and a chain of such units is required to achieve the final diameter. An alternative fabrication technique has been developed. In this process cobalt powder was compacted by cold isostatic pressing (CIP) and sintered at 1300°C for 90 minutes to produce cobalt rods. The process parameters have been standardized to prepare cobalt rods of required density. Final machining was done to produce cobalt slugs (6 x 25 mm). Figures show the macrostructure and microstructure of cobalt slug. Equiaxed grains of 15 µm size were observed in the microstructure.

This approach however did not result in consistent quality cobalt pellets (1 x 1 mm). Powder extrusion of both cobalt oxalate and cobalt metal powder was therefore taken up for preparing these pellets. Cobalt wires of 1 mm diameter and 8.6 g/cc density were produced after sintering of extruded rods/wires. Final optimization studies are in progress.



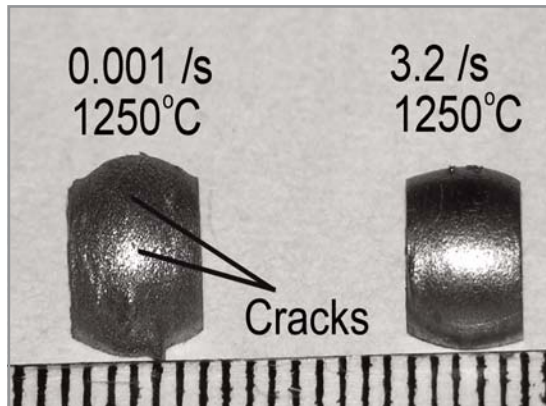
Macrostructure of cobalt slugs



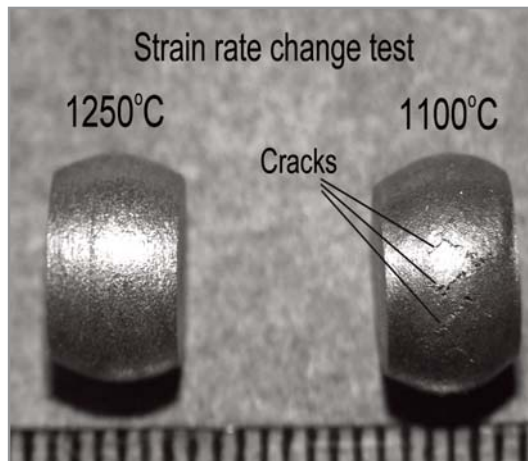
SEM image of surface of sintered cobalt showing equiaxed grain structure, average grain size of 15µm.

To optimize the hot working parameters of sintered cobalt, deformation studies have been conducted at different strain rates ranging from 0.001 s^{-1} to 3.2 s^{-1} between the temperatures from 900°C to 1300°C. The studies revealed that the hot workability of sintered cobalt is poor at low strain rates ($\sim 0.001\text{ s}^{-1}$) and good at higher strain rates (3.2 s^{-1}). Deformation at higher strain rates at 1250°C was found to result in no microcracking and higher densification. Conversely, deformation at lower strain rates at this temperature showed surface as well as grain boundary cracks.

At temperatures lower than 1200°C micro-cracks as well as surface



Photograph of samples tested at 1250°C and strain rates $0.001s^{-1}$ & $3.2s^{-1}$.



Photograph of strain rate change test samples at 1250°C and 1100°C.

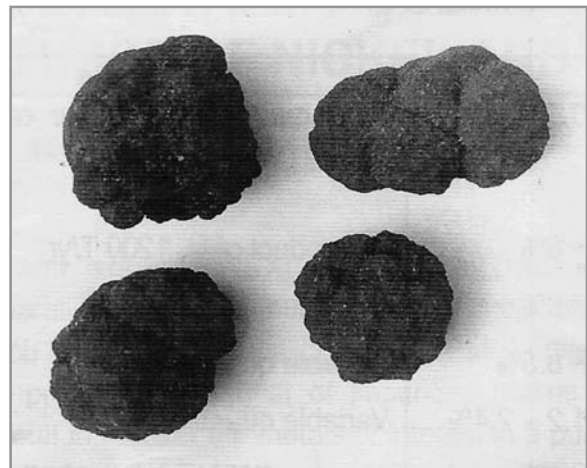
cracks were observed. Figure shows the samples deformed at 1250°C at different strain rates.

Any temperature below 1200°C is not suitable for deformation of cobalt as is evident from the figure showing presence of surface cracks on the sample deformed at 1100°C; whereas no cracks were observed in the case of the sample deformed at 1250°C.

I.G. Sharma, A.C. Bidaye, S.P. Chakraborty, P. Alex, S. Majumdar and Kishore Jugal. <igsharma@barc.gov.in>

Recovery of High Purity Nickel and Cobalt from Ocean Nodules Leach Liquor

A three-step solvent extraction process was developed for processing the leach liquor produced at RRL, Bhubaneswar containing Ni and Co, alongwith impurity metals Cu, Zn and Fe. In the first step, the impurity metals were removed by extraction with partially saponified 0.5M D2EHPA and 5% isodecanol in kerosene. In the second step, separation of Ni and Co contained in the raffinate of the first step was effected using partially saponified 0.5M PC-88A and 5% isodecanol in kerosene. The pure Co solution was recovered by stripping the loaded solvent with sulphuric acid. In the third step of solvent extraction, which was integrated with the electro winning (EW) circuit, Ni from the raffinate of second step was extracted with partially



Polymetallic Nodules from Indian Ocean

saponified D2EHPA and 5% isodecanol in kerosene. The loaded solvent was stripped with spent electrolyte to regenerate the electrolyte. The solvent extraction process was optimized and tested in mixer-settlers of 2.5 L mixer capacity to obtain pure nickel and cobalt solution with purities higher than 99% and recoveries greater than 98%.

The Solvent Extraction technology was transferred to Department of Ocean Development The process was successfully demonstrated at the PMN Pilot Plant at Hindustan Zinc Ltd., Udaipur. The SX Unit of the pilot plant has the capacity to process sulphate leach liquor in mixer settlers at a feed rate of 60 l/hr.



SX section of the PMN pilot plant at HZL, Udaipur

S.K. Tangri and A.K. Suri, *Metals Materials and Processes*, 16(1), (2004)

S.K. Tangri and A.K. Suri, *BARC Newsletter*, Vol. 239, Dec. (2003), 4-10.

S.K. Tangri and A.K. Suri, *International Symposium on Solvent Extraction*, RRL, Bhubaneswar, September 26-27, 2002.

1.5. SYNTHESIS OF METAL EXTRACTANTS FOR FRONT-END AND BACK-END OF NUCLEAR FUEL CYCLE

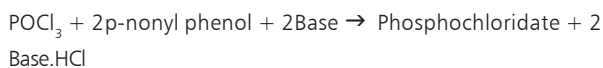
■ Di-(nonylphenyl) phosphoric acid [DNPPA].

Synthesis of DNPPA was carried out by esterification reaction of POCl_3 and p-nonylphenol, the product obtained was further hydrolyzed and purified to get ~95% selectivity of DNPPA over its monoester.

DNPPA/TOPO/NPH is a better extraction system than HDEHP/TOPO/NPH for extraction of uranium from fertilizer grade phosphoric acid.

Unit processes:

(a) Esterification Reaction:



(b) Hydrolysis:



(c) Evacuation of the low boiling components upto 80°C at 0.01mm Hg.

The knowhow for synthesis of DNPPA has been transferred to Heavy Water Board for scaleup.

■ Tri- Alkyl Phosphine Oxide [TRPO/ TAPO]

A new process route was developed for synthesis of TRPO at a purity of 98% and yield of ~90%. The steps involved are synthesis of Grignard reagents namely octyl magnesium bromide and hexyl magnesium bromide and its reaction with POCl_3 under controlled conditions. TRPO was synthesized at laboratory scale (500gm/batch) and tested for uranium extraction from phosphoric acid at REDS and found to be equivalent to imported quality. It has an advantage over TOPO in terms of its unlimited solubility in n-dodecane.

Industrially TAPO is produced by addition reaction of phosphine, 1-octene and 1-hexene. As these chemicals are highly toxic and unsafe to handle, this route was not adopted for synthesis at our end. The present route of synthesis uses safe and non-toxic chemicals and also results in high yield and purity of the product. The knowhow for synthesis of TAPO has been transferred to Heavy Water Board for scale up and production.

■ Tri- n-Octyl Phosphine Oxide [TOPO]

Synthesis of TOPO was carried out by Grignard route and with substitution reaction of Grignard reagent with POCl_3 . The overall yield and purity of the product was obtained as 85-90% and $\geq 94\%$ respectively. TOPO synthesized at laboratory scale (500 gm/batch) was tested for uranium extraction from phosphoric acid and found to be equivalent to the quality of imported chemical.

TOPO is industrially produced by addition reaction of phosphine and 1-octene. As these chemicals are highly toxic and unsafe to handle, this route was not adopted for synthesis at our end.

■ **Octyl (phenyl) N,N diisobutyl Carbamoyl Methyl Phosphine Oxide [CMPO]**

TRUEX based solvent Octyl (phenyl) N,N diisobutyl Carbamoyl Methyl Phosphine Oxide [CMPO] was synthesized at laboratory and at industrial scale at a purity of ~95% and a yield of ~85%. The process involved the synthesis of Grignard reagent and its reaction with Ethyl phenyl phosphinate and N,N diisobutyl 2-chloroacetamide.

CMPO is used for bulk separation of long-lived actinides (III) and lanthanides (III) from highly acidic high-level liquid waste. Engineering scale trial runs using simulated high-level waste were successfully carried out at user end.

■ **Tetra (2-ethylhexyl) diglycolamide [TEHDGA].**

A new metal extractant of diglycolamide class namely Tetra (2-ethylhexyl) diglycolamide (TEHDGA) was synthesized at laboratory and at industrial scale at a purity of more than 99%. The process involves a condensation reaction with an overall yield of more than 80%. TEHDGA is used for bulk separation of long-lived actinides (III) and lanthanides (III) from highly acidic high-level liquid waste. Its non-organophosphorus nature, very high extraction coefficient for trivalent actinides and lanthanides, and ease of stripping at 0.01 M nitric acid makes it a promising solvent for backend of nuclear fuel cycle. Engineering scale trial runs using simulated high-level waste were successfully carried out at user end.

J.N. Sharma, P.N. Sakhalkar, M.V. Rane & A.K. Suri. DAE-BRNS Theme meeting on 'Emerging Trends in Separation Science & Technology', BARC, Mumbai, 22nd-23rd July, 2004.

J.N. Sharma, A.K. Suri, S. Manohar, R.R. Chitnis, G.J. Shah and P.K. Wattal, DAE-BRNS Theme meeting on 'Emerging Trends in Separation Science & Technology', BARC, Mumbai, 22nd-23rd July, 2004.



2. STRATEGIC MATERIALS

INTRODUCTION

One of the highlights of the materials programme of the Department of Atomic Energy has been the development of relevant processing capability for the preparation of strategic materials. The requirement being specific, the goals identified, there has been a dedicated effort towards the successful fulfillment of the requirement conforming to stringent specifications. Nuclear grade calcium is required as a reductant for the preparation of metallic nuclear fuel in small but specific quantities. The presence of certain impurities in the reductant has a deleterious effect on the nuclear properties of the product. The preparation of uranium powder of stringent specifications with respect to the shape and size of the particulate matter as well as surface characteristics entails rigorous control over process parameters.

Boron and boron-based products with natural isotopic composition as well as those enriched with ^{10}B , find applications in the areas of neutron sensing, neutron shielding and reactor control for nuclear reactors.

Beryllia ceramics have been chosen as structural materials for compact high temperature reactors because of their excellent dimensional stability under irradiation, chemical compatibility as well as high temperature strength. Owing to the extreme toxicity, however, the preparation and handling of beryllia powders during hot pressing necessitates strict adherence to environmental safeguards.

2.1 PRODUCTION OF PURE CALCIUM

Calcium oxide is a very stable compound and can be directly reduced by carbon only above 2400 K at a total pressure of 1 atm (10^5 Pa). The reaction temperature can be lowered by operating under reduced pressure. However, the formation of calcium carbide makes this process unattractive. An alternative process for the reduction of calcium oxide is to employ metallic reducing agents. The only common metal which can be used as reducing agent for calcium oxide is aluminium. Aluminothermic reduction of calcium oxide can be represented by the reaction:



This reaction is feasible at ~ 1140 K under a reduced pressure of 10^{-6} atm (10^{-1} Pa). The products of aluminothermic reduction are not pure calcium and aluminium oxide only, as liquid aluminium absorbs calcium to form Al-Ca alloy. At a fixed temperature, the vacuum in the system determines the extent of reduction of calcium oxide. The system pressure should be maintained lower than the equilibrium vapour pressure of calcium



Assembly for production of calcium

in the system Al-Ca-O at that temperature to drive the reduction process. When this condition is achieved, the calcium content of the alloy will be less than the equilibrium value. The activity of aluminium in the alloy would be higher than the equilibrium value for the reaction. The other process control parameters are the particle size of the powders, distribution, porosity of pellets, time of reduction and the temperature of the condenser. Higher temperatures and lower pressures favour the formation of

calcium. From practical considerations on the availability of reactor materials, a temperature of $\sim 1200^\circ\text{C}$ for reduction is possible.



Assembly for purification of calcium

Considering the requirement of calcium by DAE for use as reductants in the preparation of rare earths and other metals for nuclear energy applications such as uranium, thorium and plutonium, efforts are under way to develop the technology for the production of pure calcium metal.



Pure calcium obtained by vacuum distillation

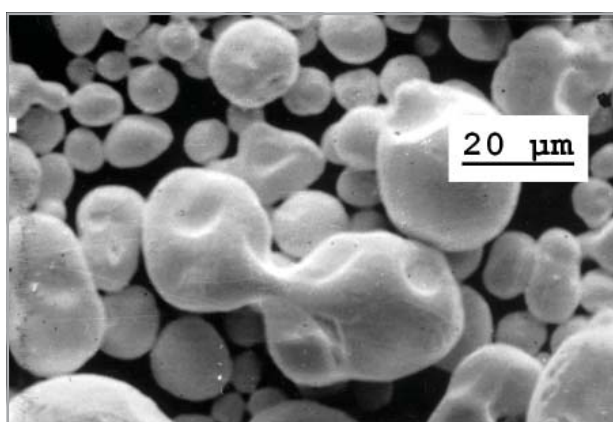
Developmental activities for the reduction of Calcium oxide by aluminium as also for the purification of calcium metal have been carried out.

R.D. Bedse, C. Subramanian and A.K. Suri,
<bedse@barc@gov.in>

2.2 URANIUM POWDER : DEVELOPMENT STUDIES, AN INDIGENOUS EFFORT

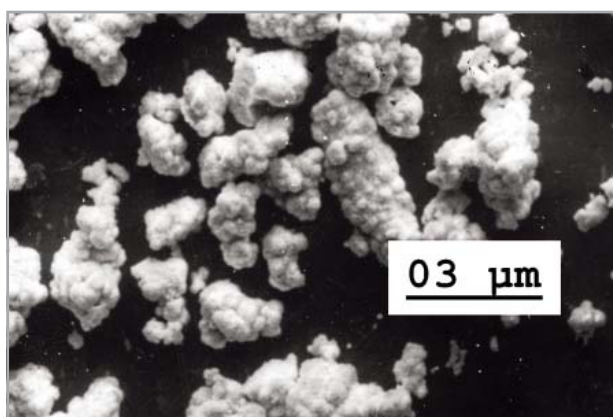
In the wide field of nuclear materials research, the massive metallic uranium ingot production used to receive major attention from researchers and quite reasonably tremendous research thrust was given in the early days. However, with the advent of novel technologies in the reactor research and other specific areas uranium is also required in the form of powder. Unfortunately, there are hardly any published useful information regarding the development of uranium powder and related topics.

Although a number of processes are available for the production

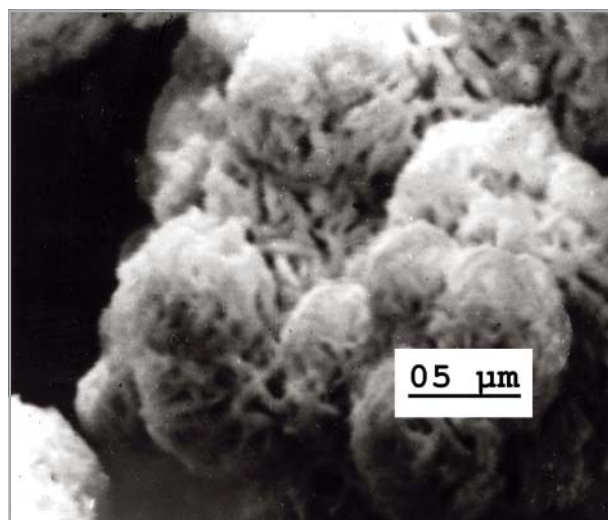


Scanning Electron Micrograph of some near spherical uranium powder

of U powder, the one adopted in the present study involves metallic reduction of UO_2 .



A Scanning Micrograph of typical Uranium di-oxide powder with O/U ~ 2.20



Electron Micrograph of UO_3 in an agglomerated state (average diameter ~60 micron)

Unlike other conventional routes, uranium powder production calls for more undivided attention as apart from having all other powder metallurgical features it poses serious problems due to the *pyrophoric* and *radioactive* nature of the powder.

For the first time in our country, excellent quality uranium powder could be made through this indigenous effort without compromising the recovery as well as the purity.

The most important parameters for controlling the shape, size, size distribution, purity and recovery are the amount of reductant, rate of heating, thickness of the slag lining, quality and type of UO_2 and reduction parameters of UO_3 to UO_2 .

Santanu Das, Sandeep Sharma, Sandeep Kumar, P.K. Rajagopalan, K.U. Nair and S.B. Roy <mrsued@barc.gov.in>

2.3 DEVELOPMENT OF BORON AND BORON BASED PRODUCTS

Boron and its compounds find extensive use in nuclear industry due to the large neutron absorption cross-section of boron. An isotope of boron, ^{10}B (19.8% in the natural boron) is found to be the best absorber of fast neutrons.

Elemental boron is used as sensor for neutrons in reactor control instrumentation. Boron carbide is used as control rod in the atomic reactor as well as shielding material for neutrons. Borides of refractory metals are being developed as control rod materials for advanced and high temperature reactors. Technology for the production of elemental boron, boron carbide powder and composites such as bocarsil, polyboron, boral etc. wherein B_4C is distributed in rubber, polythene and aluminum matrix respectively has been mastered.

Recent research and developmental activities have been focused on the preparation of enriched boron, dense boron carbide pellets and borides.

Preparation of enriched boron:

Elemental boron is generally prepared from boron carbide by fused salt electrolytic process, wherein, boron is transferred from soluble boron carbide anode to the cathode. But extraction of boron by this method is not suitable for processing enriched boron, as the recovery of boron carbide by direct carbothermic reduction is not high. Hence, a new alternative extraction route was investigated and optimised for extraction of enriched boron from boric acid. In this flow sheet boric acid is first converted to KBF_4 and boron is obtained by fused salt electrolysis of KBF_4 in a melt of KCl and KF. Enriched boron powder prepared by this method has been successfully used in the preparation of sensor elements for neutrons and also for conversion to enriched boron carbide.



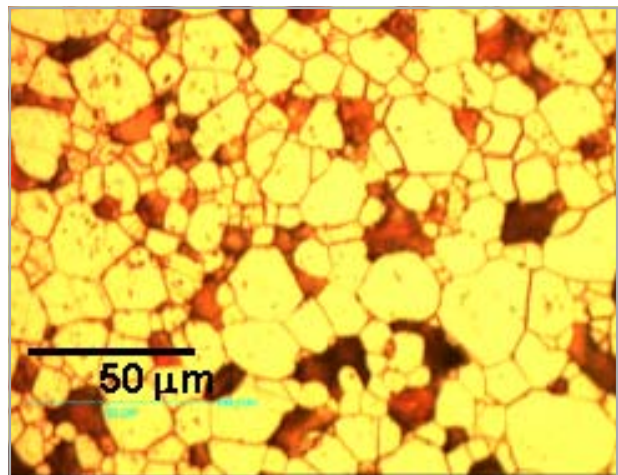
Cathode with boron deposit

Densification of boron carbide pellets:

Boron carbide pellets for the fast breeder reactors are used both as control and shielding material. For inner core control rod

application, Boron carbide enriched with ^{10}B and a high density of 95% theoretical value is prescribed, whereas, for shielding applications, natural boron carbide with 85-90% T.D is considered suitable. Due to its high melting point, covalent nature and poor diffusion constants, it is very difficult to obtain dense boron carbide shapes.

Experimental investigations were carried out to optimise the process parameters for the densification of boron carbide by pressureless sintering methods. The pellets were characterised by microstructure, SEM, X-ray diffraction, Electron Probe Micro Analysis and thermal diffusivity measurements. Pellets with a maximum density of 90% T.D have been obtained by pressureless sintering process. The pores were found to be very small and uniformly distributed throughout the body. The figure below presents a microstructure of sintered boron carbide.

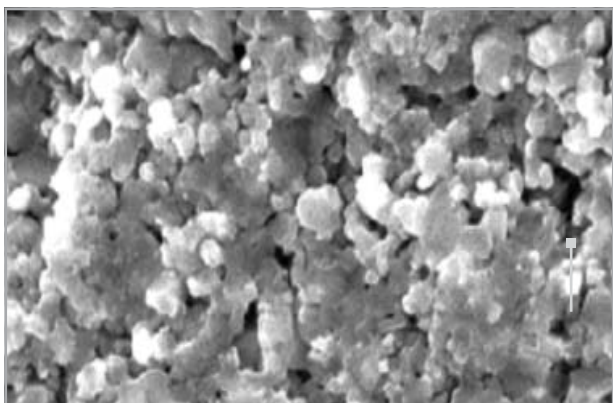


Microstructure of sintered boron carbide

Boride based control elements:

Titanium boride with high melting point and good thermal conductivity is a strong candidate as control rod material for high temperature nuclear reactors.

The process for the preparation of pure titanium boride and densification to near theoretical densities by hot pressing method with or without the addition of sintering additives has been developed and optimised. Addition of molybdenum silicide has been found to be effective in achieving higher densities.



SEM of hot pressed titanium boride with molybdisilicide

As part of material development project for Compact High Temperature Reactor (CHTR) a major milestone was achieved when an annular hexagonal beryllia block was successfully vacuum hot pressed using graphite die tooling to get 45 mm parallel face, 20 mm thick and 20 mm central hole block. The density of the block was 2950 kg/cm³ (97% theoretical density). The figure shows this block along with a cylindrical shape beryllia block (100 mm diameter, 25 mm thick, 2910 kg/cm³ density).

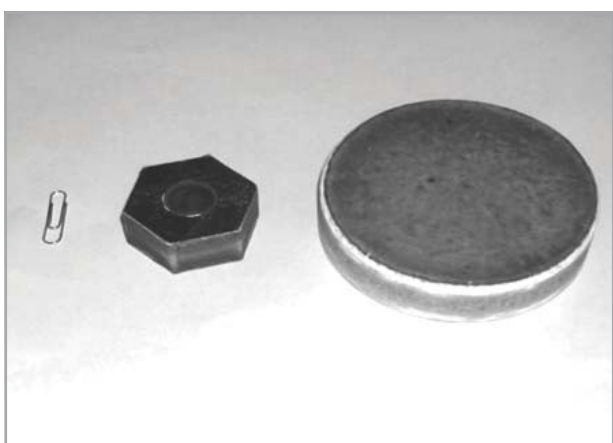
S. Saha. and B.P. Sharma., *BARC Highlights*, 85 (2003).

C.Subramanian and A.K.Suri " *Metals Materials and Processes*, 16(1) (2004), 39-52.

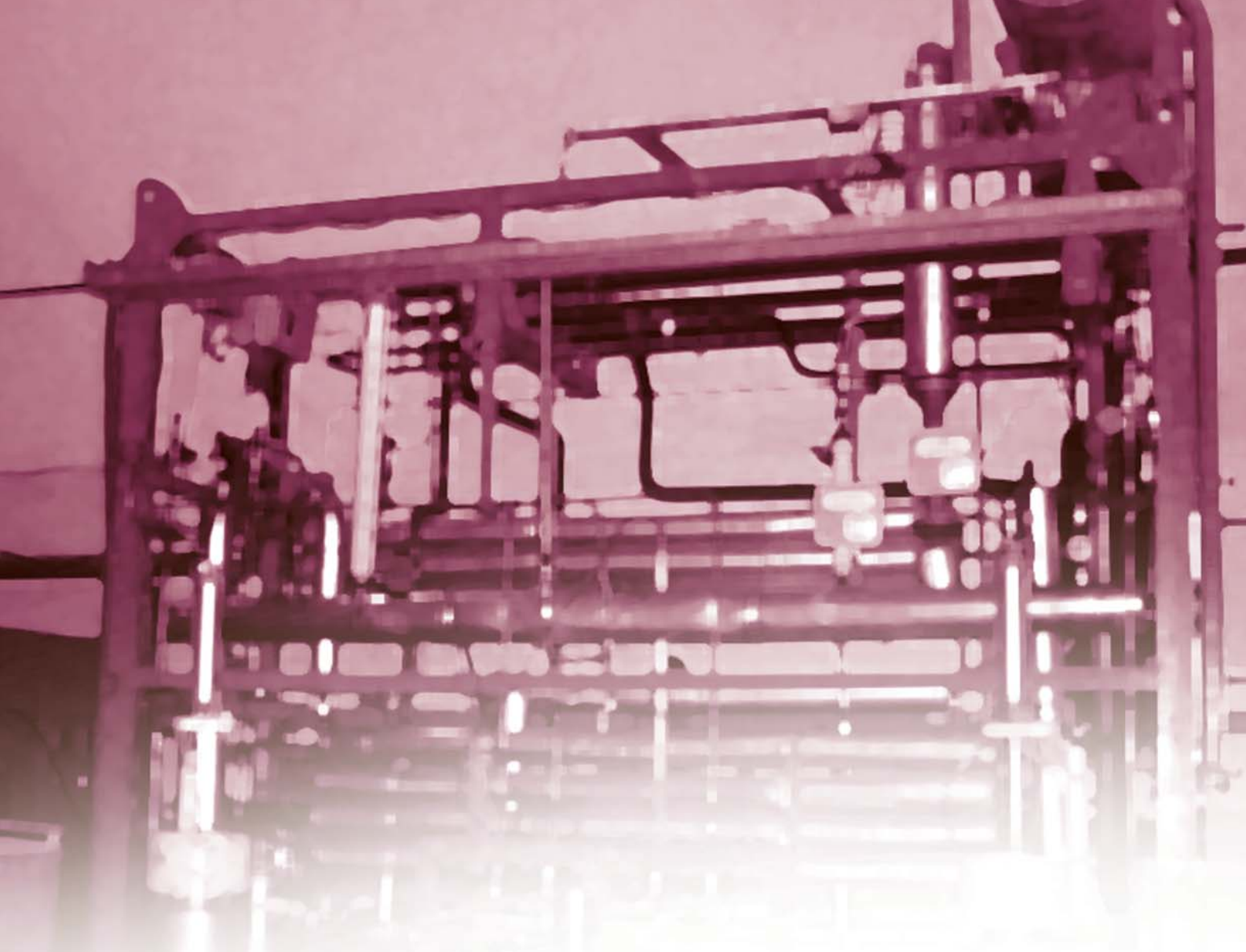
A.K.Suri and C.Subramanian, *Nuclear India*, 38(5,6) (2004).

2.4. BERYLLIA CERAMICS AND BERYLLIA SHAPE FORMATION

Beryllia is an important material for nuclear applications. To meet a specific requirement of DAE about 10 kg of this powder was produced conforming to 99.6% purity, 2100 kg/cm³ tap density and of desired granulometric composition. This powder has passed all quality control tests and was cleared by the Quality Control Committee for making desired components for our specific application.



Cylindrical and annular hexagonal Beryllia blocks by Vacuum Hot Pressing technique



3. NOVEL MATERIALS AND TECHNIQUES

INTRODUCTION

The advancements in all areas of science and technology necessitate the requirement and development of novel materials exhibiting a host of properties and techniques associated with the preparation of such exotic materials. Growth of large single crystals have extended the limits of performance of components in the fields of electronics and aerospace. Technology spinoff from the growth of single crystals has resulted in the melt texturing technique that is increasingly being adopted for high magnetic flux in magnetic bearing components made of high T_c oxide superconductors that are potential materials for magnetic bearings that show little frictional losses at high speed.

Carbon and carbon-based composites have enormous potential in the fields of electronics and nuclear energy. Large coolant channels made of high density graphite are expected to be used for compact high temperature reactors. The development of adding hydrogen to metals exhibiting solid solubility has lead to "Metallic Foam" that has exciting possibilities in heat transfer and impact absorption.

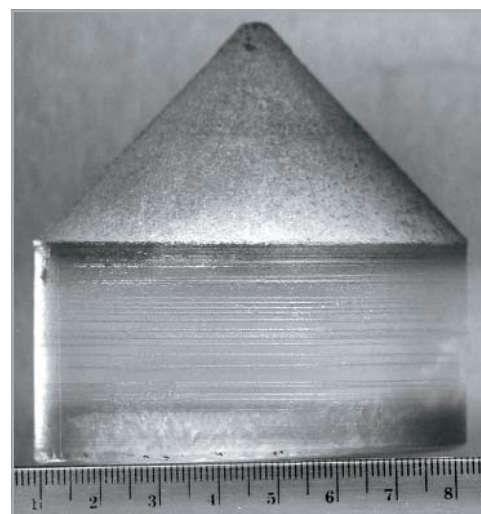
3.1. CRYSTAL TECHNOLOGY

The growth of large size LiF crystals (85 mm diameter) by Bridgman technique was simulated. For this purpose, the physico-chemical properties of LiF were investigated. Also, the experiments were conducted to obtain data required to compute the breaking strain of the crystal, maximum longitudinal thermal gradient and the crystal cooling rates. The results were used to design a hot zone assembly for the Bridgman growth of 85 mm diameter crystals. Based on this design, two vacuum furnaces having hot zone of 130 mm diameter and 160 mm length, a temperature stability of 0.1°C and capable of reaching up to 1300°C under running vacuum of the order 10^{-5} Torr were developed. The heater and the associated insulation setup were manufactured from high density graphite. The effectiveness of the simulation was verified by successfully growing LiF crystals of 75 and 85 mm diameters. A typical crystal ingot is shown in the figure.

The solidification behavior of $PbMoO_4$ was studied using the Differential Thermal Analysis (DTA) technique, with an aim to model the growth by Czochralski technique.



Lithium fluoride crystal



Lead molybdate crystal

Actual crystal growth runs were carried out to validate the modelling and identify the conditions that yielded good quality crystals. A seed oriented about 20° off the c-axis, pull rate of 3 mm h^{-1} and moderate rotation rate of 20 rpm were found to be the optimum parameters for growth of crackless crystals of 20 mm diameter and 40 mm length. The crystals if pulled along any other direction suffered extensive cracking. The changes in melt stoichiometry, which may arise due to the application of an improperly synthesized starting charge, have been found to drive the growth from an initial melt growth regime to self flux assisted growth regime. The results showed that the tolerable limit for non-stoichiometry in the present case is very small.

The crystallization behavior of LiB_3O_5 (LBO) was studied to determine conditions leading to the formation of glassy or crystalline phase on cooling the melt. The crystallization of LBO phase was investigated by seeding with a Pt wire and employing 0.1° h^{-1} as the solution cooling rate and 1 mm day^{-1} the seed pull rate. Under these conditions, the central region of the crystallized matter was found to be translucent and attached to it were a few big transparent chunks. XRD and DTA analyses showed that the presence of $Li_2B_4O_7$ (247) phase in LBO melt provides uncontrolled nucleation sites thus promoting polycrystalline growth of the LBO phase. The results for the first time have revealed the important role of the melt microstructure in governing the nature of the solidified phase. This investigation has helped in the growth of LBO single crystals by top seeded solution growth technique.

The solidification behavior of the $\text{Li}_2\text{B}_4\text{O}_7$ was also investigated to overcome a serious problem usually faced with the single crystal growth of the material namely the appearance of core defect. The application of a pull rate of 0.5 mm h^{-1} , a rotation rate of 10 rpm and higher longitudinal thermal gradient has been found to result in the growth of core free crystals, as shown in the photographs.

The single crystal growth of ZnWO_4 was studied by Czochralski technique. A major problem successfully tackled was crystal cracking. In this regard, measurements on crystal thermal expansion along different crystallographic directions were



Lithium tetraborate crystals

performed to understand the origin of the problem. Large anisotropy in thermal expansion along different directions suggested that the growth direction should have a significant influence on crystal cracking. Subsequent work on crystal growth showed that irrespective of the growth rate and / or cooling rate employed, the cracking propagates easily along certain crystallographic directions such as the cleavage plane (010). On the other hand, the cracking can be completely suppressed by effecting the growth along $\langle 023 \rangle$. The strain induced during growth in this case is so little that the grown crystal can even withstand the thermal shock caused by the cooling rate of 500°C/h . The crystal in this case exhibits the development of two very broad {010} facets, which possibly contribute significantly



Zinc tungstate crystal

to its high resistance to thermal shock.

Sangeeta, Babita Tiwari and S.C. Sabharwal, *J.Crystal Growth*, 273 (2004), 167.

Sangeeta and S.C. Sabharwal, *J. Luminescence*, 109 (2004), 69.

S.C. Sabharwal, Babita Tiwari and Sangeeta, *J.Crystal Growth*, 263 (2004) 327.

Sangeeta and S.C. Sabharwal, *J. Luminescence*, 104 (2003), 267.

S.C. Sabharwal, Babita Tiwari and Sangeeta, *J.Crystal Growth* 249 (2003), 502.

3.2. DEVELOPMENT OF NOVEL CARBON MATERIALS FOR VARIED APPLICATIONS

Carbon is a wonderful material with a wide range of structures and properties. It is a challenge to tailor its structure to get the desired properties as per requirement. On one hand the requirement is for amorphous carbon as probable scattering material in the upcoming advanced heavy water reactor (AHWR) and on the other extreme requiring graphitic carbon for the High Temperature Reactor (HTR). Brief description of the work carried out on carbon is given in the following sections.

■ Development of amorphous Carbon Composite (a-C Composite)

Two types of a-C composites have been developed so far and these are new findings. Polyacrylonitrile (PAN) fiber based C-C composites was developed using 20 vol% PAN fibers dispersed in phenolic resin matrix. In the second type, C-C composites with 15% carbon black dispersed in carbonized phenolic resin was developed. The pellets were densified by liquid resin impregnation and chemical vapour infiltration method. The samples were characterized in terms of microstructure, coefficient of thermal expansion (CTE), density and compressive strength. A density upto 1400 kg.m^{-3} and compressive strength of 65 MPa were obtained in carbon black based composites as compared to 1270 kg.m^{-3} and 32 MPa with the PAN fiber-based composites. Future efforts will be directed to achieve the required density of 1500 Kg.m^{-3} .

Irradiation of the C- C composites has been done using 145 MeV Ne^{+6} ion at different fluence levels 1×10^{13} , 5×10^{13} , 1.5×10^{14} ions. cm^{-2} at VECC. Irradiation studies confirm that these samples remain in amorphous state up to a fluence level that has been studied.

■ High-Density Graphite Channel Tube

A high-density graphite channel tube similar to dimensions for CHTR has been fabricated indigenously. This tube has the following dimensions- I.D. 35 mm x O.D. 75 mm x 1400 mm long with 12 numbers of 10 mm dia holes at 55 mm PCD running through 1050 mm deep. The other end has 6 number of holes.



Prototype hot channel tube for CHTR

The figure shows the fabricated channel tube. Fabrication of such tube poses special manufacturing challenges due to its large number of small diameter deep bores in the graphite (soft materials).

■ Binderless Microgranulation

A novel process i.e. binderless microgranulation has been developed using Centrifugal Pressure Swing Processor. The objective of the study was to granulate the nano-sized carbon black fines into dense microspheres. This dense granulated carbon black with better flowability could be used to make the C-C composites for improving the density. The granules were characterized by stereo microscope for shape and size analysis. The reduction in the surface area of the granules as measured by the surface area analyser confirms granulation. Granulation of carbon black fine powder from 3 micron to 150 micron using Centrifugal Pressure Swing Processor has been achieved. The density of a pellet using granulated carbon black is 1300 kg.m^{-3} as compared to the ungranulated one (1100 kg.m^{-3}).

K. Dasgupta and D. Sathiyamoorthy, *Materials Science and Technology*, **19** (8) (2003), p. 995-1002

K. Dasgupta, P. S. R. Krishna, R. Chitra and D. Sathiyamoorthy, *Carbon Science*, **4** (1), (2003), p. 10-13

D. Sathiyamoorthy and A. K. Suri, *Carbon Science*, **4** (1) (2003), p. 36-39

S. M. Shetty, K. Dasgupta, Ramani Venugopalan and D. Sathiyamoorthy, *Proceedings of Workshop on Carbon Materials for Energy Applications*, Nov. 25-26, 2004 Delhi. Eds R. K. Aggarwal, T. L. Dhami and O. P. Bahl, Ideal Impressions Pvt. Ltd. New Delhi (2004), p. 298-310.

3.3 MELT TEXTURED $\text{YBa}_2\text{Cu}_3\text{O}_x$ MATERIAL FOR SUPERCONDUCTING MAGNETIC BEARING (SMB)

A key component of the devices involving high circumferential speeds like energy storing flywheels, motors and centrifuges is the bearing which reduces friction and imparts rotational stability. Superconducting Magnetic Bearings (SMB), operate in non-contact mode and are therefore anticipated to have much lower frictional loss and a longer lifetime. Further SMB can stabilize the operation of rotors without requirement of any sensor and complex feedback mechanism as the diamagnetism gives vertical stability and pinning forces give lateral stability. Of late SMB

have also been used to reduce wear and tear losses in Microelectro-mechanical (MEMS) devices. High critical current density $\text{YBa}_2\text{Cu}_3\text{O}_x$ (YBCO) pellets have been developed by top seeded melt textured growth process. High T_c superconductors enable device operation at liquid nitrogen temperature and high critical current density in magnetic field is necessary for efficient devices. For preparation of high critical current pellets different dopants were added to well-sintered and oxygenated YBCO material. The pellets were heated with a seed of MgO crystal to 1050°C and then slowly cooled to room temperature. Subsequently, the material was subjected to a prolonged post growth oxygenation at 450°C .

The samples were characterized at Technical University of Budapest, Hungary under a collaborative programme. These showed a trapped field of 9 mT at temperature of 77 K when field-cooled with an applied magnetic field of 0.25 T. A pellet of 2.5 gm and 20 mm diameter showed a levitating force of 0.7 N on a small magnet having 7 mm dia, 6 mm height and 0.2 T surface field.

K. P. Muthe, Ajay Singh, D. K. Aswal and S. K. Gupta
<kpmuthe@barc.gov.in>

3.4 FABRICATION OF ALUMINUM FOAM

Hydrogen in metals like zirconium, when present as stable hydrides, renders the material hard and brittle, but in dissolved form can

reduce the phase transition temperature and improve the superplastic properties in these alloys. Hydrogen, at very low concentrations, in non-hydride forming metals like iron and steel causes low and room temperature embrittlement. But the presence of hydrogen in metals like aluminum non-hydride former results in a highly porous metal that can absorb shock and impact deformation. These materials, known in general as 'Metallic Foams', have other attractive properties as heat/sound insulation (closed pore) or efficient heat dissipation (open pore). Preliminary experiments to fabricate such metallic foams in commercial purity aluminum using zirconium hydrides were successful. Foams with dimensions of 30 mm diameter and 50 mm length could be produced with the existing facility. The foams were characterized by compression tests, measurement of pore size/distribution and bulk density. Al foams with bulk density of 0.2 gm/cc (8%) could be achieved by varying the proportion of zirconium hydride.

Foaming in commercial purity aluminum was obtained by two techniques using different concentrations of the foaming agent, zirconium hydride. The densification of the mixed powders of aluminum and zirconium hydride was obtained by (i) compacting mixture in a uniaxial press or (ii) by rolling powder in sealed aluminum cans. The foaming was obtained by heating the pressed compacts in a furnace under argon flow, and the rolled sheets under oxygen-butane flame in air. The compacts obtained using uniaxial press did not give good products while the rolled sheets showed good foaming behavior. The foamed parts (from rolled



Photograph showing levitation of a small magnet over a set of four pellets



Aluminium foams formed using Titanium or Zirconium hydrides

sheets) were characterized by measuring the pore size, distribution, bulk density and compression tests. The pore size increases, and the bulk density and the compression strength decrease with increase in the concentration of the hydride powder. The effect of addition of Al_2O_3 in Al matrix is being tried to tailor the strength of the foamed parts.

3.5. SUPERCRITICAL FLUID (SCF) PROCESSING FACILITY

Supercritical fluid is the physical state of any pure substance above its critical temperature and pressure. Once a substance attains this state, the phase boundary between the gas and liquid state disappears. Hence, the supercritical fluid exhibits properties both of gas and liquid. Supercritical fluids have low viscosities, nearly zero surface tensions, gas-like diffusion coefficients and liquid-like densities. The properties of supercritical fluids endow process engineering with novel operating regimes that can overcome several conventional barriers.

The SCF extraction is batch-wise in operation and can be carried out in 3 modes like, individual mode, series mode and parallel mode. The plant is totally automated and can be controlled through computer interface. The automation incorporates display of online status of pilot plant through mimic display, data acquisition and safety features in case of emergency shutdown.

A supercritical extraction pilot plant has been designed, fabricated and commissioned. Supercritical CO_2 is used as the extractant. The figure shows the setup of the SCF pilot plant. The plant is equipped with two extractors of 5 litres capacity. It can be operated upto a pressure of 300 bar and 150°C . The material used for construction is SS304.

Experiments have proved to extract silicone oil from alumina microspheres, the extraction of the transformer oil from soaked ceramic powders.

D. Sathiyamoorthy, S. M. Shetty, K. Dasgupta, R. Venugopalan and P.T. Rao <dsati@barc.gov.in>



Supercritical fluid extraction pilot plant

4. AMORPHOUS AND NANO-MATERIALS

INTRODUCTION

Metallic glasses and nano-crystalline solids have come in to prominence in recent times because of their extraordinary properties. Rapidly solidified metallic glasses can be produced only in very thin geometries because formation of these alloys requires very high cooling rates. But few of the alloys can be obtained in the amorphous state in bulk at relatively lower cooling rates. Crystallization of the metallic glasses leads to the formation of nano-crystals and sometimes the formation of quasicrystalline solids. Rapidly solidified metallic glasses have been made in zirconium (Zr) based iron (Fe), copper (Cu), aluminium (Al) and nickel (Ni) bearing alloys in a melt spinning device made in-house. Bulk metallic glasses have been made in Zr based Ni, Ti, Cu, niobium (Nb) and platinum (Pt) bearing alloys by casting these in copper moulds with cylindrical cavities. By suitable heat treatments nano-crystals or nano-quasicrystals have been produced in either type of glasses of different compositions. The nature of crystallographic defects like stacking faults, antiphase domain boundaries and dislocation have been examined in these nano-crystalline solids by High Resolution Electron Microscopy (HREM).

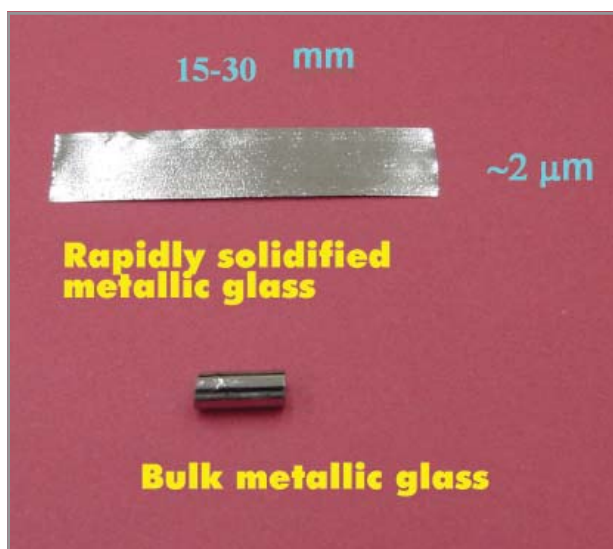
Structures with nanometer-scale dimension has attracted considerable attention of both scientific and engineering communities since their chemical and physical properties deviate from the properties of the corresponding bulk materials. The nano-structured materials have been categorized in three different subdivisions: (1) materials and/or devices with reduced dimensions in the form of isolated or self-supported or embedded nanometer-sized particles, (2) materials and/or devices comprising the nanometer-sized thickness in the form of thin film or in the surface region of bulk materials and (3) bulk solids with a nanometer-scale microstructure (nano-structure). Nano-crystalline alloys belong to the third category of nanostructured materials. Synthesis, microstructural characterization and property determination of these materials have resulted in the development of various materials with much improved properties over conventional material.

Processing of nano-structured materials is a special form of grain boundary engineering which involves increase in the area fraction of grain boundaries and number density of triple junctions over grain bodies. Among the various techniques for the large-scale production of nano-structured solids, most current efforts are concerned with consolidation of nano-crystalline precursor powders produced by different techniques, such as gas condensation, ball milling, or spray conversion. Film deposition techniques, such as physical and chemical vapour deposition (PVD, CVD) sol-gel techniques etc. are also under intensive investigation. However, electroplating has been identified as a technologically feasible and economically superior technique for production of nano-crystalline pure metals and alloys as well as nano-composites and ceramics.

4.1 METALLIC GLASSES

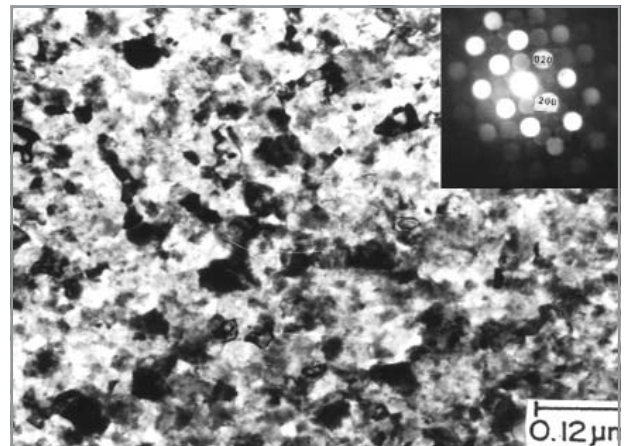
■ Rapidly solidified metallic glasses

Rapid solidification has been found to lead to the formation of metallic glasses in a variety of alloys. Keeping in view the significance of metallic glasses and nanocrystals from scientific as well as technological viewpoints, a programme of synthesis and characterization of these glasses has been pursued in BARC. The crystallization behaviour of these glasses has been examined in detail. Different types of crystallization including primary, eutectic and polymorphic, have been investigated extensively in these glasses. The deformation of these alloys in tension and bending has been examined in detail and the effect of crystalline particles on deformation behaviour and mechanical properties has been ascertained. These studies have shown that the presence



Photograph of rapidly solidified Ti-Cu alloy and Zr based bulk metallic glass

of crystalline particles in the amorphous matrix need not always lead to an improvement in the mechanical properties of the alloys. The structure of the shear bands, which are responsible for heterogeneous flow in metallic glasses has been examined by transmission electron microscopy (TEM). The corrosion behaviour of the amorphous state has been found to be superior to their crystalline counterpart. Studies are also being conducted in Fe and Co-based metallic glasses, which are of interest for application as soft magnetic materials.



Nano-particle distribution in the $Zr_{76}Fe_8Ni_{16}$
Micro-diffraction from one of the nano-particle (inset)

■ Bulk Metallic Glasses

Bulk metallic glasses have been made in Zr based Ni, Ti, Cu, Nb and Pt bearing alloys by casting these in copper moulds having cylindrical cavities and cavities with rectangular cross section. The amorphous nature of these glasses has been ascertained by carrying out X-ray diffraction, conventional TEM and high-resolution transmission electron microscopy (HREM).

The development of bulk metallic glasses and composites of crystals and glass is being carried out because of their excellent mechanical properties. These materials are finding use in bio-medical applications, application in defence, space and in electronics.

J. Basu, G. K. Dey, S. Banerjee, S. Ranganathan, *Trans IIM*, 58 (2005) p.61.

S. Banerjee and G.K. Dey, *J. Mat. Sci.* 39 (2004) p.3985

Arun Pratap, Kirit N. Lad, R.T. Savalia, G.K. Dey, S. Banerjee & A. M. Awasthi, *Physics & Chemistry of glasses*, (2006)

4.2 NANOMATERIALS

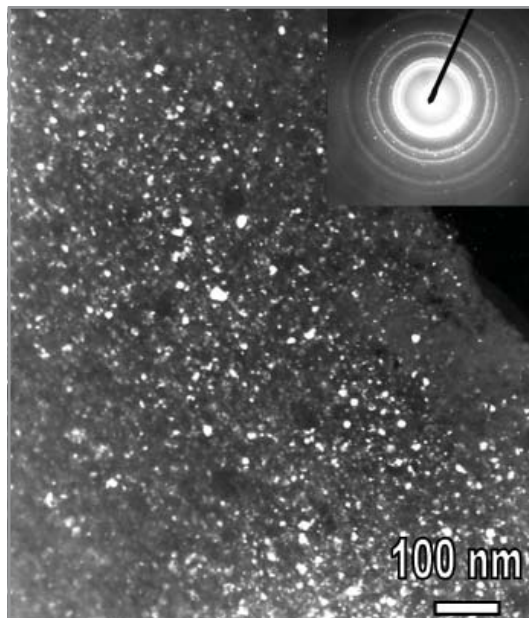
■ Nanocrystalline Solids

Crystallization of metallic glass leads to the formation of nanocrystals or nano-quasicrystalline solids. Crystallization of either type of glasses has revealed that nanocrystalline

microstructures can be produced in these after suitable heat treatments. The nature of crystallographic defects like stacking faults, antiphase domain boundaries and dislocation have been examined in these nanocrystalline solids by HREM. The structure of the nanograin boundaries in crystalline and quasicrystalline microstructures has been examined in detail by HREM and no amorphous or disordered regions could be seen at such boundaries. These boundaries have been found to have structure very similar to that of boundaries in large grained materials.

■ Nano-Crystalline Magnetic Material

The amorphous magnetic materials have been extensively used as soft magnets in transformers, inductive devices, sensors and bioengineering. The excellent soft magnetic properties like low H_c , high permeability, high magnetic saturation and low energy losses of nanocrystalline soft magnetic alloys have triggered major interest and activity in this field of research. Iron base alloy having composition $Fe_{40}Ni_{38}B_{18}Mo_4$, commercially known as METGLAS 2826MB, has been studied.



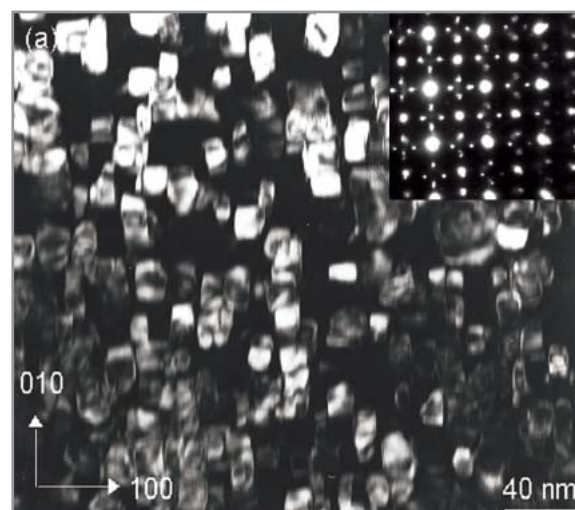
Nano-phase distribution in the $Fe_{40}Ni_{38}B_{18}Mo_4$ alloy

Amorphous $Fe_{40}Ni_{38}B_{18}Mo_4$ ribbons were obtained by using rapid solidification technique. Nano-crystalline phases were produced

in the amorphous matrix by suitable heat treatment. These cast and heat treated ribbons were characterized by DSC, X-ray diffraction, TEM. DSC studies indicated that primary and secondary crystallization occurred at temperatures around 410°C and 518.6°C respectively. Different phases formed in these alloys were analyzed and identified. The size and size distribution of the nanocrystalline phases as function of heat treatment parameter were studied and it has been found that the kinetics of the phase transformation plays a very important role to control the microstructure.

■ Phase transformations in Zirconium Niobium-based alloys

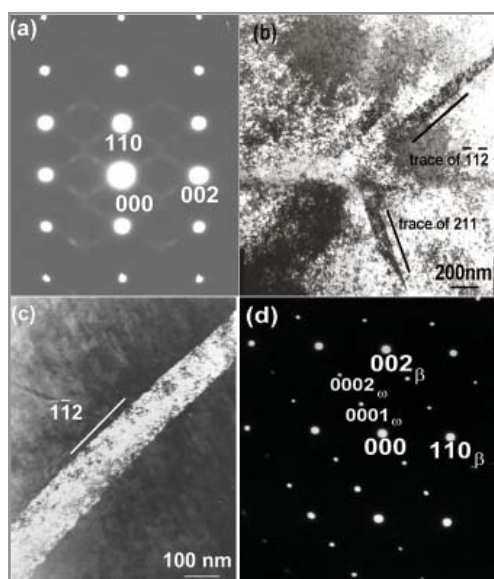
Zr_3Al -Nb based materials have been developed to explore the possibility of their usage as structural components in nuclear reactors. Several alloys were investigated and various phases have been identified. Structural relationships between various phases were established and their evolution sequence has been predicted. A pseudo-binary phase diagram Zr_3Al -Nb has also been developed. The high temperature properties of the alloys were determined using micro-indentation techniques. Using this technique high temperature creep properties have been evaluated. A deformation map has also been developed. Further investigations on evaluating irradiation behaviour of the alloys are being carried out.



Ordered omega phase in Zr_3Al -3Nb alloy

To evaluate the sequence of the omega phase transformation in Zr-20Nb by irradiation, attempts are being made to simulate the selected area diffraction patterns. Several programs generating the crystal structure of the parent phase, displacement of the atoms and generating selected area diffraction patterns of the lattice etc. have been written. A more rigorous algorithm is being developed which is sensitive to the input parameters like probability of displacement and extent of displacement.

Formation of the omega phase with a plate like morphology was demonstrated in a Zr-20Nb alloy by shock loading. Phenomenological theory of martensitic transformation has been used to explain the formation of this phase under shock loading and formation of this phase could be explained in terms of a defect akin to the twinning process. Formation of this phase in pure-Zr is being investigated to understand the underlying transformation mechanism from alpha to the omega phase.



TEM bright field micrograph and SAD pattern showing formation of the phase with a plate like morphology in a Zr-20Nb alloy by shock loading

G.K. Dey, R. T. Savalia, S. Neogy, D. Srivastava, S. Banerjee, *Trans IIM on nanomaterials* (2006)

G. K. Dey, R. T. Savalia, S. Neogy, D. Srivastava and S. Banerjee, *Journal of Nanocrystals* (2006)

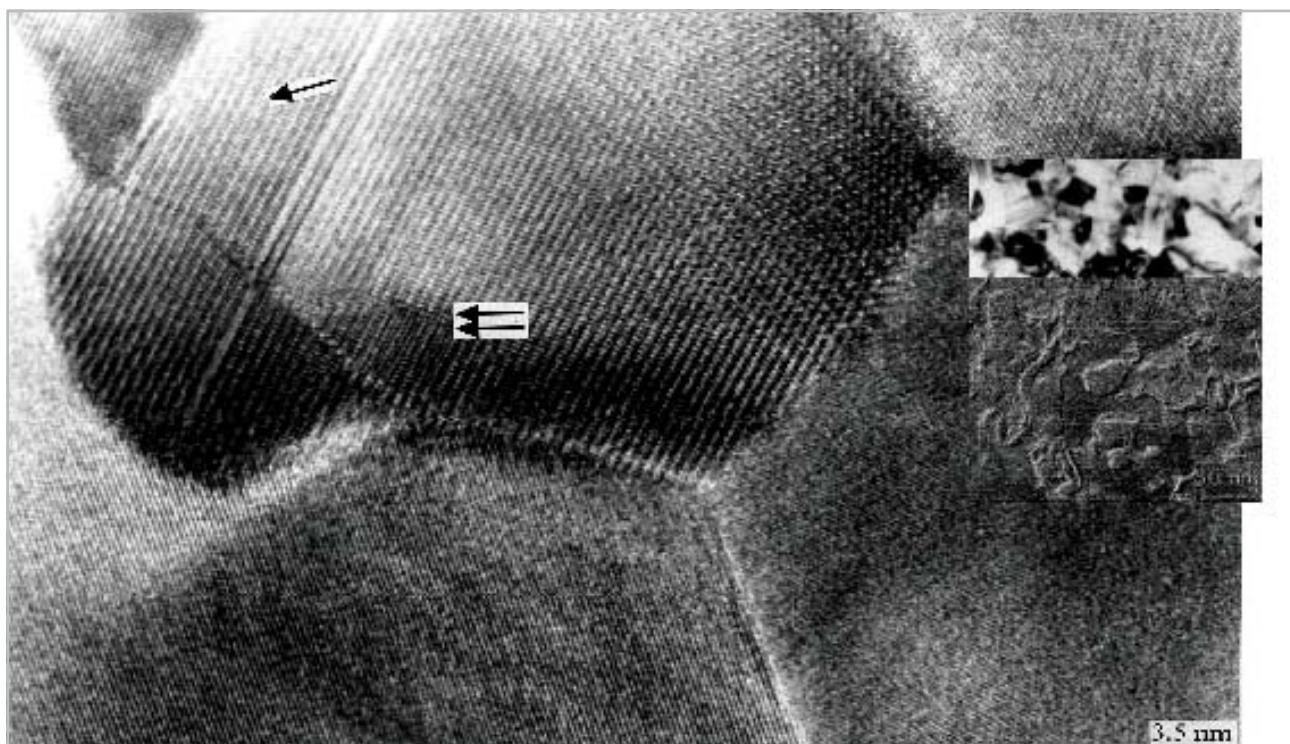
Arun Pratap, Kirit N. Lad, R.T.Savalia, G.K. Dey and S.Banerjee, *Materials Sci. & Eng.A* 375-377C (2004) p.767-771.

4.3 DEPOSITION OF NANOCRYSTALLINE NICKEL COPPER ALLOY COATINGS BY PULSE ELECTROLYSIS

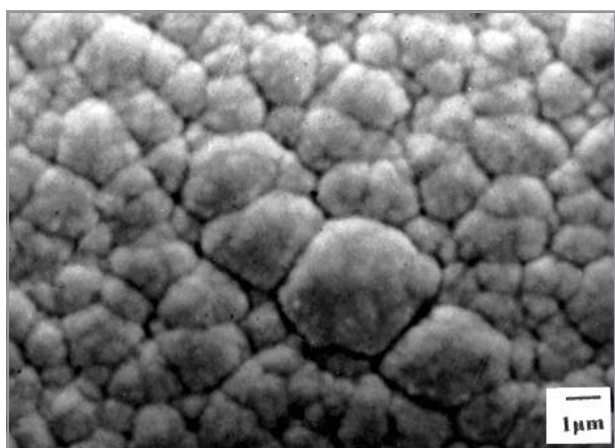
In recent years electrodeposition has emerged as a technologically and economically viable synthesis route to produce nanostructured metals, alloys and composite materials both in bulk form and as coatings of varying thickness. Among all the techniques available, electrodeposition has been identified to be a technologically feasible and, for many applications, economically superior technique for the production of nanocrystalline materials. Both direct-current (DC) and pulsed-current (PC) plating have been successful in producing a variety of nanocrystalline materials. Electrodeposition has many advantages over other *nano-processing* techniques: (1) It can be used to produce powders, thin films and bulk material as required, which is not possible with any other technique. (2) The potentially very large number of pure metals, alloys and composite materials, which can be electrodeposited with grain sizes less than 100 nm. (3) Few shape and size limitations. (4) High production rate. (5) Low initial capital investment requirements and (6) Easy technology transfer from the research laboratory to existing infrastructure in electroplating and electroforming industries.

For the last few years, the programme of synthesis of nanocrystalline (nc) alloys and metal coatings via electrodeposition route has been initiated and it was possible to deposit smooth, bright and compact Ni-Cu alloy coatings with grain size in the range of 2.5-30 nm. Pulse electrolysis has been used extensively to manipulate the deposit composition and grain size. Under pulse plating conditions surface morphology of the coating was smoother with fine grain deposit compared to the DC deposition condition. Composition of the alloy is controllable precisely with various pulse parameters. The deposit grain size decreases with the increase in pulse current and also the microhardness. Detailed microstructural characterization using X-ray diffraction (XRD), CTEM, HRTEM and differential scanning calorimetry (DSC) revealed that kinetically controlled electrodeposited Ni-Cu alloy forms not only fcc but also metastable $L1_0$ ordered phase and this novel observation is being reported for the first time of its merit in electrodeposited Ni-Cu alloys.

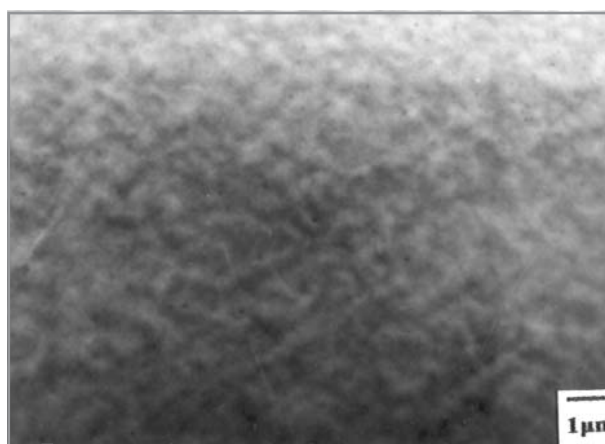
Presence of ordered $L1_0$ -phase acts as pinning site to the dislocation movement leading to higher hardness has also been



High resolution electron micrograph showing nanograin boundaries, stacking fault (single arrow) and antiphase domain boundary (double arrow) $Zr_{52}Ti_6Al_{10}Cu_{18}Ni_{14}$.



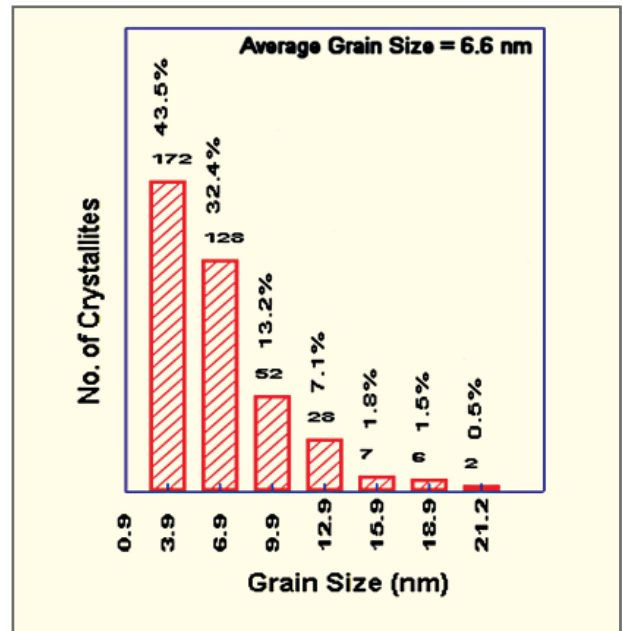
Surface morphology of direct current-plated alloy at current density = $2A.dm^{-2}$.



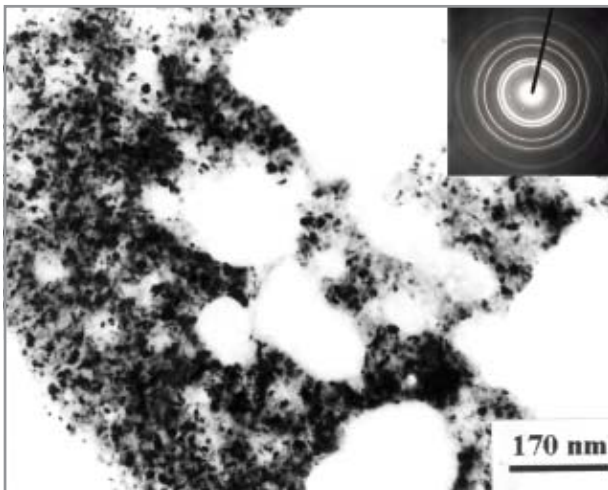
Surface morphology of pulse plated alloy at $I_a = 2A.dm^{-2}$, $I_p = 20 A.dm^{-2}$, $f = 100 Hz$.

Property data of nc Ni-Cu Alloys and Monel-400

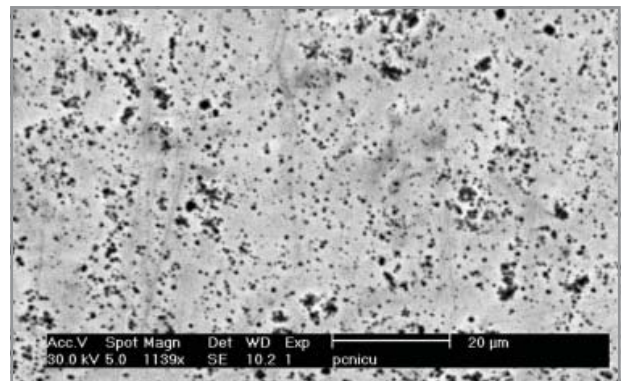
Sample wt%	Av. Grain Size (nm)	Resid. Stress (MPa)	Micro hard (KH50)	Corrosion Current Density* ($\mu\text{A. cm}^{-2}$)
PC-26.0 Cu	5.6	40.3	750	4.0
PC-27.4 Cu	7.8	63.2	480	7.0
PC-35.8 Cu	12.7	45.5	452	1.5
DC-30.6 Cu	27.8	400	6.0	
Monel-400	~15,000	-	260	2.2



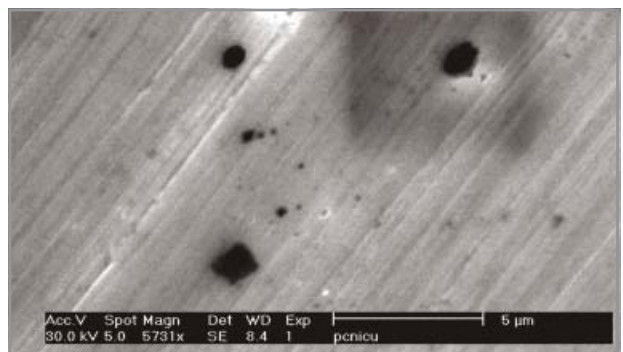
Grain size distribution of nano-crystalline PC-Ni-26.0wt% Cu alloy



Bright-field image and SAED pattern (inset) of PC-Ni-26.0wt% Cu alloy

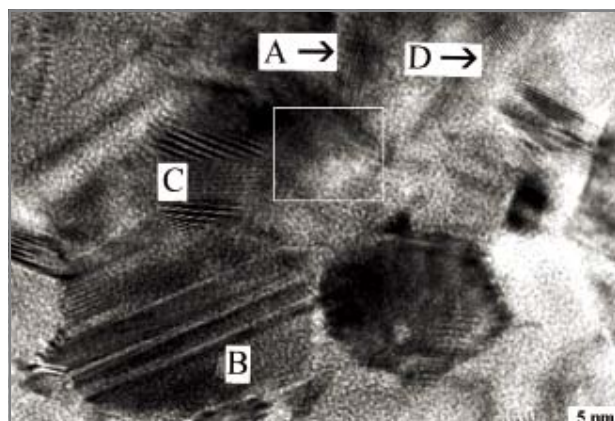


(A) SEM image of Corroded surface of Monel-400 and (B)nc PC-35.8wt% Cu alloy



noticed.

Detailed corrosion behaviour study in 3.0 wt% NaCl solution at RT as well as at 50°C revealed that PC-plated alloys were more corrosion resistant as compared to their DC counterpart. It also revealed that commercial Monel-400 alloy showed pitting type of attack at RT, however, PC-plated alloys undergo general type of attack with numerous shallow pits, akin to homogeneous corrosion, as seen under SEM but passivity for Monel-400 was superior.



HRTEM image of nc PC-27.4wt% Cu alloy
[A: Phase Separated region, B: Stacking faults,
C: Twins, D: Low angle grain Boundary]

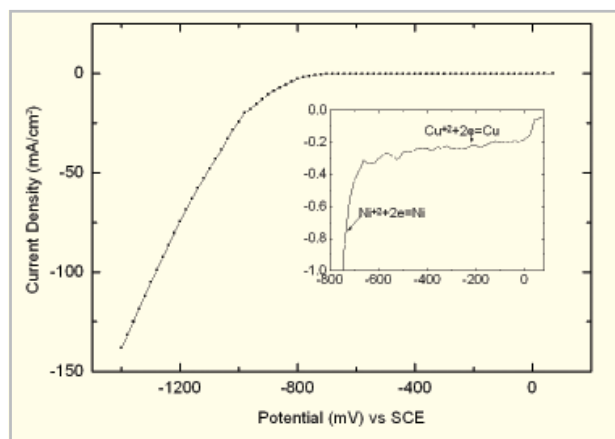
S.K. Ghosh, A.K. Grover, G.K. Dey and A.K. Suri, *Defence Science Journal*, 55 (1), (2005) p.63.

S.K. Ghosh, A.K. Grover and M.K. Totlani, *Trans. Inst. Met. Finis.*, 80(2), (2002) p.56.

S.K. Ghosh, A.K. Grover, G.K. Dey and M.K. Totlani, *Surface and Coatings Technology* 126 (1), (2000) p.48.

4.4 NANOSTRUCTURED Ni/Cu MULTILAYER COATINGS BY PULSE ELECTROLYSIS

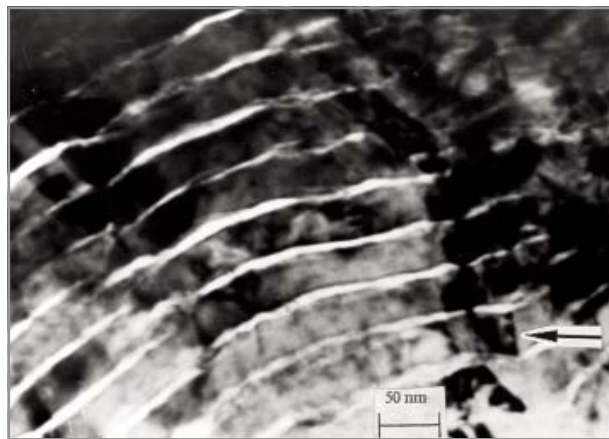
The deposition of artificially layered structures using multiple metals having different behaviour with respect to their mechanical or magnetic properties, has become important because of its widespread applications in areas like



Cathodic polarization curve to select deposition regions

interconnects, giant magnetoresistive sensors and data storage devices. Among the various techniques, sputtering and molecular-beam epitaxy are mainly used to produce multilayers with good physical properties, however, electrodeposition (ED) could obviously be a simple and significantly low-cost alternate technology and it could be used to prepare multilayers in geometries inaccessible to other fabrication methods.

Nickel/Copper (Ni/Cu) multilayer has received significant attention recently because of their high strength. Growth of coherent epitaxial layers is possible because the two metals have the same crystal structure (fcc) and have a lattice mismatch of



Cross-Sectional TEM of The Electroformed
(30nmNi+5nmCu)₂₀₀ Multilayers.

~2.6%. Results of the electrosynthesis of Ni/Cu multilayers, characterisation using cross section transmission electron microscopy (XTEM) and XRD analysis are also presented.

Electrodeposition of Ni/Cu multilayers was done galvanostatically in such a manner that deposition would occur in diffusion controlled mode for copper and activation controlled mode for nickel. Cathodic polarisation was carried out potentiostatically to determine the deposition voltage and current separately for Cu²⁺ and Ni²⁺ ions. The entire process was carried out in a two compartment electrolytic cell separating the anolyte and catholyte by anion-exchange membrane to maintain the pH. A three-wave pulse generator has been used for the growth of the multilayer specimen.

X-ray diffraction analysis has revealed the presence of both Ni and Cu in the electroformed multilayered material. Layers were

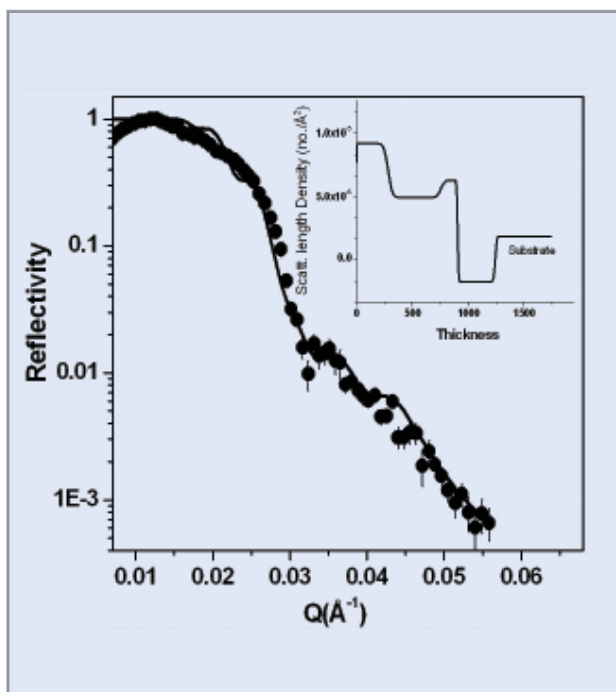
textured in the (111) direction but there was no evidence of superlattice formation. This was further, confirmed by transmission electron microscopy. Cross-sectional TEM micrograph of Ni/Cu multilayer containing a total of 200 sublayers of each metal. The presence of two distinct phases of nickel and copper could be clearly seen. The thicknesses of nickel and copper sublayers were 30 ± 1 nm and 5 ± 1 nm respectively.

Recently Ni/Cu bilayer sample was electrodeposited on a 20 nm thick Cu seed layer on a buffer layer of 45 nm Ti layer from a single solution electrolyte. The film was grown on Si (111) substrate at room temperature. Both seed and buffer layers were grown by magnetron sputtering methods. Ni/Cu bilayer structure was characterized by using the Polarized Neutron Reflectometer at Dhruva reactor in Trombay. AFM images of the top surface of the sample were obtained using an NT-NDT's Solver P-47 H multimode instrument with a Si_3N_4 tip.

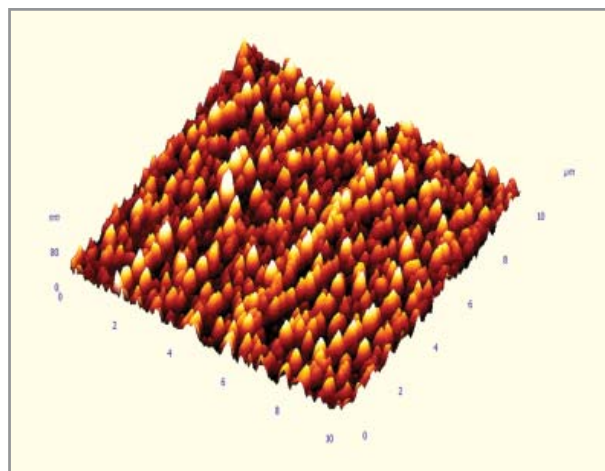
Fitting the NR data gives thickness of 338 Å and 150 Å for Ti buffer and Cu seed layer respectively, comparable with the designed values of thickness. The roughness value at the Si/Ti, Ti/Cu and Cu (seed)/Cu(ED) layers are 9.0 Å, 11.0 Å and 7.0 Å

respectively. The Ti and Cu (seed) layers are deposited by the sputtering technique so the roughness values are low. The thickness for Cu and Ni layers grown on seed layer by ED method was 473 Å and 281 Å respectively. The roughness values at the interfaces Cu(ED)/Ni(ED) and Ni(ED)/air have increased to 28 Å and 30 Å respectively. The scattering length density for the Cu layer grown by ED method is 4.95×10^{-6} per Å², which is lower as compared to 6.30×10^{-6} per Å² (~bulk) grown by sputtering method. The scattering length density of the ED Ni layer is 9.2×10^{-6} per Å². This is also lower as compared to the bulk value. It shows that the layers grown by ED is porous compared to that grown by sputtering method.

In order to visualize the local growth of film in the ED method the AFM image of the uppermost i.e. Ni surface of Ni/Cu multilayers was taken. The AFM analysis of Ni/Cu bilayer gives an rms roughness of 36.5 Å, which is comparable to that obtained from the reflectivity measurement. The NR and AFM measurements both indicate several distinctive features of the ED technique. The layers grown by ED have lower densities and also the interfaces of the ED layers are having much larger roughnesses (~30 Å) as compared to the sputter-deposited layers (~10 Å).



The measured and calculated unpolarized neutron reflectivity profile for the sample.



The Atomic force microscope image of Nickel surface of Ni/Cu multilayers.

Element	Thickness (Å)	Scatter Length Density (Nb _{coh}) (10 ⁻⁶ / Å ²)	Roughness (Å)
Nickel	281	9.2	30
Copper	473	4.95	28
Copper (seed)	150	6.30	7
Titanium(buffer)	338	-1.72	11
Silicon Substr.	-	1.90	9.0

Physical parameters of sample extracted from best fit of unpolarized reflectivity data.

A.K. Grover, S.K. Ghosh and A.K. Suri, *Indian Surface Finishing*, 1 (1), (2004) p.69.

S.K. Ghosh, A.K. Grover, G.K. Dey and M.K. Totlani, *TMFAI*, Jan-Mar, (2002) p.37.

4.5 SYNTHESIS OF CARBON NANOTUBE BY CATALYTIC CHEMICAL VAPOUR DEPOSITION

Carbon nanotube has been synthesized by Catalytic Chemical Vapour Deposition (CCVD) of acetylene (diluted with nitrogen) at different temperatures (600, 700 and 800°C) in a quartz tube reactor. Nanosized catalyst like nickel, cobalt and iron were synthesized respectively from nickel formate, cobalt formate and ferrocene. The concentration of the catalysts was varied between 5, 10 and 15 wt%. These precursors directly yield metal nanoparticles on supported materials and thus eliminate the lengthy process of supported catalyst preparation. The purity and yield of the nanotubes were found out using thermogravimetric analysis in air upto 1000°C. Nanotubes synthesized at 700°C on Ni-magnesia supported catalyst with 15 wt% Ni loading have the maximum purity (90%) and yield (72 times that of the catalyst loading). Figure shows the nanotubes synthesized by the above method.



Helical multiwall nanotube from Fe catalyzed CCVD. The background artifacts (cuboids) are from the coated grid used for making TEM sample



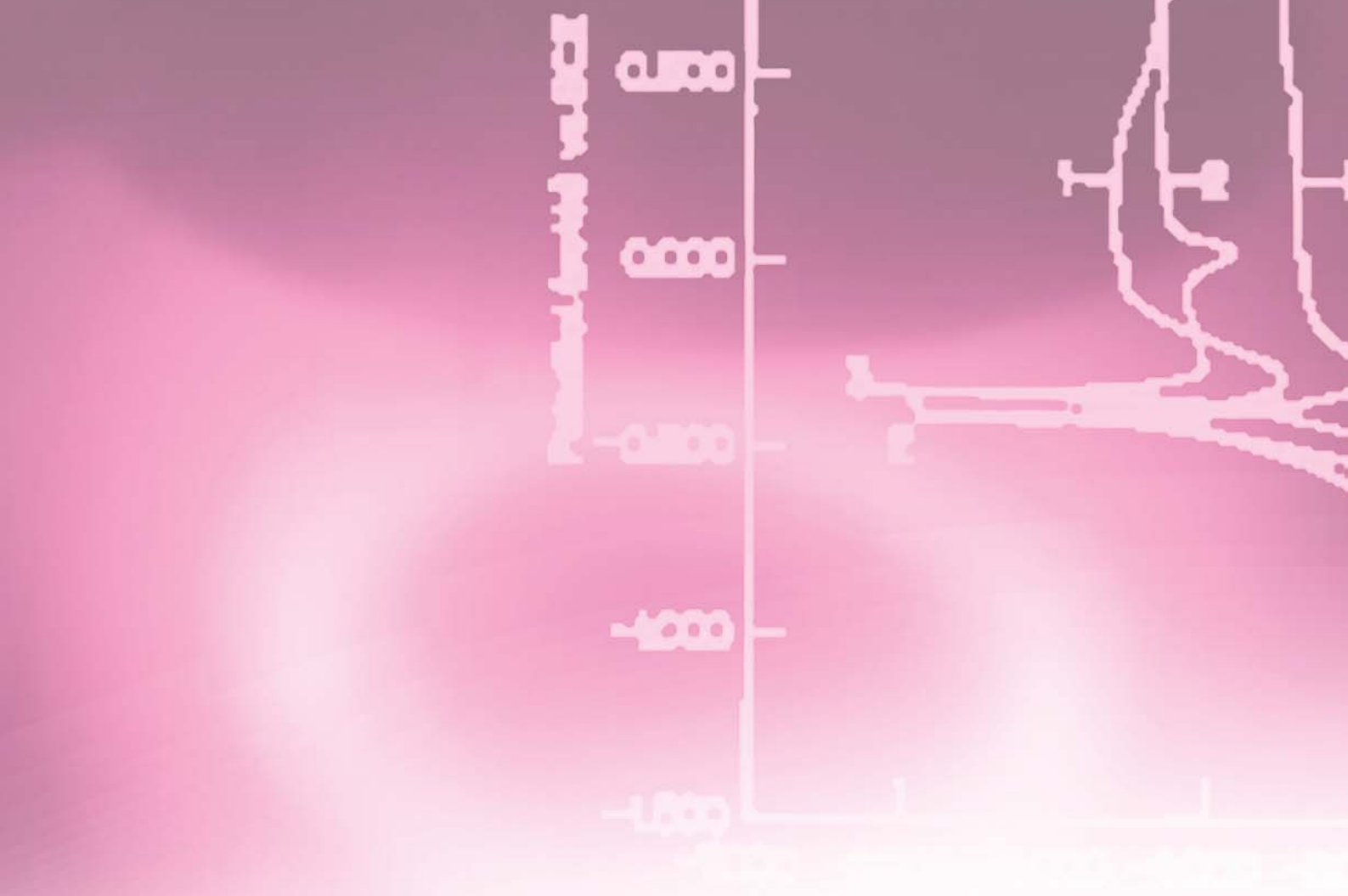
Nanotube rope from Ni catalyst. The background artifacts (cuboids) are from the coated grid used for making the TEM sample.



Purity : 86%

Carbon nanotubes obtained by catalytic chemical vapour deposition techniques with different catalysts.

K. Dasgupta and D. Sathiyamoorthy < kdg@barc.gov.in >



5. SURFACE ENGINEERING

INTRODUCTION

Advances in Surface Engineering technologies enable surfaces with improved hardness, superior wear resistance, friction behaviour, heat resistance, corrosion characteristics and nuclear properties without altering the desired bulk mechanical properties. Variety of techniques involving electroplating, electroless plating, magnetron sputtering etc are being utilized to deposit metals, alloys, compounds, composites, multicomponent and multilayer coatings. A host of techniques are utilized for characterization and performance evaluation of these coated materials.

Fission type ($^{235}\text{UO}_2$ based) sensors for various flux levels for different projects Tarapur Atomic Power Station (TAPS), PRP and Advanced Heavy Water Reactor (AHWR) having different enrichment and Absorption type (^{10}B based) neutron sensors have been developed with the complete flow sheet right from the starting material boric acid. Electroless nickel (EN) coatings have been applied for mirrors in CO_2 laser, structural components used in fluoride vapours, helical springs of seal and shield plug assembly of Dhruva, Rosemount pressure sensors of heavy water plant, housing of liquid scintillation counters etc. Composite coatings are being developed for water lubricated ball bearings and nickel plating applied on difficult-to-plate uranium components of first indigenously built ^{60}Co Teletherapy unit, Bhabhatron. Hard nitride coatings have been developed by magnetron sputtering. These find variety of applications in tribology and corrosion resistance areas. Work has been initiated for developing a process for TRISO coating of fuel particles for Compact High Temperature Reactor (CHTR).

5.1 NEUTRON SENSORS

Neutron detectors are used as **out-of-core and in-core devices** for monitoring neutron flux in nuclear reactors. This requires the application of controlled quantity of fissile or neutron sensitive material on sensor electrodes. Two types of neutron sensors have been developed as import substitutes

(1) **Fission type ($^{235}\text{U}_2$ based)**

(2) **Absorption type (^{10}B based)**

UO_2 was electrodeposited from a complex uranyl nitrate electrolyte. A very close control of operating conditions such as pH, temp., current density, agitation and circulation is required to get coherent, adherent stress free deposits.

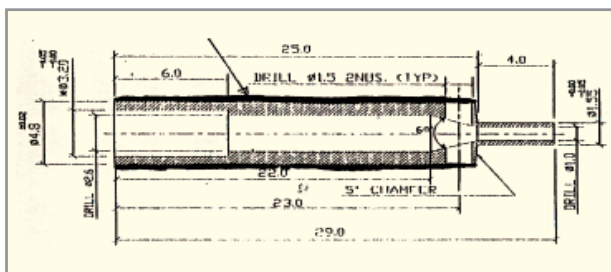
Applications:

Four different types of uranium based (^{235}U : 93%) sensors have been developed and are being used at **TAPS**. These are

- (1) **Short-range monitor** (UO_2/Ti 1.5mg.cm⁻²) to measure the neutron flux at source during start-up.
- (2) **Intermediate range monitor** (0.54 mg.cm⁻²) to measure the flux in the range of 10^7 - 10^8 .
- (3) **Linear power range monitor**(0.5 mgcm⁻²) for full power flux measurement (10^{12} - 10^{14}).
- (4) **Travel-in-core probe.**

The **indigenously developed neutron sensors for Tarapur Atomic Power Station** have a **better signal to noise ratio** over its entire life span due to switch-over from SS to Ti as the electrode material.

The uranium-based sensors having low enrichment of 20% have also been developed with deferent Uranium (UO_2/SS 0.75-0.8 mg.cm⁻²) and (UO_2/SS 0.25 mg.cm⁻²).



Neutron sensor for critical facility (AHWR)

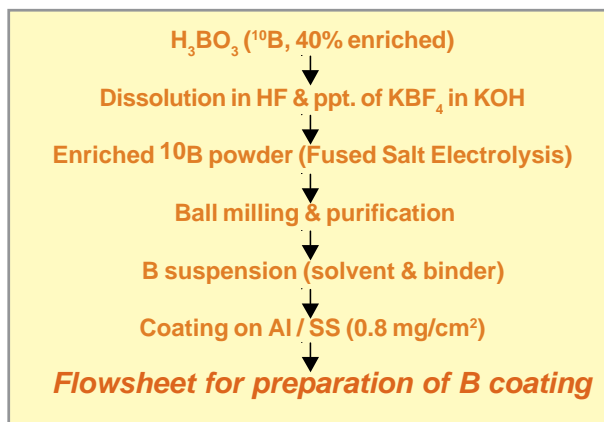
Boron Based Neutron Sensors have been developed as import substitute. A complete flow-sheet for preparation of

boron from starting material boric acid has been developed. It was possible to have better control of viscosity in the indigenously developed suspensions. This ensured uniformity in the thickness of boron coating.

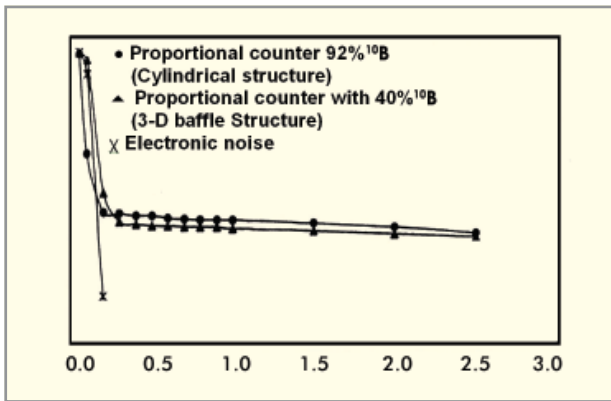


Neutron sensor electrodes (PRP)

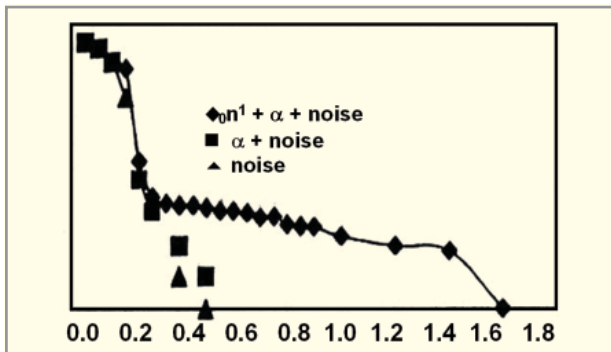
Integral Bias Curves for the neutron sensitivity show the usefulness range for bias voltage. The performance of indigenously developed 40% enriched boron counter having 3-D baffle structure was almost the same as that of 92% enriched imported cylindrical boron counter.



Boron coated neutron sensors, Ion chamber



Disc bias (volts) ¹⁰B lined proportional counters at 150 nv thermal neutron flux, 800V



Disc bias (volts) ²³⁵UO₂ (20% Enriched) coated fission detector, Uranium : 0.8 mg.cm⁻² Neutron Sensitivity : 0.166 cps/nv 600V

The respective thermal resistance of the developed neutron sensors of fission and absorption type are 600 K and 423 K and each type of sensor has good neutron sensitivity because of better control in coating thickness. Following the success of these developments, it is proposed to setup a larger electrolyzer unit incorporating newer features such as solution circulation, continuous make-up of solution pH, uranium (U) ion concentration and novel design of mechanical agitator. This will help in developing U coated neutron sensors for PFBR operating at higher temperatures of 823-873 K. The challenge will be to meet the requirement of higher coating thickness of about 2 mg.cm⁻² and coating on difficult-to-plate upon Inconel-600 electrode material.

¹⁰B-coated neutron sensors of higher surface area in a given volume of tubular geometry incorporating novel design such as finned internals are also being developed.

The indigenously developed neutron sensors meet the requirements of various departmental projects.

Mary Alex, D.N. Prasad, K.R. Prasad, S.K. Kataria, S.N. Athavale, A.L. Pappachan, C. Subramanian, A.K. Grover and A.K. Suri, *Jl. of Sci. & Indl. Research*, 62 (2003) p.1057-1062.

P.M. Dighe, D.N. Prasad, K.R. Prasad, S.K. Kataria, S.N. Athavale, A.L. Pappachan and A.K. Grover, *Nuclear Instruments and Methods in Physics Research. Section (A)* 496 (1) (2003) p.154.

G. C. Panchal, A. Topkar, S. K. Kataria, A. L. Pappachan, A. V. Sathian, *Proc.:Symp. on Compact Nuclear Instruments and Radiation Detectors (CNIRD-2005)*, BRNS, Jodhpur 2-5th March 2005 p. 110.

5.2 DEVELOPMENT OF HARD NITRIDE COATINGS BY MAGNETRON SPUTTERING

In sputtering, a glow discharge (10⁻³ – 10⁻² torr) is created of inert gas (usually argon). These ions strike the target with high energy under the influence of high negative potential applied to the target and sputter out the target material primarily in atomic form. A magnetic field is applied to constrain secondary electrons to follow a helical, rather than straight-line path resulting in enhanced ionization and sputtering rates. Magnetron sputtering differs from a conventional diode sputtering that it operates at a lower pressure (4 - 20X10⁻³ mbar). Advantages of magnetron sputtering are lesser impurities (and inert gas) in the deposited films, better adhesion because of the higher energy of the sputtered atoms and increased deposition rates.

In sputtering, since the coating material is passed into the vapour phase by mechanical means rather than a chemical or thermal process, virtually any material is a candidate for sputtered coatings. These coatings show exotic properties with respect to hardness, wear, oxidation and corrosion and, therefore, find applications in many areas.

System : The indigenously built system consists of 6" dia target with 0-1000 V variable DC power supply (0-6 A) for target, substrate biasing 0-300 V (negative), gas purification system and flow control for input gases. Fairly uniform coatings can be carried out over a flat surface of about 4" by 4" size.

Coatings studied : Magnetron sputtered titanium nitride (Ti-N), chromium nitride (Cr-N), titanium aluminium nitride (Ti-Al)N coatings and duplex coatings having top coat of TiN

with interlayers of Cr, Ni and electroless nickel (EN) deposited by plating have been studied at various deposition parameters. NbN and (Ti-Nb)N coating systems are being studied currently.



Plasma inside the chamber

Characterization : Coatings were evaluated by X-ray diffraction (XRD), scanning electron microscope (SEM), energy dispersive X-ray analysis (EDX), surface hardness, adhesion, electrochemical (in 1N H₂SO₄), and wear tests. Some of the typical results are being reproduced below.

Parameter	Value
Base pressure	8 x 10 ⁻⁸ mbar
Operating pressure	4-6x 10 ⁻³ mbar
on gas flow rate	20 cc/m
Nitrogen flow rate	0-10 cc/m
Substrate biasing	-50 to -250 V
Target current	0.6-0.8 Amp
Target-subst distance	~ 60 mm

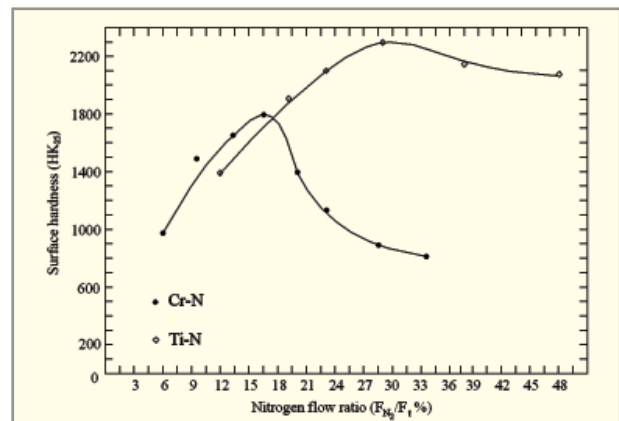
Operating parameters for deposition

Deposition rates were found to decrease almost linearly with the increase in nitrogen flow and substrate biasing.

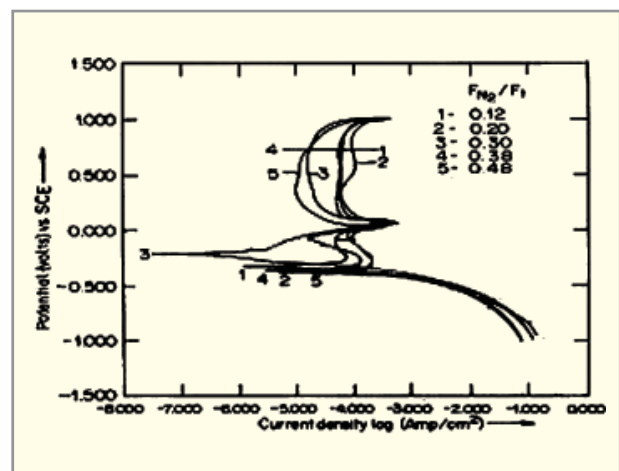
Crystallography : In Ti-N system under stoichiometric TiN phase was observed to be the hardest phase while in case of Cr-N system Cr₂N was found to be the hardest phase.

In case of (Ti-Al)N coatings NaCl type cubic TiN structure was observed. With increasing nitrogen flow hAlN structure was also observed leading to sudden drop in hardness 1746 from 2790 HK₂₅. Hardness of the coatings increases consistently with the increase in substrate biasing (negative).

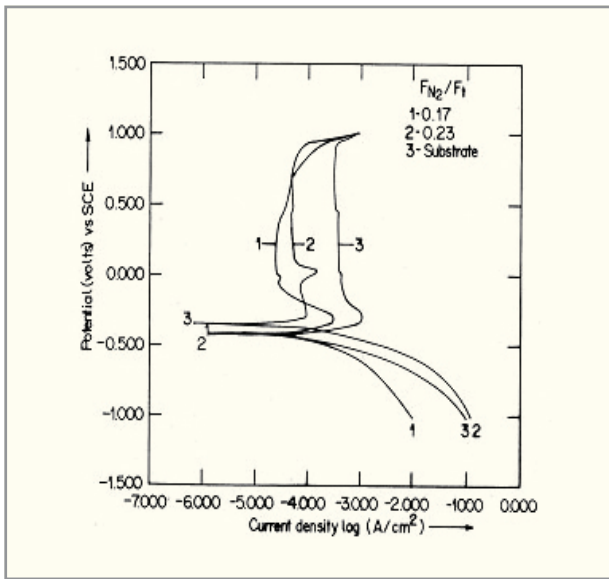
Corrosion : Increase in nitrogen partial pressure in general caused the corrosion resistance to increase (increase in corrosion potential E_{corr} and decrease in corrosion current density I_{corr}). Increase in substrate biasing from -50V to -250V resulted in consistence increase in corrosion resistance. TiN coatings have been applied on mild steel with Cr, Ni and EN interlayers and were found to show considerable improvement in corrosion resistance.



Surface hardness Vs N₂ flow



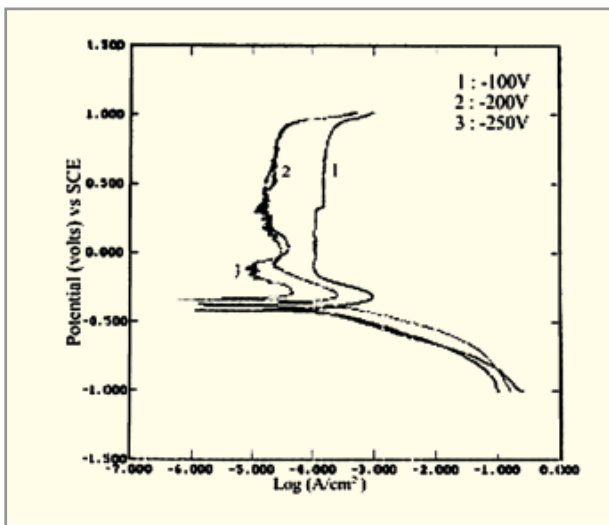
Potentiodynamic curves for Ti-N coatings



Potentiodynamic curves for TiAlN coatings

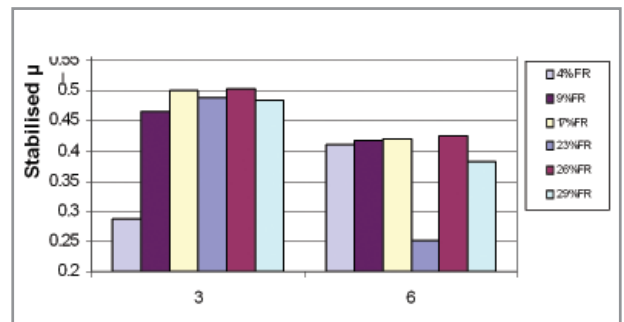
HARDNESS & I_{CORR} FOR TiN WITH INTERLAYERS

COATING	H_{25}	I_{CORR} mA cm ⁻²
SUBST (MS)	<200	1440
TiN (2.0)	1064	478
Ni(4)+TiN	1289	31.1
Cr(4)+TiN	1907	9.3
EN(4)+TiN	1484	0.45

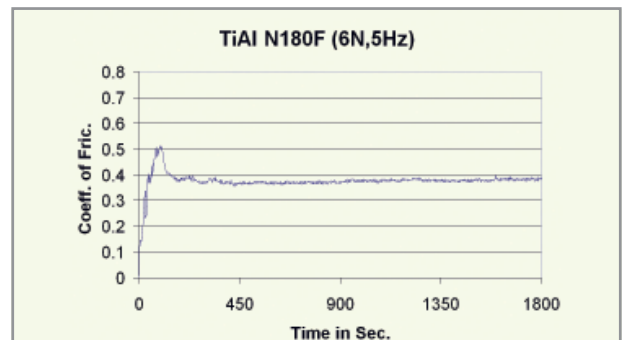


Effect of substrate biasing on CrN coatings

Tribological properties of (Ti-Al)N coatings were studied at 3 and 6N load, 5 & 15 Hz frequencies for 10 and 30 minutes in a ball-on-plate configuration. Short duration tests were also carried out to study the coating ball interaction mechanism and pictures were taken after 10, 30 and 60 sec for all the samples. Lowest friction was observed at 6N load & 5 Hz for coatings deposited at 23% N₂ flow while highest wear rate (of counter body ball) was observed at 6N, 15Hz for coatings deposited at 17% N₂ flow.



Coefficient of friction (μ) Vs load (N) for (Ti-Al)N coatings



Coeff. of friction Vs time

It was possible to produce hard nitride coatings having better corrosion resistance and favourable mechanical and tribological properties through proper control of deposition parameters.

K. Singh, A.K. Grover, and A.K. Suri, *Wear* 258, June (2005), p.1813–24.

K. Singh, A.K. Grover, and A.K. Suri, *Metals Materials and Processes*, 16 (1) (2004) p.111.

K. Singh, A.K. Grover, and A.K. Suri, *Trans. IMF (UK)*, 81(4) (2003) p.131-35.

5.3 ELECTROLESS NICKEL (Ni-P) AND COMPOSITE COATING

Electroless coating is an autocatalytic process. The bath consists of source of metal ion, complexing agent, reducing agent and sometimes a poison to control spontaneous decomposition and an exaltant to accelerate the deposition process. EN basically is a Ni-P coating and the phosphorous content is controlled by maintaining a careful control of pH and temperature. This in turn controls the stress in the coating. The nanocrystalline structure of EN is responsible for some of its unique properties - high hardness, wear resistance, inherent lubricity, and good corrosion resistance. The basic reaction is



Depending upon phosphorous (P) content (Wt% 4–11) the coatings are designated as low, medium or high phosphorous. EN coatings have hardness in the range of 500-600 VHN, which can be increased to about 900 VHN by heat treatment (Ni₃P precipitation).

Ra: 0.05µm, Reflectivity: 96%



Coated metal mirrors for lasers

Applications: High phosphorus (10-11%P) EN has been extensively plated for a variety of applications for use in our DAE programmes e.g., for coated metal optics - as mirrors for use in CO₂ laser, as corrosion resistant coating on structural components used in fluoride vapours, helical springs of seal and shield plug assembly of Dhruva, Rosemount pressure sensors of heavy water plant, housing of liquid scintillation counters etc.

EN-Composite Coatings: Incorporation of hard particles like diamond, SiC, Al₂O₃, B₄C, Si₃N₄ into the nickel matrix improves wear, corrosion and impact resistance. A recent development in the field of composite coating is co-deposition of luminescent particles with EN which, otherwise appear normal under visible light, emit fluorescence on exposure to UV of suitable wavelength. Such coating can be used either as a functional coating or as an

under coat to act as indicator coating and has potential use for authentication of products.

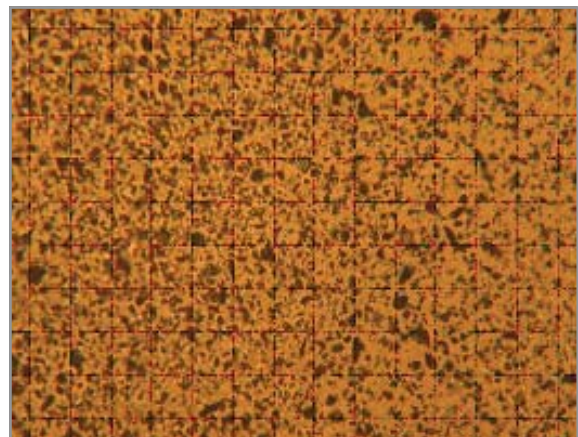
EN-silicon nitride (Si₃N₄) coatings for water lubrication

applications: Fuel handling equipment and control-rod-drive systems operating under aqueous (pH 8 and temperature around 60°C) use cobalt-based ball bearings. Such environment is highly aggressive towards commonly used AISI 52100 bearing steel. Thin EN composite coating with Si₃N₄ as second phase can possibly alleviate wear and corrosion problems of AISI 52100 ball-bearings because of high hardness and chemical inertness of Si₃N₄ particles. Although corrosion resistance of EN increases with the phosphorous content, hardness decreases and, therefore, medium and low phosphorous EN coating can serve for both low corrosion and wear in aqueous environments, Tribological requirements for water lubricated ball-bearing are manifold:

1. Withstand accelerated 4-ball-wear tester for 18 hrs of life.
2. Corrosion resistance in lithiated water
3. Wear <50% of coating thickness
4. Pitting factor (noise) < 10
5. Low coefficient of friction

Medium and low phosphorous composite EN-Si₃N₄ coatings have been developed. SEM picture shows a very uniform distribution of Si₃N₄ particles.

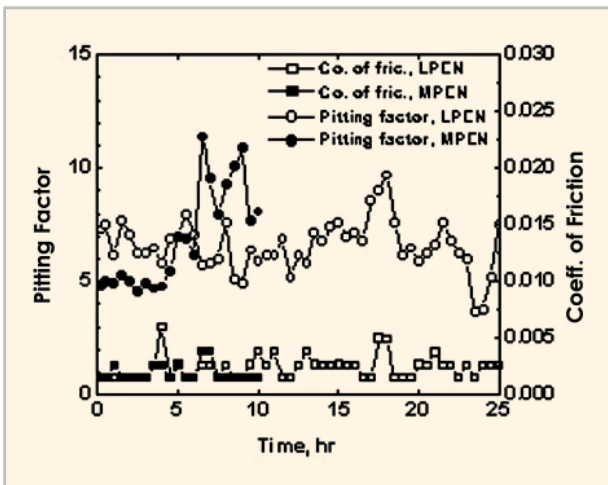
Low phosphorous composite coating showed lower pitting factors up to 25 hrs of testing compared to about 10 hrs for



Surface topography of Ni-P-2.9wt% Si₃N₄

E_{corr} and I_{corr} in 0.125N H_2SO_4 and hardness for substrate, EN and composite coating

Material	E_{corr} (mV)	I_{corr} ($\mu A.cm^{-2}$)	Hardness
CS	-481	186	-
EN	-452	9.1	474.5
EN-2.9Si ₃ N ₄	-476	118	583.7



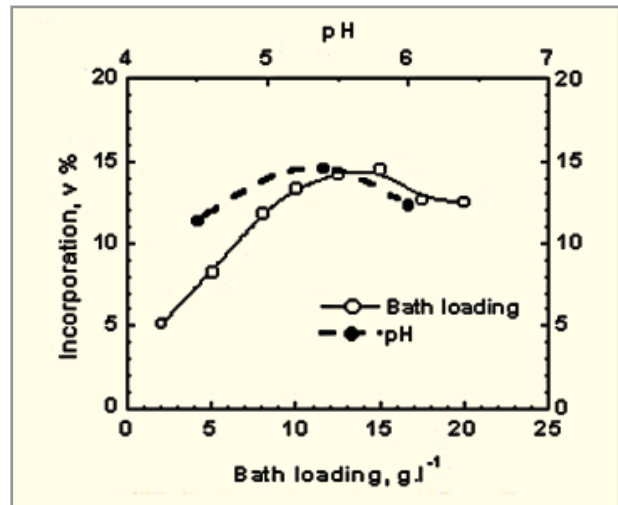
Comparative performance of 4mm thick low and medium phosphorous EN-Si₃N₄ coating

medium phosphorous coating although the coefficient of rolling friction were similar. Composite coating did not affect corrosion rates.



EN composite coated Balls and Races

EN composite-coated balls and racers have given encouraging results with all the requirements being met in the four ball wear tester and they have the potential for use in water-lubricated applications.



Effect of pH and bath loading

Luminescent EN composite coatings: Luminescent EN composite coatings were prepared by co-depositing YVO₄:Eu⁺³ into the nickel matrix 15 g.l⁻¹ bath loading at 90 °C and pH 5.4. Increasing the concentration of the suspension of YVO₄:Eu⁺³ in the EN bath increases the incorporation of luminescent particles in the coating up to 15 g.l⁻¹.

Ni-P-YVO₄:Eu⁺³ coating emits bright red luminescence when exposed to UV light. Composite coating containing 5.16 volume % of YVO₄:Eu⁺³ is good enough to be used as indicator undercoat but not as a functional coating due to its poor corrosion protection characteristics as compared to Ni-P coating.

C.M. Das, A.K. Grover and A.K. Suri, *Trans. Inst. Metal Finish* 80(4), (2002)p. 128

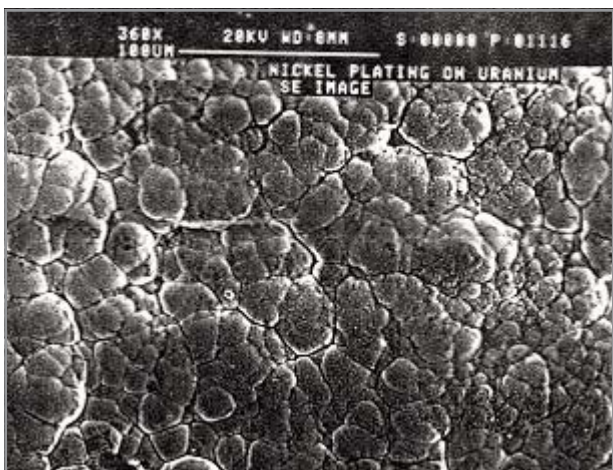
C.M. Das, P.K. Limaye, A.K. Grover and A.K. Suri, *Proc.12th National Congress on Corrosion Control*, Visakhapattanam 20-22 Sep. (2004) p.1-6

5.4 PLATING ON DIFFICULT-TO-PLATE METALS: NICKEL ON URANIUM

Uranium readily oxidizes in air or in water at room temperature. It is one of the most difficult-to-plate upon metals due to the passive film present on its surface. This surface film is often difficult to remove as it is re-formed immediately when the cleaned surface is exposed to air or water. To overcome this

Surface pre-treatment for uranium

- | | |
|-----------------------------------|----------------------------|
| 1. Degrease in Acetone | 10. Nitric acid dip |
| 2. Degrease in Alkaline | 11. H ₂ O Rinse |
| 3. Water (H ₂ O) Rinse | 12. Sod.- silicate |
| 4. Desmut in HNO ₃ | 13. H ₂ O Rinse |
| 5. H ₂ O Rinse | 14. HNO ₃ dip |
| 6. Sod.-silicate | 15. H ₂ O Rinse |
| 7. H ₂ O Rinse | 16. Electroplate |
| 8. Etch with FeCl ₃ | Nickel from |
| 9. H ₂ O Rinse | (Sulphamate Bath) |



Surface topography of Ni plated U

Corrosion performance was assessed by exposure of Ni-plated uranium coupons to atmosphere at ambient room temperatures and also some accelerated tests were carried out by exposing the coupons to boiling water and moist oxygen at higher temperatures.

Applications: Nickel has been electroplated on components of Teletherapy unit – the first indigenous ⁶⁰Co Teletherapy machine developed by BARC for cancer treatment. Uranium has been used because it is a good shielding material due to its high density and high mass number. Various components that have been electroplated are primary definer, trimmers and jaws. An electroplating facility with elaborate pre-treatment sequence as outlined earlier was set up. Variety of jigs were designed and fabricated to accommodate different components based on its geometry and weight e.g. the primary definer weighed about 75 Kilograms.

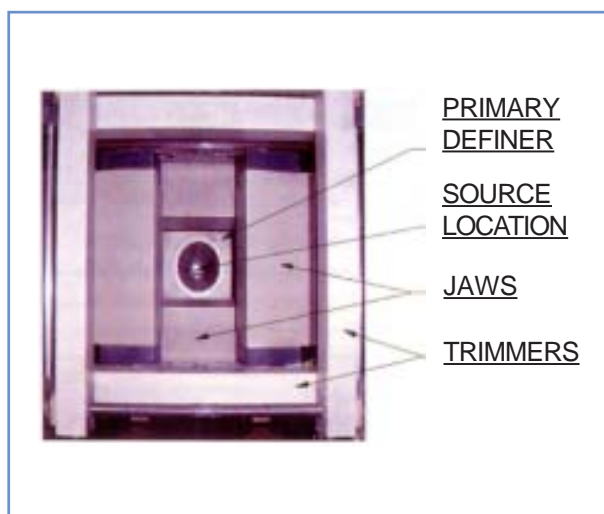


Primary Definer, Trimmers and Jaws of

problem uranium is etched to effect mechanical keying between the coating and the uranium substrate. A comprehensive pre-treatment procedure has been standardized to get adherent nickel coating on uranium to afford a long term protection to uranium exposed to normal atmosphere at room temperature. Nickel has been plated from nickel sulphamate bath.

Property data:

Thick ness	Moist O ₂ 94-96 ⁰ C 312 hours	Boiling H ₂ O 144 hours	Room Temp. Exposure 2000 Hours
25.0 µm	No corrosion	Failed after 48 hours	No Corrosion
37.5 µm	No corrosion	No corrosion	No Corrosion



Collimator at ACTREC

The first state-of-the-art ⁶⁰CoTeletherapy unit Bhabhatron has been installed at **Advanced Centre for Treatment, Research and Education on Cancer (ACTREC), Navi Mumbai.**

The other uranium components that have been electroplated with nickel are bobbins, spacers of remote field eddy current probe assembly being developed at IGCAR, Kalpakkam.

A. L. Pappachan, S. N. Athavale, A. K. Grover and A. K. Suri. <papachan@barc.gov.in>

Initial studies have started on the development of pyrocarbon (PyC) coating using alumina microspheres. PyC was deposited at 1400°C using methane-argon and acetylene-argon mixture. A good adherent coating was obtained. The optical microstructure shows that the deposited carbon has the isotropic structure. Further studies are going on with sintered alumina and stabilized zirconia.

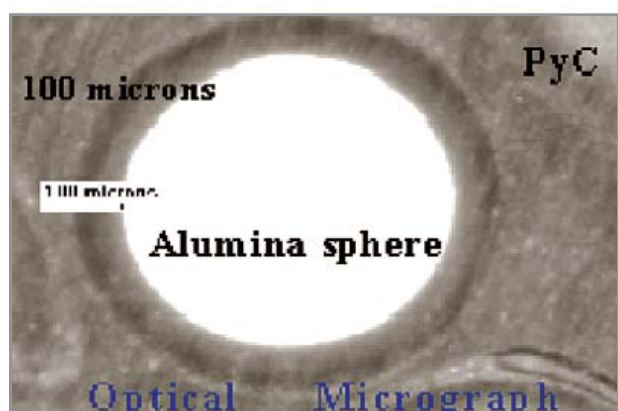
D. Sathiyamoorthy, S. M. Shetty, K. Dasgupta, R. Venugopalan and P.T. Rao. <dsati@barc.gov.in>

5.5 HIGH TEMPERATURE SPOUTED BED COATING FACILITY FOR PARTICULATES

Development of TRISO coating of fuel particles for compact high temperature reactor (CHTR) has been initiated. An 18 kW spouted bed graphite resistance (1700°C, protective atmosphere) furnace has been designed, fabricated and commissioned.



High temperature fluid/spout bed furnace



Microstructure of PyC coated alumina sphere



6. ADVANCED CERAMICS

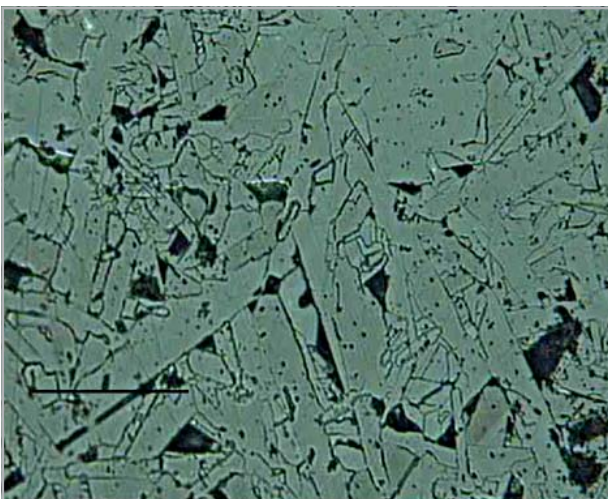
INTRODUCTION

Advanced ceramic materials (oxide and non-oxide) are used in a wide variety of novel applications. They are materials which exhibit superior mechanical properties, oxidation resistance, and thermal, electrical, optical or magnetic properties. Sol-gel, co-precipitation and combustion synthesis are some of the newer preparation methods for formation of the powders. Silicon carbide and zirconia-based ceramics exhibit attractive high temperature mechanical properties making them useful for structural applications. Nano-crystalline oxides such as alumina, ceria, titania etc. are used as catalyst/catalytic support for a wide variety of novel applications. Hydroxyl apatite and calcium sulphate are some of the bio-ceramics used for prosthetic and orthopaedic applications. Sol-set technique has been exploited for the development of high purity Nd-YAG powder for laser applications and $\text{Bi}_2\text{O}_3\text{-BeO}$ for rechargeable neutron source and high surface area catalytic base alumina microspheres of controlled porosity. Special sealing glasses and glass ceramics are yet another new class of materials used in vacuum, high voltage and spectroscopic applications. Lead zirconium titanate (PZT) piezoelectric ceramic finds application in acoustic emission sensors.

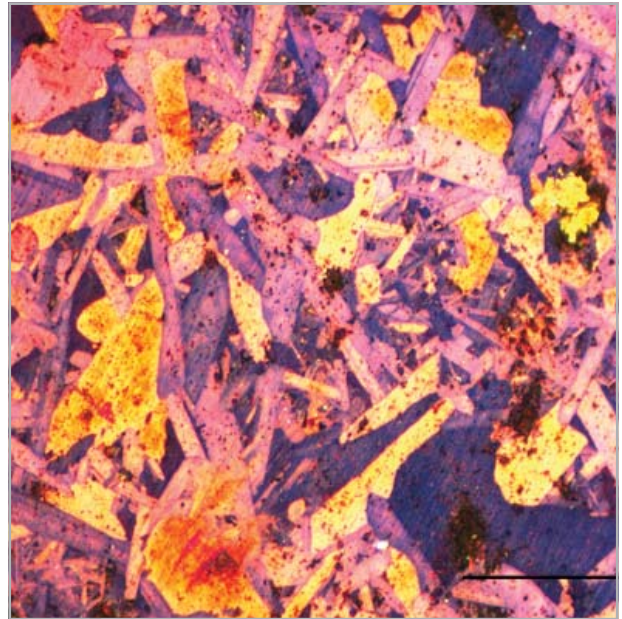
6.1 SILICON CARBIDE CERAMICS FOR STRUCTURAL AND TRIBOLOGICAL APPLICATIONS

Densification behavior of fine β -SiC (0.5 μm) powder along with different sintering additives by hot pressing and pressureless sintering was studied. Hot pressing was carried out in graphite dies in the temperature range of 1700-1900°C where as pressureless sintering was conducted in the temperature range of 1800-1900°C. Reaction-bonded silicon carbide was fabricated by infiltration of molten silicon in a preform made of SiC and C. For microstructural studies the fine polished and etched (Murakami's reagent) surfaces were examined under optical microscope for all the samples.

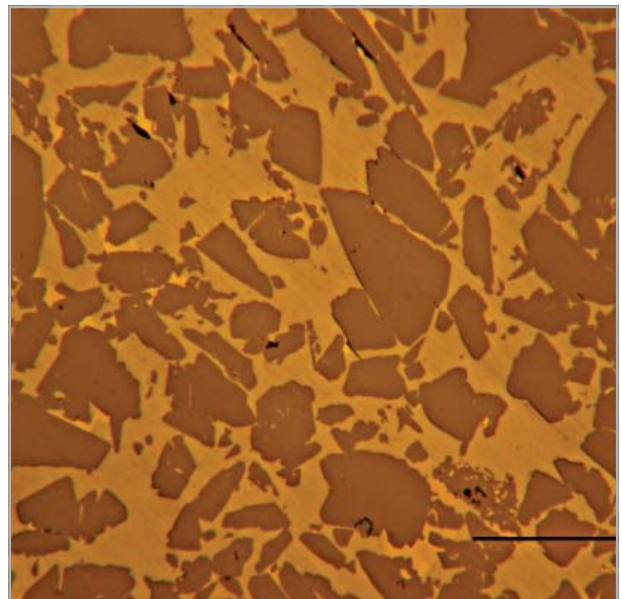
Fully dense (bulk density 3.18 $\text{g}\cdot\text{cm}^{-3}$) SiC samples were obtained after hot pressing (HP) at 1900°C. Typical optical micrograph shows the characteristic plate like morphology of α -SiC grains having an aspect ratio of about five. Conversion to high temperature α -phase is generally very rapid at these temperatures in the presence of additives used here. The grain boundaries appear generally free of secondary phase as seen in bright field conventional TEM images. The prominent features are about the polytypes of SiC, which are a complex mixture of different variants. The presence of other fine scale features like the in-grown dislocation network is also observed. High Resolution Electron Microscopy (HREM) analysis, however, provides evidence for distribution of amorphous phase, at the grain triple-junctions and as very thin (< 2 nm) intergranular film.



Optical micrographs of SiC hot pressed at 1900°C. (Bar is 20 μm)

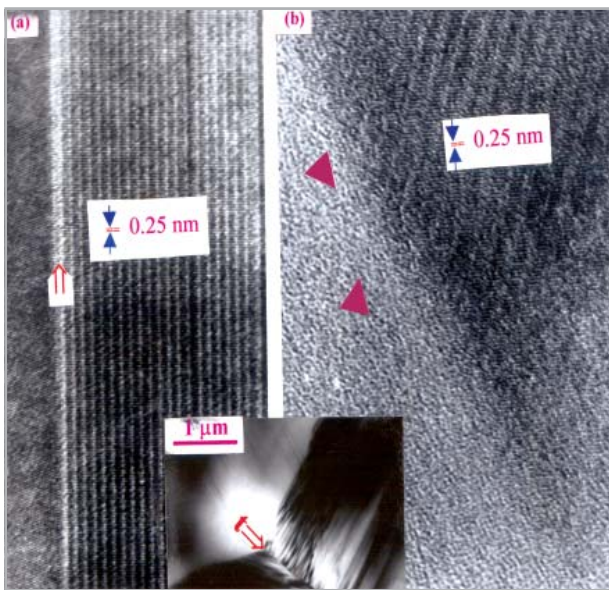


Optical micrographs of SiC pressureless sintered at 1850°C. (Bar is 20 μm)



Optical micrographs of reaction bonded SiC. (Bar is 50 μm)

The typical mechanical properties of the H.P. SiC is given in the table. Results are very significant for the development of strong and creep-resistant ceramic components.



HREM image of HP-SiC. Fig (a) shows presence of clean boundary (marked by “⇒” where as (b) indicates amorphous phase in the triple grain junction (marked by arrow head). Inset shows a typical triple junction (marked by “t”).

Sample Details	Hardness (Kg.mm ⁻²)	Toughness (MPa√m)
1800°C HP	1900	2.0
1900°C HP	2100	2.5

Mechanical properties of HP-SiC

A.Ghosh, A. Gulnar, R.K. Fotedar, G.K. Dey, D.D.Upadhyaya, Ram Prasad and A.K.Suri, Proc. XXV Annual Conf. of Electron Microscopy Society of India on Electron Microscopy and Allied Fields, IIT Mumbai, (2002) pp.130-132.

K. Rastogi, A. Ghosh, D.D.Upadhyaya and Ram Prasad, Trans. Ind. Ceram. Soc. (2006).

6.2 SOL-GEL, SOLUTION COMBUSTION AND NANOMATERIAL PROCESSING

■ Sol-Gel Technology for Non-Nuclear Materials

Sol-gel technology has been exploited for the development of materials for catalytic and laser applications. Studies have been carried out on the preparation of porous titania microspheres

by internal gelation technique by adding cationic surfactants such as Cetrimide (C₁₇H₃₈BrN) or CTAB (C₁₉~2BrN) in the feed broth prior to gelation. Batch experiments on the sorption of tetravalent ions particularly Pu(IV) on this material from various carbonate/bicarbonate solutions showed high distribution ratio values in the range of 600 to 1500 indicating the suitability of this material for the removal of plutonium from carbonate waste streams. Disc electrodes made of haematite doped with Mg, Si, Ti, Zr and Ca were prepared to investigate their use in photo-electrochemical cells. With the aim of technology development for phosphors based on rare-earth doped materials, YAG (Yttrium Aluminium Garnet) doped with Ce³⁺ was synthesized by Gel Entrapment Technique and the samples were characterised by different techniques.

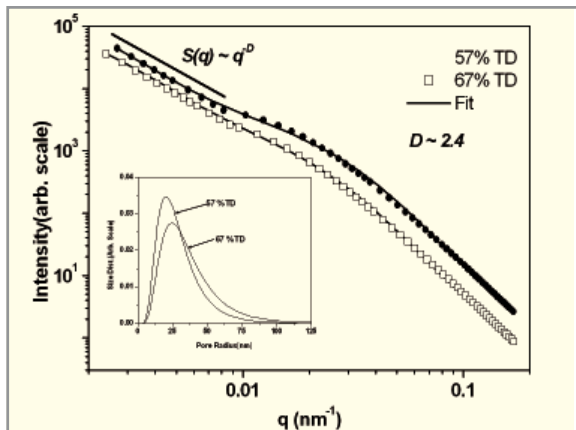
This technique has been used to prepare pellets of Bi₂O₃-BeO to be used for rechargeable neutron source. Homogeneous mixture of Bi₂O₃ and BeO in the form of cylindrical pellet were irradiated to give neutron yield of 5000 n/sec/cc. A novel type of low-cost Po-Be source, which is rechargeable, has been developed. The device is a convenient short-life source having negligible gamma dose and can be recharged in a reactor whenever the neutron yield falls below a specified strength.

With a view to prepare Nd-doped YAG crystals indigenously, kilograms scale batches of high purity Nd-YAG powder were prepared by gel entrapment technique, maintaining dust-free conditions. The quality of the powder was ascertained by XRD, specific surface area analysis, SEM and spectrographic analysis.

High surface area alumina microspheres of controlled porosity are of immense use as a base for a variety of catalysts and for several other applications. Internal gelation technique was exploited to prepare good quality alumina gel spheres.

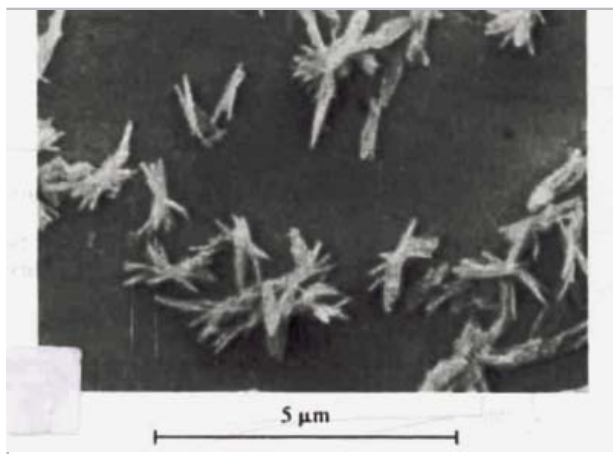
■ Controlled morphology oxide powders by solution sol-gel processing

Solution-based ceramic processing provides many advantages such as formation of compound at lower temperature with controlled morphologies and hence helps in the formation of the component with tailored microstructure at relatively lower sintering temperatures. Processes for synthesis of controlled morphology precursor powders were developed through methods such as homogeneous precipitation, thermal hydrolysis, gel crystallization and co-precipitation techniques for formation



SANS profile and pore-size distribution in sol-gel derived TiO₂ compact indicating the nanoporous structure.

of alumina, titania, ceria, hematite, nickel oxide, yttria stabilized zirconia, yttrium aluminum garnet and lanthanum strontium manganite. The role of reaction conditions on the powder characteristics has been studied. Powders with narrow size distribution could be formed by appropriately adjusting the reaction conditions so that the process of nucleation occurs for a short time followed by selective growth regime. Dispersion condition to form into stable slurries of ceria required for glass polishing applications has been established. Powder characteristics of YAG have been tailored to form transparent bodies which find application as laser components. Conditions have been optimized to form nano-crystalline titania powder. The pore size evolution during sintering of the nano-structured titania and ceria compacts, an aspect of interest for catalytic application, has been studied using Small Angle Neutron Scattering (SANS).



Nitrate route



Sulphate route Morphology of precursors for alumina by homogeneous precipitation method

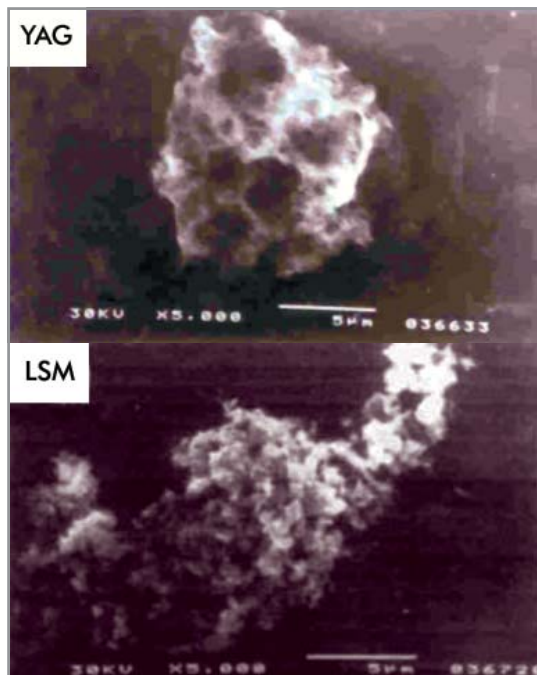
Sub-micron size hematite powder has been prepared that find applications in studies of adsorption of radioactive nuclides.

The nature of anion of the salt on the morphology of the precursor for alumina formed during homogeneous precipitation has been brought out by the elongated fibrillar and spherical shapes for precursors formed from nitrate and sulphate of aluminum.

■ **Soft agglomerated oxide powders by solution combustion method**

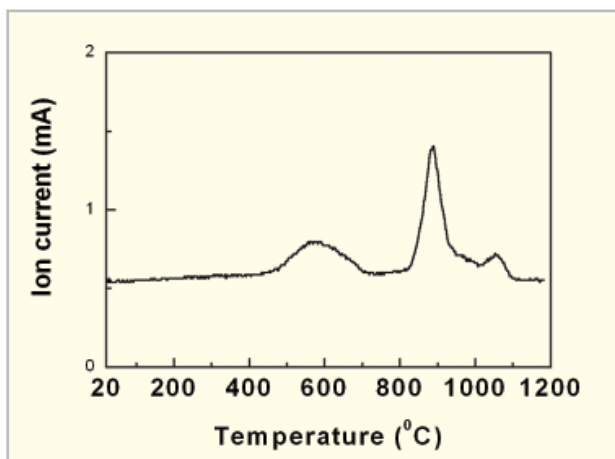
Solution combustion is an easy and pollution free method to form fine powders. The formation of powder precursors for yttrium aluminum garnet, lanthanum strontium manganite (LSM), nickel oxide, ceria-yttria and lanthanum strontium chromite (LSC) has been studied. The conditions have been optimized to make the combustion reaction smooth enough to form large batch sizes of the powder feasible by choosing the appropriate fuel (eg. glycine for YAG and YSZ-NiO; citric acid for LSM, CeO₂ - Y₂O₃, LSC, and NiO). The powder formed were in the form of soft agglomerates of nano-particles that could be easily ground to form powders of desired size required for various applications.

The intermediates involved in the combustion reaction (e.g. for formation of YAG) have been characterized that throws light on the mechanism of compound phase formation. A detailed thermo-gravimetry, differential thermal analysis-evolved gas

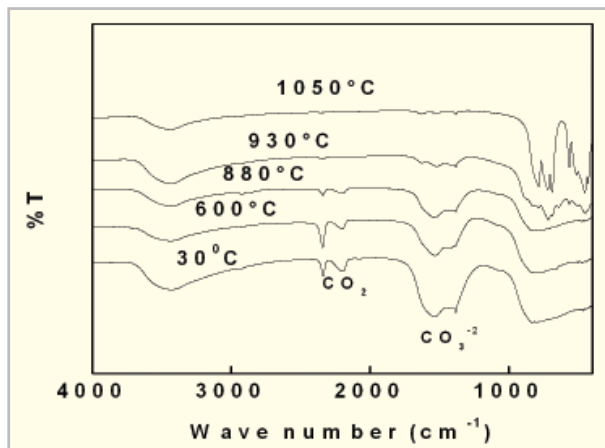


Porous morphologies of YAG and LSM formed by nitrate – glycine & nitrate – citric acid combustion reactions

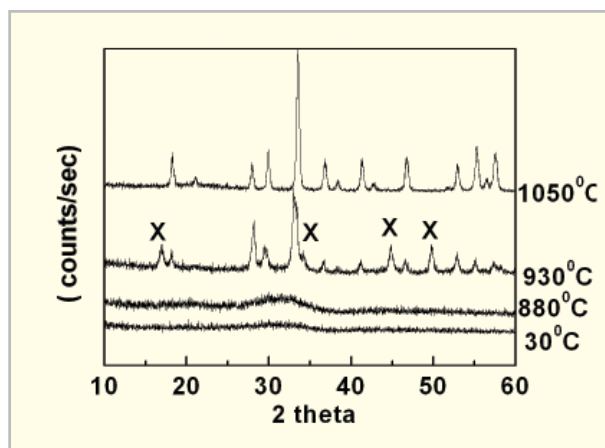
analysis (TG-DTA-EGA), XRD and Fourier Transformation Infra-red spectroscopy (FTIR) characterization study of the precursor of YAG formed by nitrate - glycine combustion has revealed that the formed precursor contains trapped carbon dioxide and carbonate which is evolved at the crystallization stage.



EGA pattern showing evolution of carbon dioxide during crystallization in TG-DTA run



FTIR spectra of precursor showing loss of CO₂ & CO₃²⁻ while heating above 930°C



XRD pattern of precursor showing crystallization above 930°C (X refers to an intermediate YAP like phase)

The powder treatment conditions to tailor the characteristics suitable for the applications have been established.

M. B. Kakade, S. Ramanathan and P.V. Ravindran, *Journal of Alloys and Compounds* 350 (2003), p.123-129.

S. Ramanathan, K.P. Krishna kumar, P.K. De and S. Banerjee, *Bulletin of Materials Science*, 2 (2005) p.109-14.

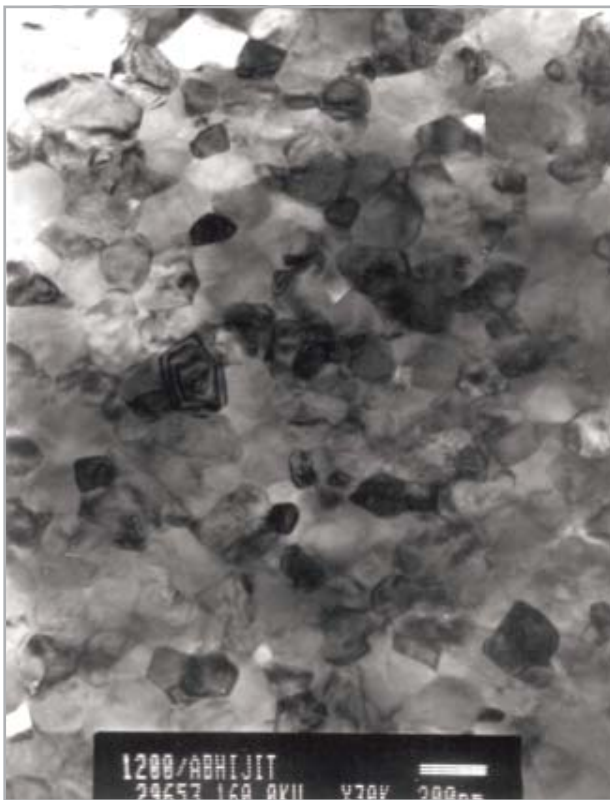
D. Sen, A.K. Patra, S. Mazumder and S. Ramanathan, *Journal of Alloys and Compounds*, 361 (1-2) (2003) pp. 270-75.

A.K. Patra, S. Ramanathan, D. Sen., S. Mazumdar, *Pramana, Journal of Physics*, 63 (2) (2004) pp.327-331.

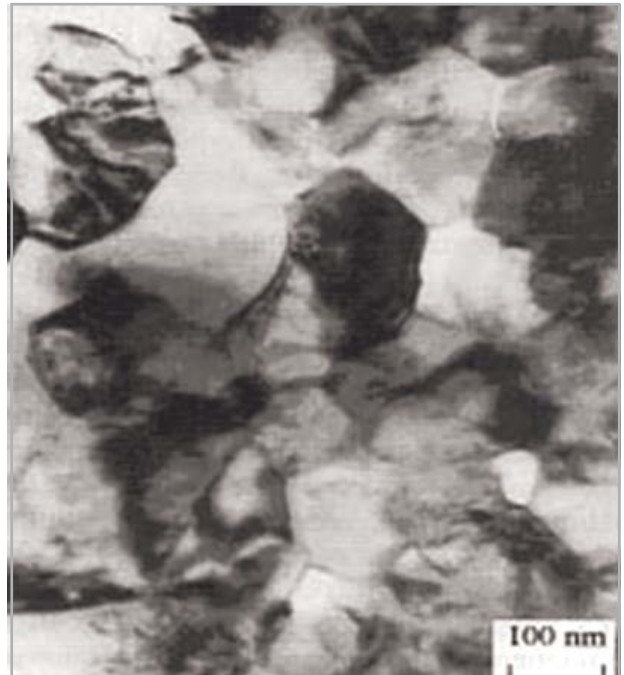
■ **Processing of Zirconia Based Nano-Ceramics : Synthesis, Crystallisation & Densification Studies**

The zirconia-yttria system provides a wide variety of ceramics for high performance applications. Hydroxide coprecipitation process is the most cost effective process for the formation of $ZrO_2 - Y_2O_3$ solid solution phases.

cystallite size occurred. Microstructures of the sintered products have been investigated using TEM techniques. In this process it has been proved that a high bulk density (>96%TD) can be achieved by sintering the powder at a relatively lower temperature (1200°C) while retaining the nano size grain structure (<100 nm) in the ceramics.

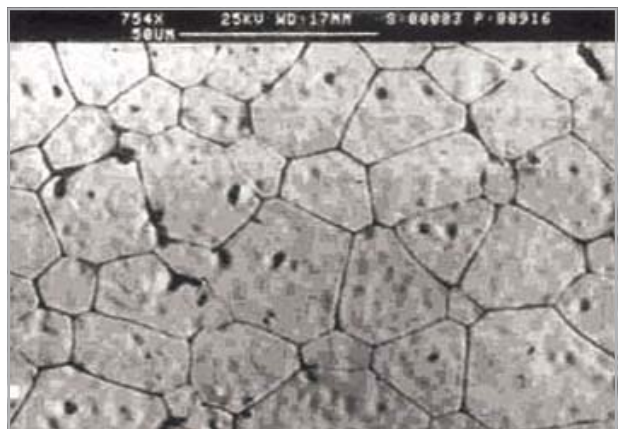


TEM image of microwave sintered 3Y-TZP ceramic



TEM micrograph of 1200°C sintered 3Y-TZP ceramics.

The mechanism and kinetics of primary crystallization in $ZrO_2 - Y_2O_3$ solid solution systems was studied by in-situ hot stage XRD technique under both isothermal and isochronal heating conditions. Compositions selected fall into the three distinct regions of the phase diagram, viz (a) single phase tetragonal polycrystals (3Y-TZP), (b) partially stabilized zirconia containing t (tetragonal) and c (cubic) zirconia (5Y-PSZ) and (c) fully stabilized monophasic c- ZrO_2 (9Y-FSZ). Activation energy for amorphous to crystalline phase transformation was observed to be a linear function of solute concentration. Existence of a critical temperature was noted beyond which a sudden increase in



SEM micrographs of microwave field sintered 9Y-FSZ ceramics

Detailed investigations have been undertaken towards harnessing the phenomenon of microwave heating (MWH) for the sintering of nano-zirconia ceramic materials.

Sintering assembly was constructed by modifying a 2.45 GHz microwave oven of 1.5 kW capacity. A special arrangement was made to form the heating zone. Samples of 9Y-CSZ and 3Y-TZP were sintered at 1625°C and 1350°C respectively, in microwave furnace. Conventional sintering of the above materials was carried out at 1700°C and 1400°C respectively to achieve comparable density. Microstructural features of 9Y-FSZ show an equiaxed grains (~20 nm) with finely dispersed porosity for 3Y-TZP, grains were ~100 nm with a monomodal distribution. The grain boundaries were completely free of amorphous phase which indicates that the high purity of the material is retained. These features have important implications in terms of improved mechanical properties of ceramics as shown in the table.

Sl. No.	Materials & Sintering Treatment	Bulk Density (gm.cm ⁻³)	Hardness H _v (Gpa)	Toughness K _{IC} (MPa√m)
1.	3Y-TZP (con)	5.86	6.6	8.7
2.	3Y-TZP (mw)	5.83	8.3	8.6
3.	3Y-TZP + MnO ₂ (mw)	5.82	4.5	4.2
4.	3Y-TZP + TiO ₂ (mw)	5.77	3.3	4.7

Comparative study of conventional (con) and microwave (mw) sintered 3Y-TYP ceramics

D.D. Upadhyaya, A. Ghosh, K.R. Gurumurthy and Ram Prasad, *Ceramics International*, 27 (2001), p.415-418.

A. Ghosh, D. D. Upadhyaya and Ram Prasad, *J. Amer. Ceram. Soc.*, 85 [10] (2002) pp.2399-2340.

6.3 DEVELOPMENT OF BIOCERAMICS FOR ORTHOPAEDIC APPLICATIONS

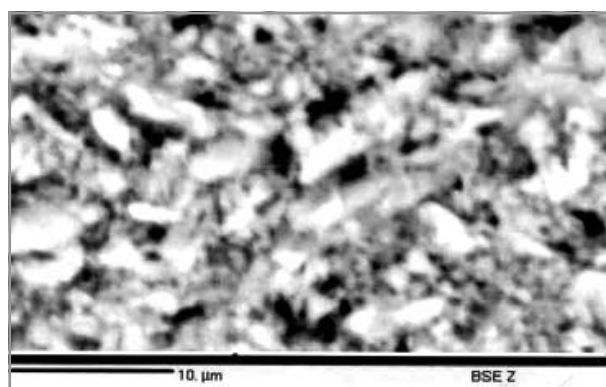
Hydroxylapatite

Hydroxylapatite (HA) based ceramics find application as prosthetic implants. The synthesis protocol for reproducible grade HA powders has been established through a detailed characterisation for particle size distribution, chemical composition, phase purity and thermal stability.

Porous components using pure HA & composites of HA - β tricalcium phosphate (TCP) to attain improved mechanical strength for structural applications have been fabricated & characterized for their microstructure & porosity. Currently, techniques for producing stable HA coating on titanium based implants are explored.

Calcium sulphate

The use of calcium sulphate as a carrier of antibiotic in the human body is a recent phenomenon. Commercially it is marketed as 'Osteoset' and is imported for use in surgical interventions inside the human body. Hence, work was carried out to develop it indigenously. The conditions were optimized for obtaining predominantly α -CaSO₄ 0.5 H₂O (α HH) through controlled dehydration process to match the microstructure of the compacts prepared from 'Osteoset'. Clinical testing of the compacts supplied to Tata Memorial Hospital and LTMG Hospital, Sion have shown encouraging results. The microstructure of the compact and the clinical applications of α HH, are shown in the figures.



SEM micrographs of α HH pellet



Clinical application.

- A** : Cavity in tibia
- B** : Flap cover to close the defect
- C, D** : Pre Op. X-ray AP and lateral view
- E, F** : Post Op. X-ray
- G, I** : Post Op. clinical picture

R. P. Tangri, Ram Prasad, A. K. Suri & P. R. Agrawal, *BARC Newsletter*, 245, Jun (2004), p. 5-9.

R. P. Tangri, Ram Prasad, G.B.Kale, A.K.Suri & P. R. Agrawal, *Trans. Indian Ceramic Society*, 63 (4) (2004) pp. 227-229

6.4 SYNTHESIS OF THERMAL SPRAY-GRADE YTTRIUM OXIDE POWDER

Yttrium oxide is used for coating crucibles and moulds that handle highly reactive molten metals like uranium, titanium, chromium, beryllium and their alloys. Hence, work was carried out to synthesize plasma spray-grade powder and coating formation.

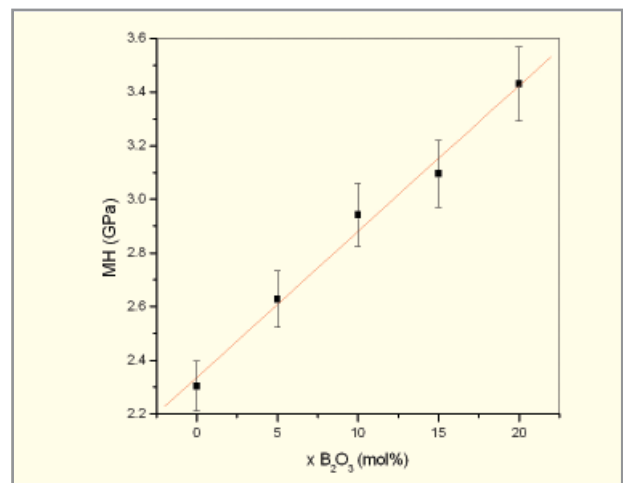
The granulation of yttrium oxide powder from IRE Ltd. was carried out by both isostatic pressing (followed by milling and sieving) and spray drying techniques. The powder granules were sintered up to 1600° C to improve the density. A study of the plasma spray behavior of the powder on various substrates has established that the flowability and deposition efficiency were the best for granules formed by isostatic pressing method with particle size in the range of 53-75 microns as compared to that prepared by spray drying.

R. U. Satpute, K. P. Srikumar, P. V. A. Padmanabhan & S. Ramanathan <satputer@barc.gov.in>

6.5 INDIGENOUS DEVELOPMENT OF SPECIAL SEALING GLASSES AND GLASS CERAMICS: PREPARATION AND CHARACTERIZATION

The developments related to glass to metal seals for vacuum devices and vacuum systems, level sensors and conductivity probes for HWP's were carried out using the glass powders/tubes procured from overseas suppliers. In recent years attention has been focused on the materials development of special glasses and glass-ceramics for different applications in the field of vacuum, high voltage, spectroscopy etc. During the course of the development various related investigations were pursued. Significant progress has been made in developing high quality machinable glass ceramics based on magnesium aluminium silicate, lead silicate glass for compression type seals, borosilicate and phosphate glasses for matched seals and arsenic chalcogenide glass windows for IR applications.

Developmental work has been carried out on phosphate glasses and lithium zinc silicate (LZS) glass-ceramics for fabrication of hermetic seals with various metals/alloys. Glasses and glass ceramics have been prepared using four stage processing involving calcination, glass melting/pouring, annealing, and controlled crystallization. The properties like thermal expansion coefficient, glass transition temperature, micro hardness, chemical durability etc, have been studied as a function of glass composition and process parameters.



Dependence of micro hardness for (40Na₂O-10BaO-xB₂O₃-(50-x) P₂O₅, x = 20 mol%).



Photograph of a glass-to-metal seal fabricated using Al as outer body.

Glass composition:
 $(40\text{Na}_2\text{O}-10\text{BaO}-x\text{B}_2\text{O}_3 - (50-x) \text{P}_2\text{O}_5, x=10 \text{ mol}\%)$

M.Goswami, K.Shah, Arjun Sarkar, Shobha Manikandan, Rakesh Kumar, V.K.Shrikhande, G.P.Kothiyal, and J.V.Yakhmi <mgoswami@barc.gov.in>

6.6 DEVELOPMENT OF PZT CERAMIC AE SENSOR ELEMENT

Some major applications of AE are in continuous monitoring of the pressure vessels, storage tanks, heat exchangers, piping, reactors, aerial lift devices, nuclear power plants etc. for any failure event. Most AE measurements are done with piezoelectric ceramic, which have high detection sensitivity. They are used in the form of circular discs and truncated cones in the devices.

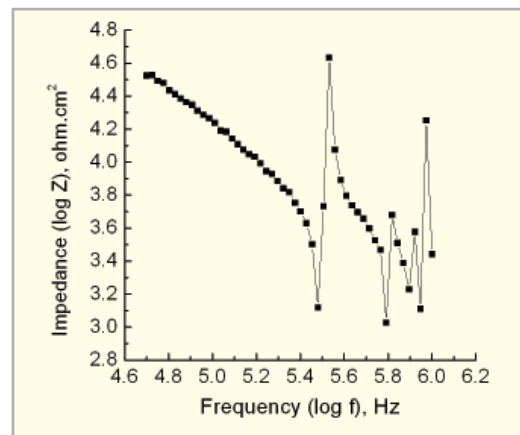
The present study was aimed at developing sensitive piezoelectric PZT ceramic sensor element with high g_{33} (piezoelectric voltage

constant) values. A detailed process development work was carried out and is described in the flow sheet.

Poling treatment to these sintered pellets was carried out at 120°C using DC voltage of the order of 3.2 KV/mm applied for 10 minutes. The dielectric, piezoelectric and impedance spectroscopic data obtained exhibited the suitability of the material for the application.

Dielectric & piezoelectric properties obtained

Parameter	Range
Dielectric constant	500-900
Loss Tangent	.007-.02
Resistivity	$10^{12} - 10^{13} \text{ ohm-cm}$
d_{33}	150-200 C/N
g_{33}	.028-.04 V-m/N

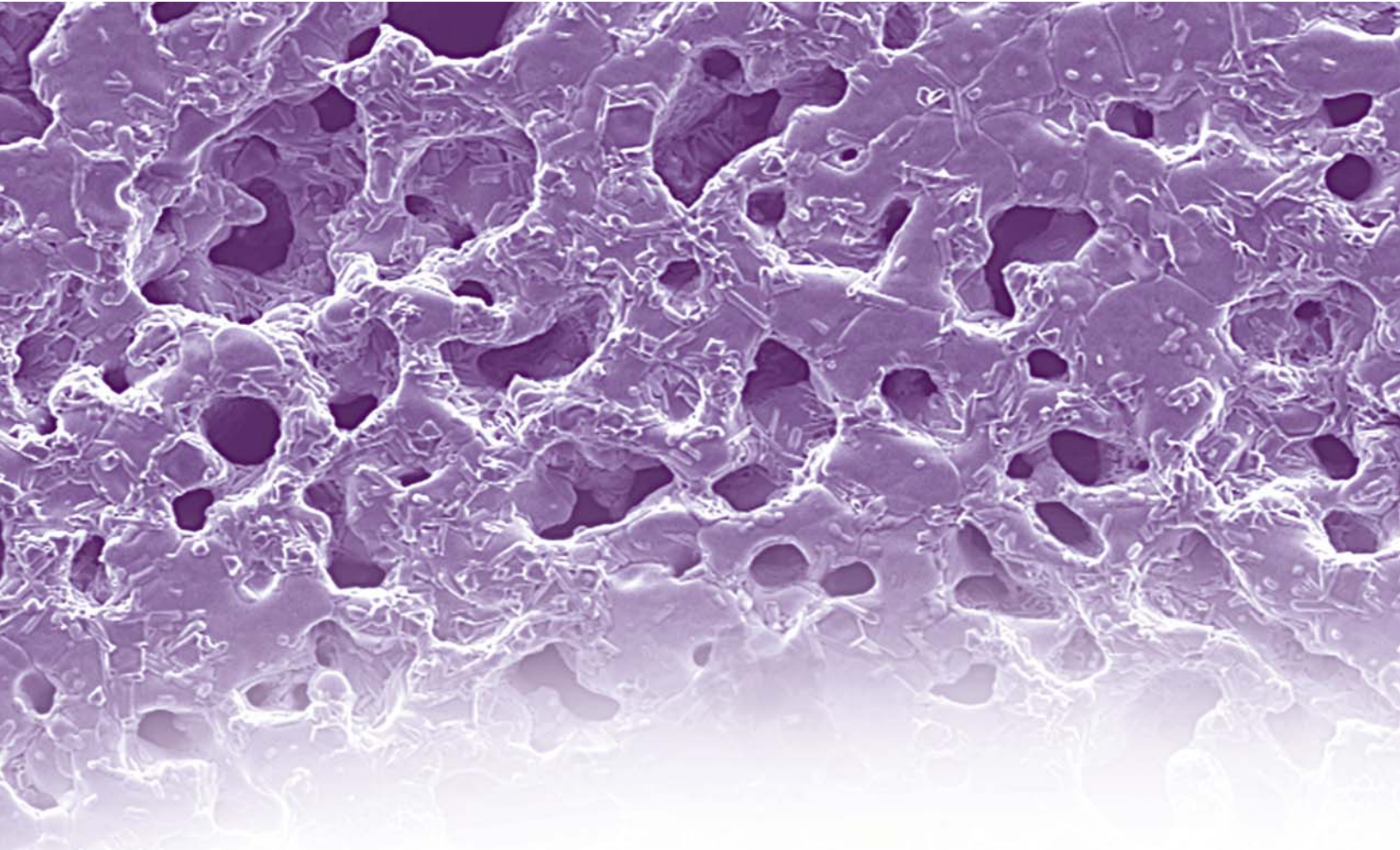


Impedance versus frequency plot of PZT



PZT sintered products

A. K. Sharma, Dharendra Mohan, H.R. Mehta, S. Bhattacharya, 'National workshop on Online diagnosis of Power Transformers by Acoustic Emission techniques, Feb., (2005) Central Power Research Institute, Bangalore.



7. MATERIALS FOR FUEL CELLS

INTRODUCTION

Fuel cells are considered as clean and alternative power sources for the future and there has been considerable research the world over in recent years. Development of Solid Oxide Fuel Cells (SOFC) and Polymer Electrolyte Membrane Fuel Cells (PEMFC) form an important area of our research activities. SOFC is a direct energy conversion device that produces electricity by electrochemical combination of a fuel (e.g. hydrogen) with oxygen. It is an attractive means of electricity generation due to its high conversion efficiency, flexibility regarding fuel, environment friendliness and low levels of noise during operation. Formation of a fuel cell pack based on multiple tube assembly for 1 KW power has been proposed.

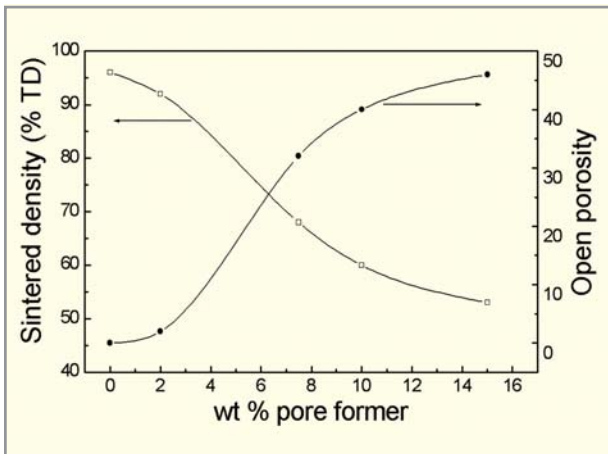
With this objective, work on the synthesis and processing of materials of various components (cathode, anode, electrolyte and interconnect) for SOFC and polymer electrolyte membranes for PEMFC has been carried out. Studies on development of lanthanum strontium manganite (LSM) cathode material comprises of powder synthesis by solution based techniques (combustion-synthesis and co-precipitation) and formation of porous tubes by standard ceramic fabrication techniques (extrusion, isostatic pressing and slip casting) using the powder containing a carbonaceous pore former. Studies on formation of porous composite coating of yttria stabilised zirconia - nickel oxide (YSZ-NiO) as anode and lanthanum calcium chromite (LCC) powder for interconnect have been carried out. Flat sintered tapes of YSZ, LSM and YSZ-NiO for planar test cell studies have been prepared by aqueous tape casting technique. A facility for evaluating the electrical behavior of the planar cell characteristics has been established while setting up of a facility to evaluate tubular cells is being planned.

7.1 CATHODE MATERIAL DEVELOPMENT

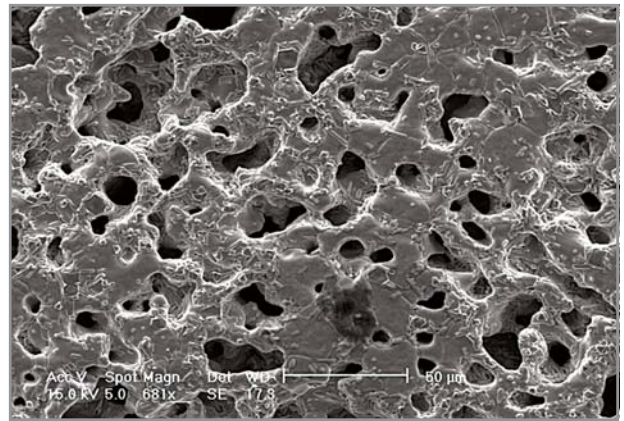
Development of Lanthanum Strontium Manganite Support Tubes

Lanthanum strontium manganite (LSM) is known to be a potential cathode material for SOFC based on stabilized zirconia electrolyte. The co-precipitation method was adopted for preparation of the powder with the composition $\text{La}_{0.85}\text{Sr}_{0.15}\text{MnO}_{2.93}$. A powder of basic carbonate mixture of La^{3+} , Mn^{3+} , and Sr^{2+} was coprecipitated. The precipitate, after washing and drying was calcined at a temperature of more than 1000°C to form phase pure compound which was confirmed by X-ray diffraction technique. Densification

studies on pure as well as on powders with different concentrations of pore former have been performed. SEM micrograph of a 1400°C heat-treated porous body has indicated uniform distribution of porosity in the sintered product.

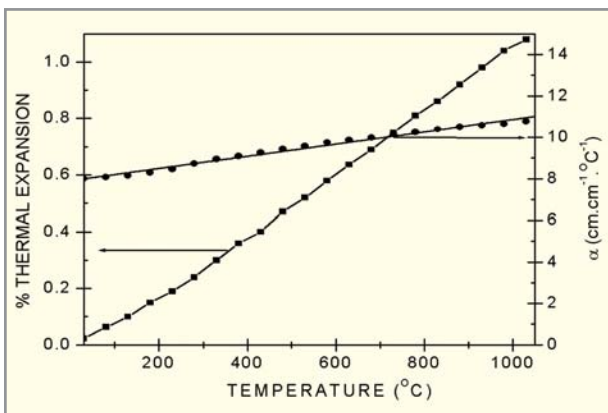


Effect of pore former on densification behaviour of LSM

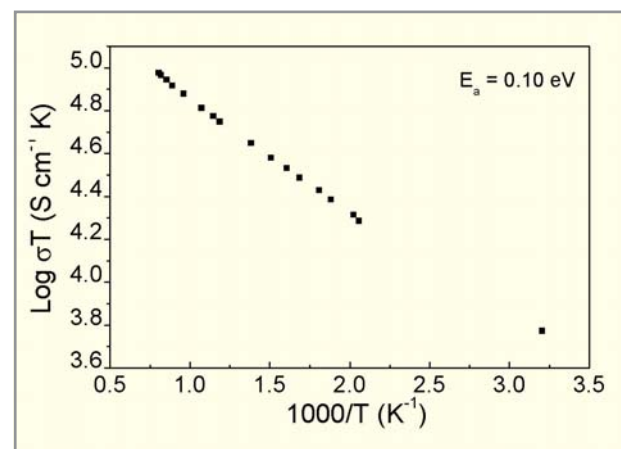


Scanning electron micrograph of thermally etched surface of sintered LSM

Thermal expansion behaviour of 40% porous material has been studied and values are in good agreement with that of yttria stabilised zirconia sintered body. Electrical conductivity of the porous body measured at 1000°C was around 80 S/cm , which is very close to the value required for a cathode material in SOFC device. The activation energy for conduction was around 0.1 eV .



Thermal expansion behaviour of porous LSM



Electrical conductivity variation with temperature of LSM with 40% porosity



Sintered porous LSM tube

Required shape with proper dimension has been fabricated by extrusion method.

<aghosh@barc.gov.in>

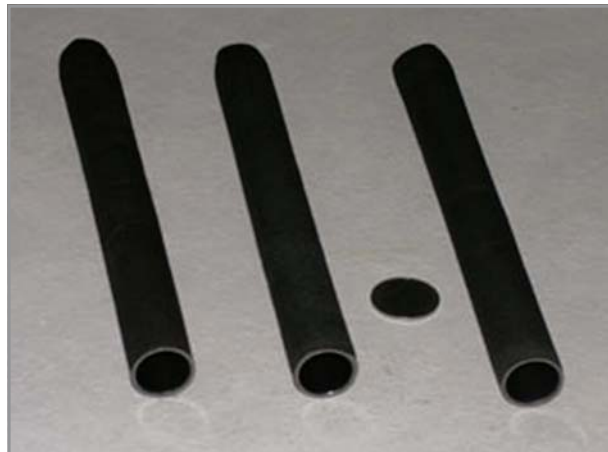
■ Development of $\text{La}_{0.75}\text{Sr}_{0.20}\text{MnO}_{3-8}$ tube by cold isostatic pressing

A safe method of combustion synthesis of Strontium-doped lanthanum manganite (LSM) was developed using nitrate as oxidant and acetate as fuel. This method was safe due to gradual combustion without forming any vigorous/explosive/fire hazard condition as has been usually found in most of the combustion synthesis reactions. Using this method about 3 kg of nano-size (5-15 nm) LSM powder was produced.



Set up for combustion synthesis

Strontium doped lanthanum manganite (LSM) powder having the composition $\text{La}_{0.75}\text{Sr}_{0.20}\text{MnO}_{3-8}$ was synthesized through



Green LSM cathode tubes, made by CIP



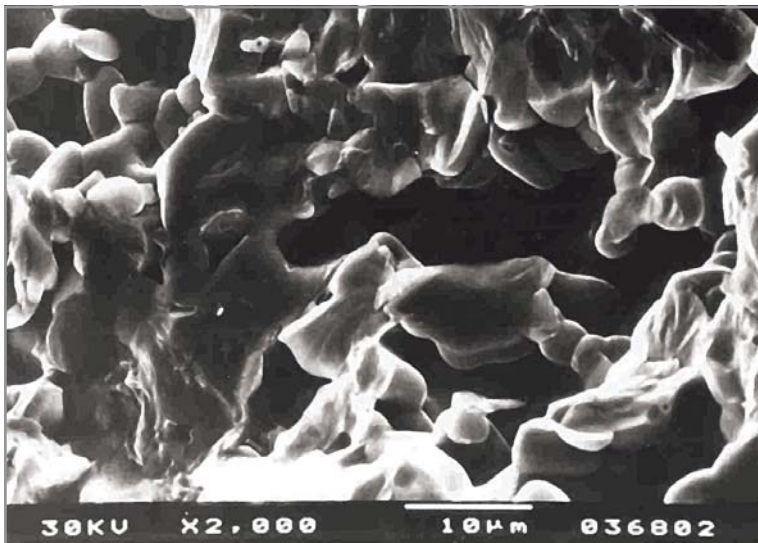
Porous sintered LSM cathode tube

wet chemical processing technique. The powder produced was characterized by X-ray diffraction, particle size distribution, and specific surface area analysis. The material exhibited high electrical conductivity ($\sim 190 \text{ S cm}^{-1}$ at 1000°C). The value of thermal expansion coefficient of this cathode material ($11.7 \times 10^{-6} \text{ K}^{-1}$) was found to be close with that of YSZ ($10.8 \times 10^{-6} \text{ K}^{-1}$). The desired degree of interconnected porosity (40 v/o) in the material was developed by introducing suitable pore-former during processing. The process for preparation of LSM powder has been scaled upto 500 g per batch. Using this powder with pore former, porous tubes have been fabricated through Cold Isostatic Pressing (CIP)

followed by air sintering.

■ **Dispersion characterization and slip casting studies on $\text{La}_{0.85}\text{Sr}_{0.15}\text{MnO}_3$**

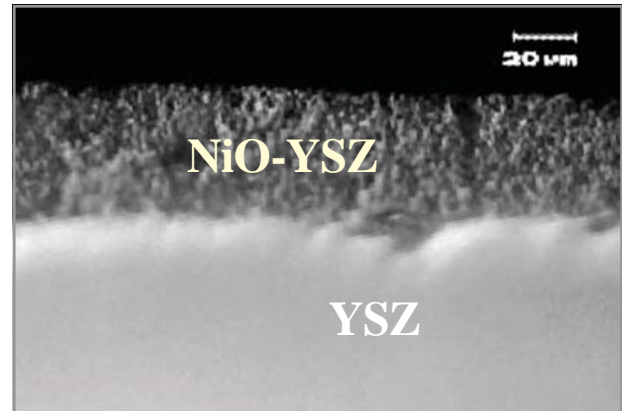
Dispersion conditions for slip or slurry formulation of a powder mixture of lanthanum strontium manganite ($\text{La}_{0.85}\text{Sr}_{0.15}\text{MnO}_3$ - LSM) and carbon (pore former) in water was studied through detailed zeta-potential and rheological measurements. The zeta potential window for their co-dispersion and pseudo-plasticity of the slurry were optimized to form long tubes with uniform wall thickness (wall thickness 2 to 3 mm and length of 200 mm). The tubular specimens formed after controlled carbon burn out and sintering at 1400°C for 1 hour possessed about 35 percent open porosity. The porosity remained the same upon further sintering at 1400°C for 8 hours, establishing stability of the porous structure formed towards further sintering. The evaluation of the density/porosity data and morphological features established the homogeneity in the microstructure of the bodies.



Porous microstructure of slip cast LSM

7.2 ANODE MATERIAL

Porous coating of anode material nickel- yttria stabilized zirconia (Ni-YSZ cermet) on the electrolyte surface calls for the development of two major processes preparation of NiO-YSZ mixed powder and technique for dip-coating of NiO-YSZ suspension on YSZ electrolyte substrate. NiO powder



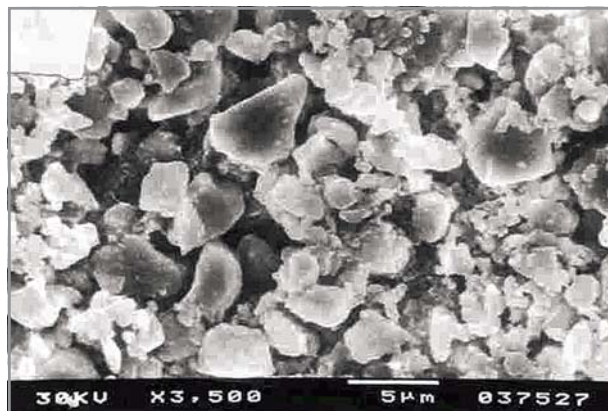
Microstructure of YSZ- (YSZ-NiO) interface

prepared by citrate – nitrate combustion route and YSZ powder were found to be suitable feed materials for dip coating process. With the optimized coating process uniform porous coatings on YSZ tube was obtained.

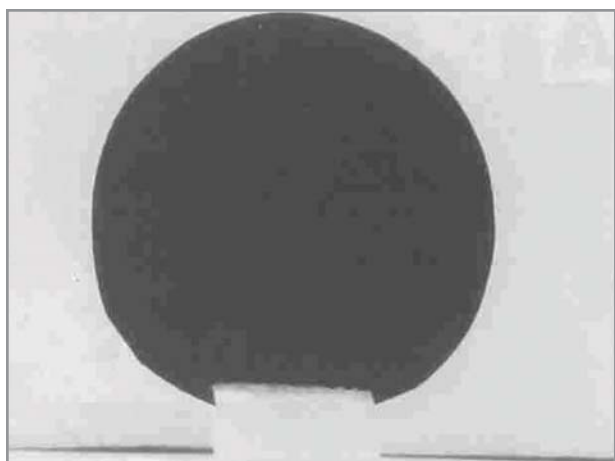
7.3 SLURRY CHARACTERIZATION & TAPE CASTING OF ELECTROLYTE / ELECTRODE SUPPORTS FOR SOFC

An extensive study for the formation of flat thin tapes (thickness of about 100 to 500 μm) of systems such as yttria-stabilized zirconia, lanthanum strontium manganite and nickel oxide – yttria stabilized zirconia composite for solid oxide fuel test cell applications has been carried out through aqueous tape casting. The pH of maximum zeta-potential for these oxides is found to be characteristic of the system. All were sufficiently charged to be dispersible in alkaline pH. The zeta-potential window for co-dispersion of YSZ and NiO and LSM and carbon pore former have been established.

The rheological behavior of the tape cast slurries were optimized to have the desired amount of pseudo-plasticity to enable formation of flexible tapes of desirable thickness and a uniform green microstructure that can be sintered to flat sheets of required density (>99% & ~80% T.D. for YSZ & LSM, YSZ-NiO). The typical sintered flat tapes (YSZ and LSM) and the porous microstructures (LSM, YSZ-NiO) are shown in the figures.



Porous microstructures of YSZ-NiO

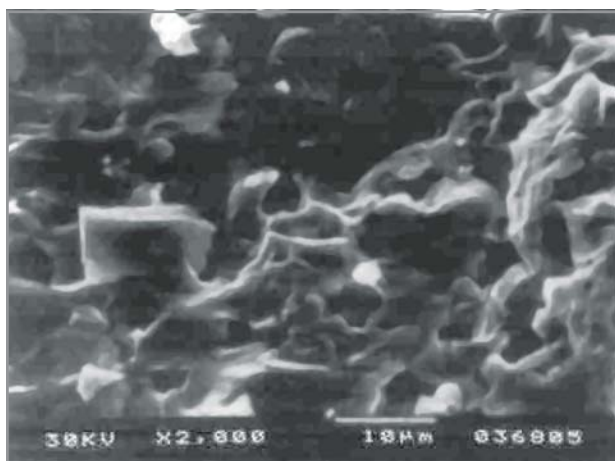


Flat sintered tapes of YSZ (dense) and LSM (porous)

7.4 INTERCONNECT MATERIAL

Calcium-doped lanthanum chromite powder was prepared by combustion synthesis method starting from nitrates of lanthanum, chromium and calcium as raw materials. The powder was characterized for particle size analysis, specific surface area and XRD. Sintered samples were evaluated for density and electrical conductivity. The material sintered at 1300° C showed density better than 90% TD and electrical conductivity was 28 S/cm at 1000° C.

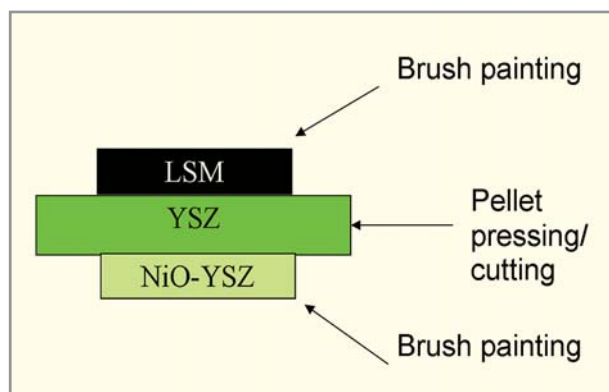
R. D. Purohit, Amit Sinha, S. J. Ghanwat and S. Saha
<asinha@barc.gov.in>



Porous microstructures of LSM

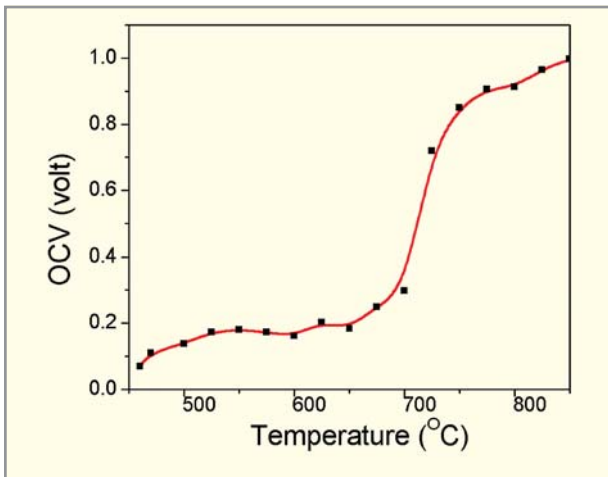
7.5 PLANAR SOLID OXIDE FUEL CELL

A facility for electrical characterization of single button cells of SOFC was set up. The system maintains oxygen and



Schematic of test cell configuration.

hydrogen atmospheres in two chambers separated by a single cell (i.e. self supporting YSZ electrolyte of about 20 mm diameter and 700 mm thickness with the cathode (LSM) and anode (Ni-YSZ Cermet) Coating on its either side. The chambers were formed using the above cell, alumina tubes and ceramic as sealant. Electrical contacts were made using Pt lead wires and the open circuit voltage measured was around 1.08 V at 1000 °C.



Variation of open circuit voltage (OCV) with temperature

A. Ghosh, A. K. Gulnar, D.D. Upadhyaya, Ram Prasad and A.K. Suri Presented in the Annual Technical Session of IIM, Vadodara, Nov. (2002).

A. K. Sahu, A. Ghosh, A. K. Suri, P. Sengupta and K. Bhanumurthy, *Mater. Letts.* 58 (2004) p. 3332-36

A. Ghosh, A. K. Sahu, A. K. Gulnar and A. K. Suri, *Scripta Materialia* 52 (2005) p. 1305-09.

M.B. Kakade, S. Ramanathan and P.K. De, *British Ceramic Transaction*, 102 (5) (2003) p. 211-215.

S. Ramanathan, K.P. Krishnakumar, P.K. De and S. Banerjee, *Journal of Materials Science*, 39 (10) (2004) p. 3339-3344.

S. Ramanathan, Peeyush Kumar Singh, M.B. Kakade and P.K. De, *Journal of Materials Science*, 39 (9) (2004) p. 3207-10.

S. R. Nair, Deep Prakash, P. K. Sinha & B.P. Sharma, *Int. Symp. On advanced Materials and processing*, ISAMAP 6-8 Dec 2004, IIT Kharagpur.

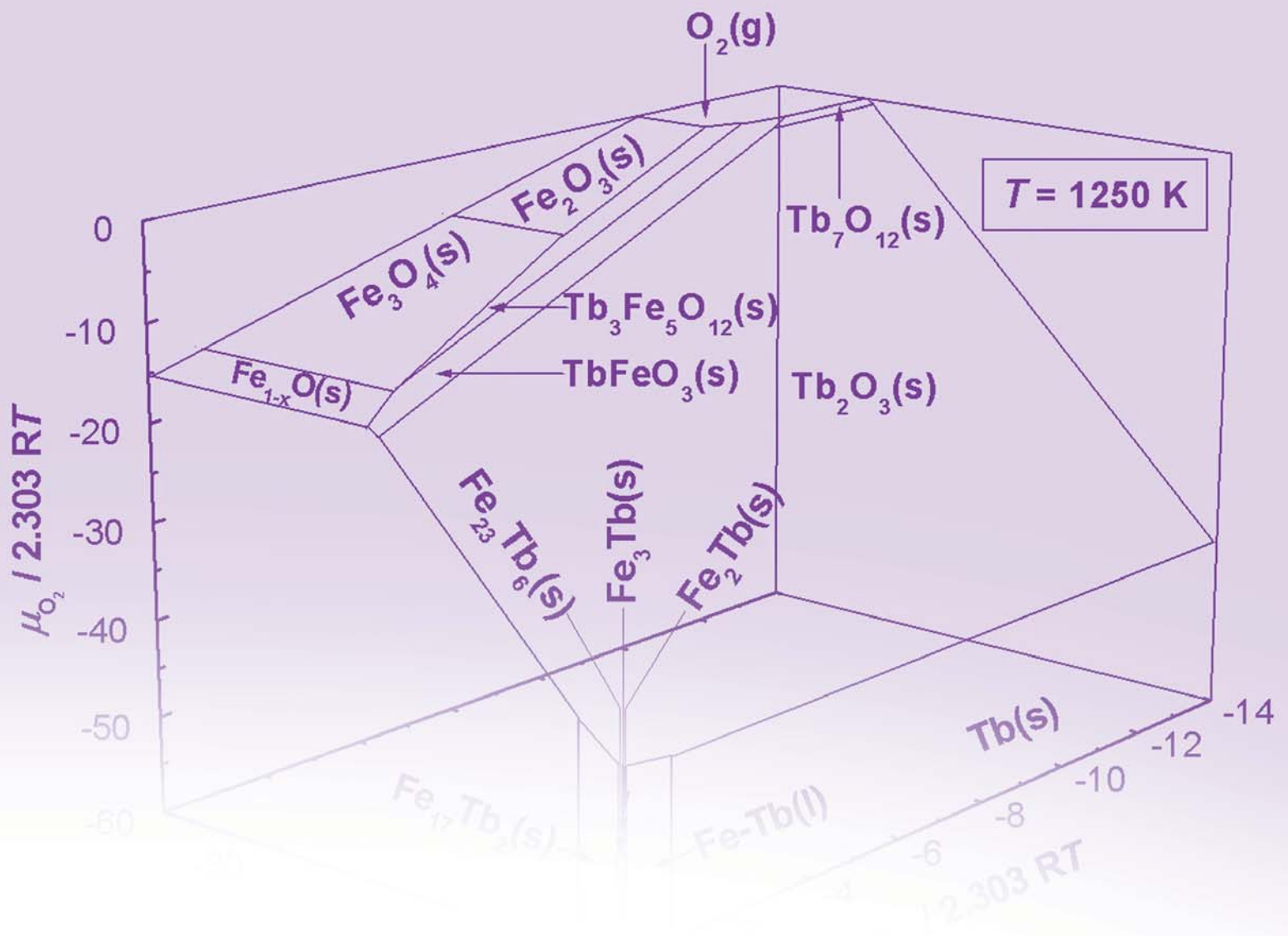
<ashok@barc.gov.in>

7.6. POLYMER ELECTROLYTE FOR PEMFC

PEMFCs are used to convert chemical energy (i.e. from the reaction of H₂ and O₂) directly into electrical energy. Cation exchange membrane is used as an electrolyte in these cells and has exchangeable H⁺ ions. These membranes are available commercially, e.g., Nafion-117. However, high cost of these membranes has prohibited their wide commercial use in Polymer Electrolyte Membrane Fuel Cells (PEMFC).

Currently alternate membranes are being developed to be used as solid polymer electrolyte fuel cells. The membranes are made by sulfonation of different polymers followed by membrane casting, resulting in the ion exchange membrane with capacity 0.1 - 1 meq/g (Nafion-117 IEC ~0.9 meq/g). Efforts on improving the mechanical stability of these membranes by different methods are underway.

H.S. Sodaye, S. Prabhakar and P.K. Tewari
<hemant@barc.gov.in>



8. EQUILIBRIUM PHASE DIAGRAMS

INTRODUCTION

Equilibrium phase diagrams are important to assess mutual compatibility of materials. These diagrams are also important in assessing the stability of a material.

The phase diagrams can be experimentally determined or computed using appropriate solution models and thermodynamic properties of components involved. Experimental determination and computer calculations can be used to complement the information provided by each other and can be used to synergistically improve the reliability of the final phase diagram.

Phase diagrams of some complex oxides have been generated using experimentally determined data on heat capacity and Gibb's energy.

Phase diagrams of ternary and quaternary U-O systems have been generated using high temperature X-ray diffraction and thermal analysis methods.

8.1 THERMODYNAMIC PROPERTIES AND PHASE DIAGRAMS OF RARE EARTH REFRACTORY METAL SYSTEMS

Phase diagrams of refractory metals like tantalum and tungsten with the rare earths are vital for any meaningful assessment of the interactions in the preparation of rare earth metals and alloys as well as their usage. By analogy, these diagrams provide important information of the nature of certain actinide systems as well. Determination of these diagrams entirely by experiments is rather challenging because of the high temperatures involved and the physical properties of the component metals. The computational approach is presently pursued. The thermodynamic properties and binary phase diagrams of all the 16 naturally occurring rare earth (RE) elements with tantalum and with tungsten have been calculated using a regular solution approximation. The regular solution parameters were calculated from the experimental data on the solubility of tantalum and tungsten in liquid RE metals and the thermodynamic properties of pure RE metals, tantalum and tungsten. The thermodynamic properties of all the liquid RE-Ta and RE-W solutions were obtained and expressed in the form of the regular solution parameter α as,

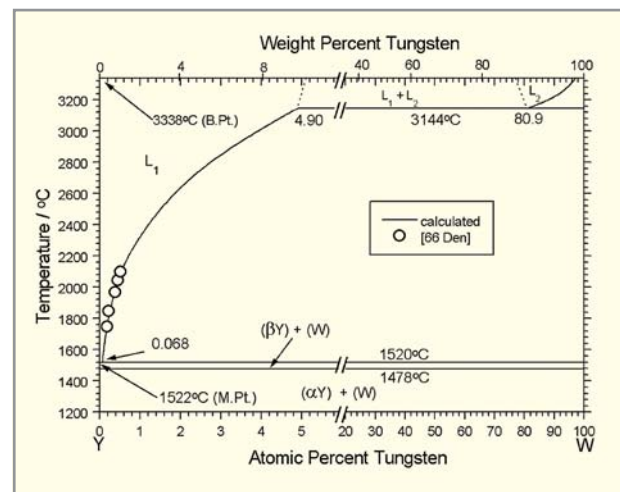
$$\alpha = G^{xs}(M,L) / (1 - X_M)^2$$

Using the α values, the liquidus over the entire composition range was obtained by solving the following equation at various temperatures.

$$\alpha (1 - X_M)^2 + \Delta_{fus} G_M + RT \ln X_M = 0$$

In the absence of any miscibility gap in the liquid solution, this equation has only one real solution, which corresponds to the liquidus composition at a given temperature.

All the rare earth-tantalum systems, and all the rare earth – tungsten systems except Sc-W exhibit liquid immiscibility. For all these systems, the values for the monotectic temperature and composition were also obtained by computation.



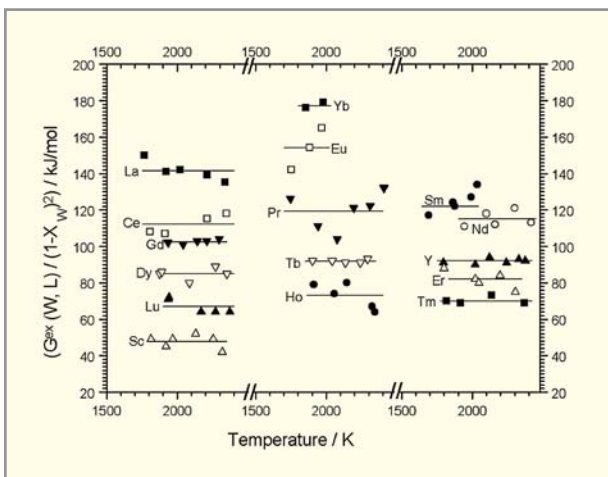
The Y- W Phase Diagram

All the RE- refractory metal systems exhibit eutectic reactions. The eutectic temperature and composition were also calculated for each of the systems. The eutectic lies very close to the pure rare earth metal’s melting point.

The phase diagrams thus generated have been accepted by ASM International as the most reliable ones and have been included in their literature.

N. Krishnamurthy, A. Awasthi and S.P. Garg

<nkrishna@barc.gov.in>

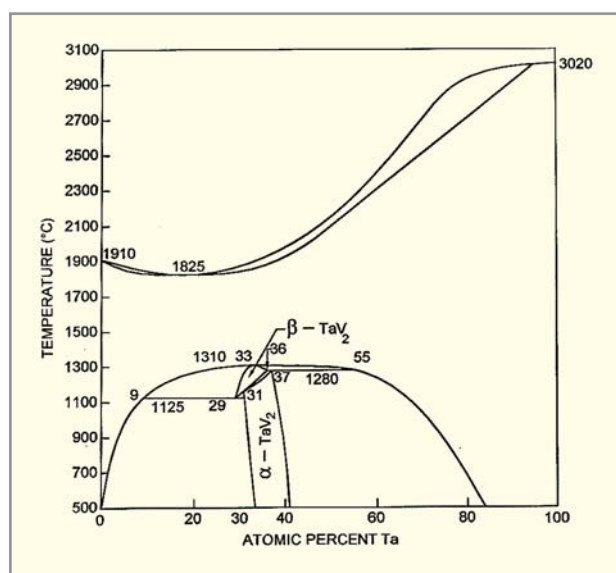


Regular solution parameter as a function of temperature for RE-W systems

8.2 CRITICAL EVALUATION OF BINARY PHASE DIAGRAMS

BARC is engaged in the international program conducted by Materials Science International Team (MSIT) for critical evaluation of binary phase diagrams. The programme essentially involves the critical evaluation of the published thermodynamic, crystal structure data and phase equilibria and suitable modifications/ amendments to the existing phase diagrams.

Critical evaluation of Ta-V system has been carried out and modifications in the phase fields have been made and included in the phase diagram. As the experimental data agrees well with recently computed data, it is accepted. The existing azeotropic melting point and composition have been modified. The azeotropic melting minimum at 1825 °C and 15 at% Ta is included in the phase diagram. Considering the variation in congruent transformation temperature of TaV_2 to solid solution, the congruent transformation at 33 at% Ta was placed at 1310 ± 10 °C the mid point between two transformation temperatures with uncertainty encompassing both the values. The crystal structure of TaV_2 at high temperature is still unclear and controversy on the possible polymorphic transformation of TaV_2 still exists. The eutectoid transformation temperature, peritectoid transformation temperature and two phase regions reported experimentally



The Ta-V phase diagram

agree well with those computed and these results have been accepted. The low temperature TaV_2 is designated as α - TaV_2 and has C15 structure whereas high temperature TaV_2 is designated as β - TaV_2 and has C14 structure.

The phase diagrams of 14 systems viz Ag-Ta, Au-Ta, Cl-Ta, Cs-Ta, Ga-Ta, Ge-Ta, H-Ta, Hf-Ta, Rh-Ta, Ta-Th, Ta-U, Ta-V, Ta-W and Ta-Zn have been evaluated after reviewing the existing literature and assessed phase diagrams have been drawn. The data on crystal structure, phase equilibria and thermodynamics has been compiled.

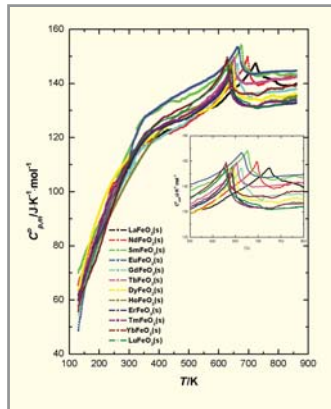
G.B. Kale, K. Bhanumurthy and S.P. Garg; Inter-national programme of Materials Science International Team (MSIT) (2005)

8.3 THERMODYNAMIC STUDIES ON COMPLEX OXIDES

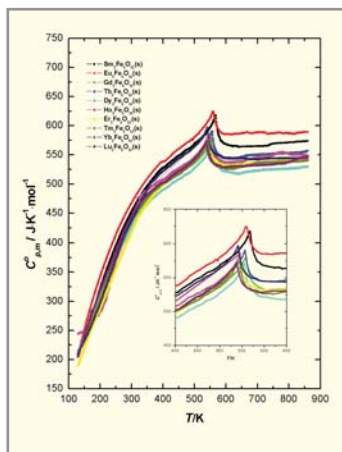
Complex oxides like perovskites, garnets, spinels, double oxides etc. have extensive applications in materials science and technology owing to their interesting physico-chemical properties. The high temperature stability of these compounds is generally predicted from their thermodynamic properties. This work presents thermodynamic studies on complex oxides of the type: $RFeO_3$ (orthoferrites: perovskite-type) and $R_3Fe_5O_{12}$ (Garnet-type) of rare earths ($R = La$ to Lu) and ternary compounds in the system Ba-Fe-O. Thermodynamic parameters of these complex oxides are determined by experimental techniques like differential scanning calorimetry and solid-state electrochemical methods using oxide and fluoride ion conducting electrolytes. Different types of stability diagrams like oxygen potential diagrams, two- and three-dimensional chemical potential diagrams and ternary isothermal sections are computed.

Heat capacity measurements

These oxides are prepared by citrate-nitrate gel combustion method and heat capacities are measured from 130 to 860 K by using a differential scanning calorimeter. The heat capacities of $RFeO_3(s)$ and $R_3Fe_5O_{12}(s)$ are shown in following figures.



Plot of $C_{p,m}^o$ against T for $RFeO_3(s)$ ($R = La$ to Lu). Insert: magnified portion of the plot near the transition region indicating distinct values of Néel temperatures for different $RFeO_3(s)$.



Plot of $C_{p,m}^o$ against T for $R_3Fe_5O_{12}(s)$ ($R = Sm$ to Lu). Insert: magnified portion of the plot near the transition region indicating nearly same values of Curie temperatures for different $R_3Fe_5O_{12}(s)$.

Lattice, electronic and magnetic contributions to the total heat capacity of $RFeO_3(s)$ and $R_3Fe_5O_{12}(s)$ are calculated in the present study from 0 to 860 K. The Debye temperatures of these compounds are calculated as a function of temperature. The excess heat capacity function is used to calculate the magnetic entropy due to order-disorder transition.

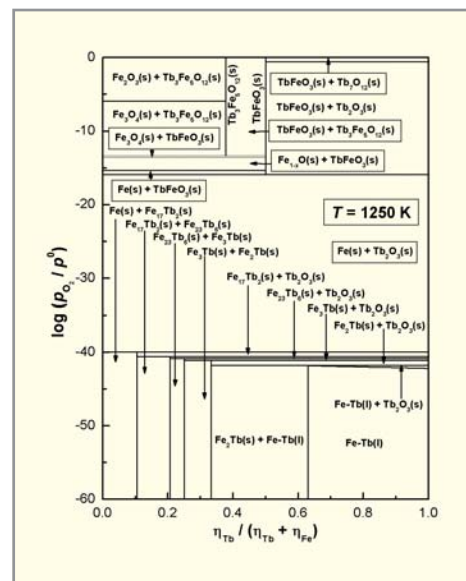
■ Solid-state electrochemical technique

The solid oxide electrolytes used in the present study are CSZ, YDT and YSZ whereas the fluoride electrolyte used is single crystal CaF_2 . The standard molar Gibbs energy of formation,

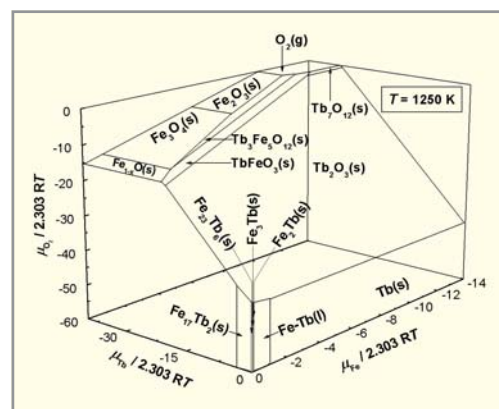
$\Delta_f G_m^o(T)$, for $RFeO_3(s)$, $R_3Fe_5O_{12}(s)$ and ternary oxides in the system Ba-Fe-O are calculated from the emf data.

■ Computation of chemical potential diagrams

The oxygen potential diagram, two- and three-dimensional chemical potential diagrams are computed for any selected system using the available thermodynamic data. The oxygen potential diagram and the 3D-chemical potential diagram for the system Tb-Fe-O are shown in the following figures.



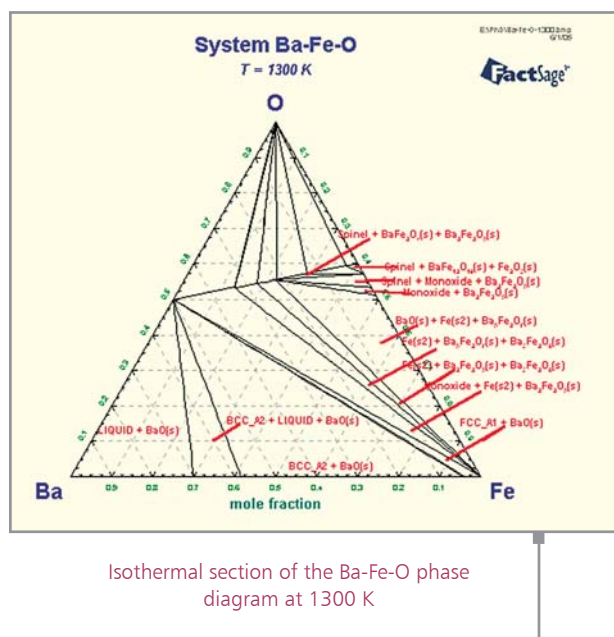
Isothermal oxygen potential diagram for the Tb-Fe-O system at 1250 K



Three-dimensional chemical potential diagram for the system Tb-Fe-O at 1250 K

■ Computation of phase diagram for Ba-Fe-O System

The phase diagram for the system Ba-Fe-O is computed by the CALPAHD approach. A consistent set of thermodynamic data is generated for this system using the optimization program available in the CHEMSAGE/ FACTSAGE software package. Using the optimized thermodynamic data, the isothermal section of Ba-Fe-O system is calculated and is shown in the figure at 1300 K.



S.K. Rakshit, S.C. Parida, Ziley Singh, R. Prasad and V. Venugopal, *J. Solid State Chem.*, 177 (2004), p. 1146-1156.

S.K. Rakshit, S.C. Parida, S. Dash, Ziley Singh, R. Prasad and V. Venugopal, *J. Chem. Thermodyn.*, 35 (2003), p. 1793-1807.

S.C. Parida, S.K. Rakshit, S. Dash, Ziley Singh, R. Prasad and V. Venugopal, *J. Solid State Chem.*, 172 (2003), p. 370-380.

8.4 EQUILIBRIUM STUDIES IN URANATE SYSTEMS

■ Thermal expansion studies

Na-U-O and Sr-U-O system: UO_2 is known to form an extensive range of substitution type solid solutions with oxides of alkaline earths, rare earths and actinides. In Na-U-O system, $\text{Na}_y\text{U}_{1-y}\text{O}_{2\pm x}$ with $0 \leq y \leq 0.2$ form fluorite type solid solution. In Sr-U-O system, strontium dissolves up

to 30 atom % in UO_2 lattice forming $\text{Sr}_y\text{U}_{1-y}\text{O}_{2\pm x}$. Thermochemical studies have shown that $\text{M}_y\text{U}_{1-y}\text{O}_{2\pm x}$ solid solutions have higher kinetic stability than uranium oxide and fluorite structure is retained up to 773 K in air. The lattice parameters as a function of temperature of $\text{M}_y\text{U}_{1-y}\text{O}_{2\pm x}$ solid solutions with $y = 0.08, 0.10$ and 0.14 for $\text{Na}_y\text{U}_{1-y}\text{O}_{2\pm x}$ and $y = 0.15, 0.20$ and 0.25 for $\text{Sr}_y\text{U}_{1-y}\text{O}_{2\pm x}$ were determined from 298 K to 1273 K using High Temperature X-ray diffraction (HT-XRD). Thermal expansion coefficients for the solid solutions were derived from HT-XRD data and compared with the thermal expansion of UO_2 . It is found that the average thermal expansion coefficient increases with increase in Na or Sr concentration in UO_2 lattice.

Strontium aluminates: Strontium aluminates doped with different rare earth elements have technological importance because of their after-glow long-lasting phosphor properties. SrAl_2O_4 was synthesized by citrate-nitrate gel combustion route where nanocrystalline material was formed on decomposition at 1073 K. HT-XRD studies revealed a structural phase transition of SrAl_2O_4 at 923 K from monoclinic to the hexagonal crystal system. The thermal expansion coefficients of both the phases were determined from the lattice parameter values of the respective systems as a function of temperature. A plot of the lattice volume/molecule against temperature showed discontinuity at 923 K, due to crystallographic modification.

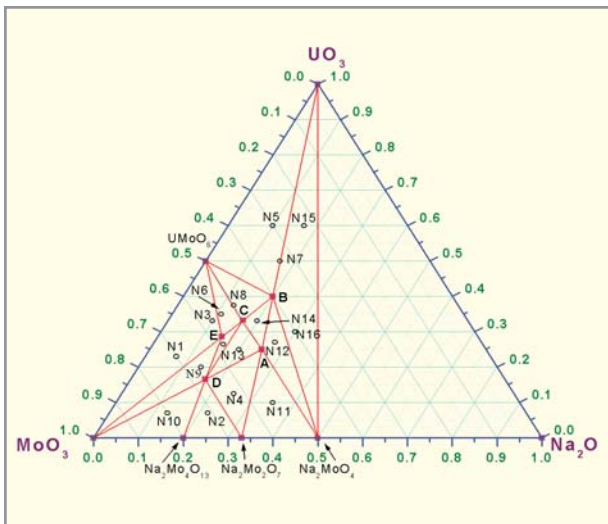
K. Krishnan, S.K. Sali and K.D. Singh Mudher

<krishnan@barc.gov.in>

■ X-ray and thermal studies on Na-U-Mo-O system

In Na-U-Mo-O system five compounds with compositions $\text{Na}_2\text{UMo}_2\text{O}_{10}$, $\text{Na}_2\text{U}_2\text{Mo}_2\text{O}_{13}$, $\text{Na}_2\text{U}_2\text{Mo}_3\text{O}_{16}$, $\text{Na}_2\text{UMo}_4\text{O}_{16}$ and $\text{Na}_2\text{U}_2\text{Mo}_4\text{O}_{19}$ were prepared at 550°C by solid state reactions of UO_3 with $\text{Na}_2\text{Mo}_2\text{O}_7$ and $\text{Na}_2\text{Mo}_4\text{O}_{13}$ in the required stoichiometric ratio. All these compounds were characterized by X-ray powder diffraction and thermal analysis techniques. X-ray powder diffraction data of above-mentioned compounds were indexed to derive lattice parameters. TG curves of all the compounds showed thermal stability up to

600°C. These compounds when further heated in air at 950°C decompose to form $\text{Na}_2\text{U}_2\text{O}_7$. A pseudo-ternary phase diagram of $\text{Na}_2\text{O}-\text{UO}_3-\text{MoO}_3$ was drawn using these quaternary compounds, and various phase mixtures were established by XRD to draw the phase boundaries.

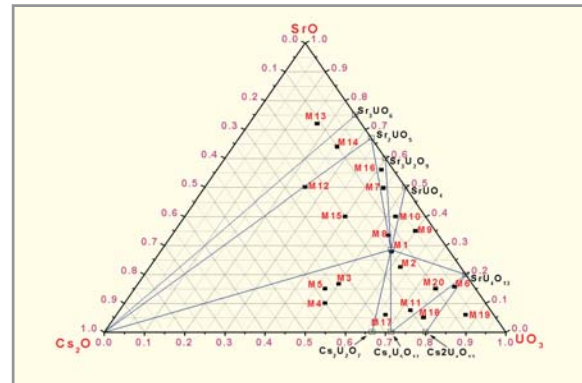


Phase diagram of Na-U-Mo-O system

N.D.Dahale, Meera Keskar, R. Agarwal and K.D.Singh Mudher, Proceedings Nuclear and Radiochemistry Symposium (NUCAR 2005), Amritsar, March 15-18, 2005, p-221.

■ X-ray and thermal studies on Cs-Sr-U-O system

The phase diagram of Cs-Sr-U-O system was analysed at 900°C. A novel quaternary phase, $\text{Cs}_2\text{Sr}_2\text{U}_4\text{O}_{15}$ in the system was identified by heating the respective oxides at 900°C in air and X-ray powder diffraction data was indexed on a monoclinic system with cell parameters, $a = 9.627(6) \text{ \AA}$, $b = 13.742(8) \text{ \AA}$, $c = 7.681(5) \text{ \AA}$ and $\beta = 107.72(5)^\circ$. A pseudo-ternary phase diagram of $\text{Cs}_2\text{O}-\text{SrO}-\text{UO}_3$ system, shown in the figure, was drawn on the basis of the knowledge of $\text{Cs}_2\text{O}-\text{UO}_3$ and $\text{SrO}-\text{UO}_3$ systems and new phase $\text{Cs}_2\text{Sr}_2\text{U}_4\text{O}_{15}$. The compositions investigated by XRD to establish the coexisting phases are shown as points, the stable phases are drawn on the basis of the reported compounds and the new compound. Phase analysis of most of these compositions confirmed the expected phase boundaries.



Phase diagram of Cs-Sr-U-O system

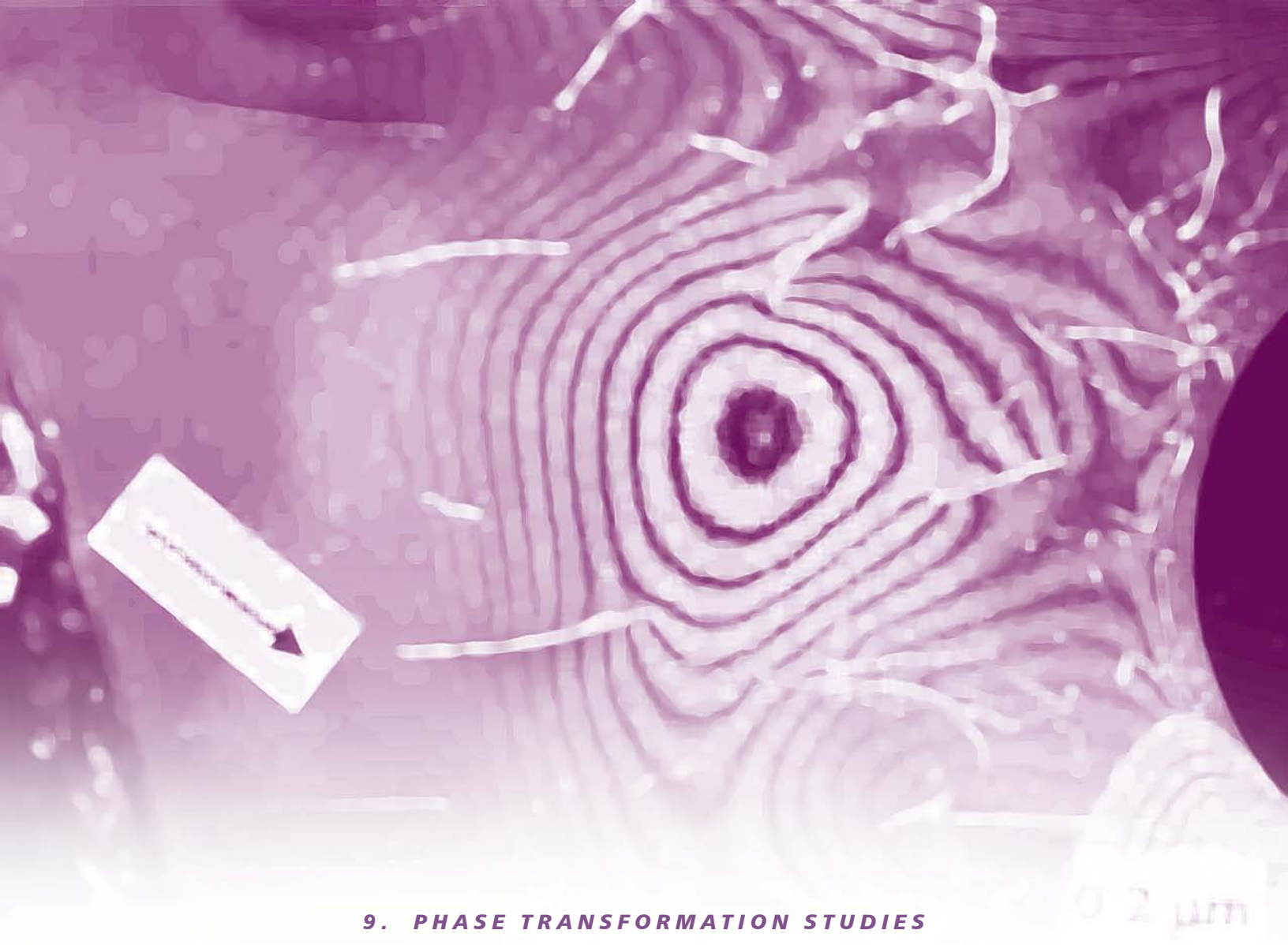
Meera Keskar, R. Agarwal & K.D.Singh Mudher, Proc. Nuclear and Radiochemistry Symposium, Amritsar, March 15-18, 2005, p-219.

■ Thermal studies on alkali uranates

Various alkali uranates have been reported but limited literature is available on the solid solubility among themselves. With a view to study the Na-K-U-O and Na-Rb-U-O systems, studies have been carried out on the solid state reactions of mixtures of $\text{Na}_2\text{U}_2\text{O}_7$ with $\text{K}_2\text{U}_2\text{O}_7$ and $\text{Rb}_2\text{U}_2\text{O}_7$. Mixtures of $\text{Na}_2\text{U}_2\text{O}_7 + \text{K}_2\text{U}_2\text{O}_7$ and $\text{Na}_2\text{U}_2\text{O}_7 + \text{Rb}_2\text{U}_2\text{O}_7$ containing different proportions of Na : K and Na : Rb were heated in air up to 1200°C. X-ray diffraction pattern of the product showed formation of complete range of solid solutions of type $(\text{Na}_x\text{K}_{1-x})_2\text{U}_2\text{O}_7$ and $(\text{Na}_x\text{Rb}_{1-x})_2\text{U}_2\text{O}_7$. The reduction behavior of these solid solutions in Ar/ H_2 atmosphere up to 700°C showed the formation of ABO_3 type perovskite phases. Thus the reduction of $(\text{Na}_x\text{K}_{1-x})_2\text{U}_2\text{O}_7$ and $(\text{Na}_x\text{Rb}_{1-x})_2\text{U}_2\text{O}_7$ where $x = 0$ to 0.5 forms cubic phases indicating solubility of 50 atom% of Na in KUO_3 or RbUO_3 phase. For $0.9 < x < 1$ only orthorhombic phase of NaUO_3 containing KUO_3 or RbUO_3 was observed. For $0.6 < x < 0.9$ a mixture of orthorhombic phase containing K or Rb and cubic phase containing Na was observed. Further enthalpy of oxidation of MUO_3 ($M = \text{Na} + \text{K}$ and $\text{Na} + \text{Rb}$) determined by DTA peak area measurement was found to be in the range of 40 to 90 kJ/mol.

S.K.Sali, N.K.Kulkarni and K.D.Singh Mudher

<sksali@barc.gov.in>



9. PHASE TRANSFORMATION STUDIES

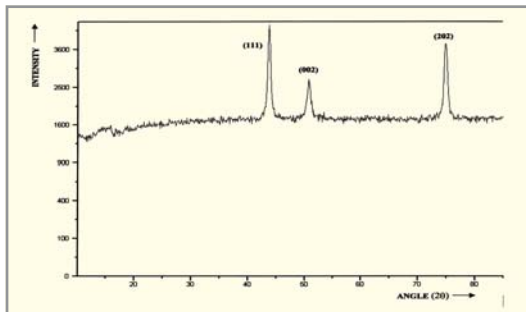
INTRODUCTION

Phase transformations occur to lower the energy of the body. But it is not always that they are useful in their lowest state of energy. A material may, sometimes, be more useful in its metastable state if, in a given environment, the kinetics of its transformation to the stable state is slow enough to permit its use for the desired duration. Materials scientists focus on the study of the thermodynamics of the equilibrium phases, the kinetics of transformation of the metastable phases under desired environments and, most importantly, the combinations of stable and metastable phases that would give the desired properties for a given application. Developing a microstructure, constituted of the stable and not so stable phases, to suit a given end use and, at the same time, delineating the mechanisms involved in the development of this microstructure and its degradation during use are central to studies on phase transformations. The studies carried out with the above in view on various alloys of interest using transmission electron microscopy, electron probe microanalysis, dilatometry and acoustic emission are described below in brief to give a bird's eye-view of the recent activity in this interesting area of development of materials and their characterization.

9.1 COLD WORKED MICROSTRUCTURE OF ALLOY 800

To simulate the deformation that steam generator tubes experience while bending into hairpin shape in some cases, cold-worked (~50%) state of Iron-Nickel-Chromium (Fe-Ni-Cr) based Alloy 800 has been considered. The cold worked microstructure of the alloy under an optical microscope revealed deformation bands and random distribution of large, faceted, undissolved primary titanium nitride (TiN) particles in the matrix. X-ray diffraction performed on cold-worked alloy indicated the presence of austenite phase.

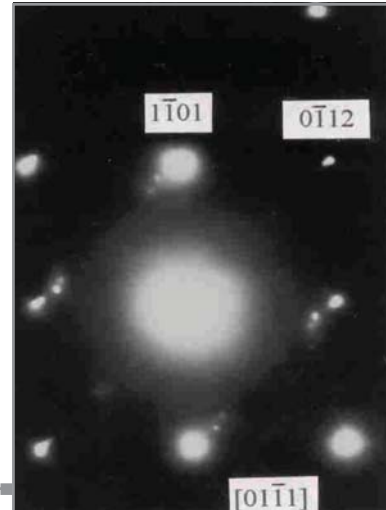
Transmission electron microscopy (TEM) studies carried out on the deformed sample revealed the presence of a small volume fraction of martensite-like phase with the appearance of plates. Selected-Area Diffraction (SAD) pattern analysis confirmed that the phase has been isostructural with ϵ -martensite having hexagonal structure. The formation of hexagonal ϵ -martensite in Alloy 800 during deformation could be due to overlapping stacking faults.



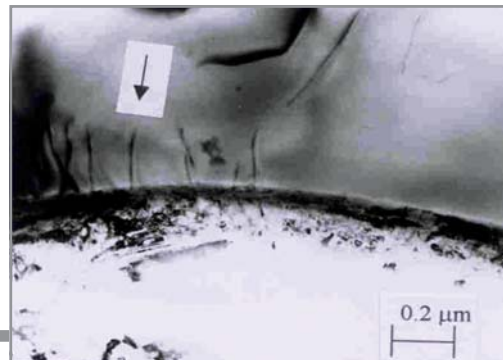
X-ray diffraction of cold worked Alloy 800 revealing austenite phase

TEM examinations revealed that although the matrix contained very high dislocation density owing to heavy deformation, the interface region between matrix and large, faceted primary TiN particle having hexagonal structure has been relatively cleaner.

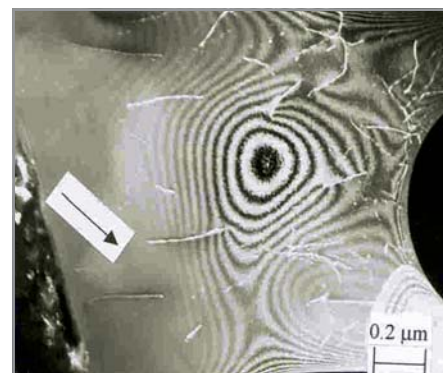
It has been indicated from the deformation behaviour of large, faceted TiN particle that the particle has been very hard since only a few dislocations were generated within the particle after heavy deformation of the alloy.



Selected area diffraction pattern of ϵ -martensite (hexagonal) along specified zone axis



Cold worked Alloy 800 revealing TiN particle/matrix interface.



A few dislocations within primary TiN particle after heavy cold deformation.

R.S.Dutta and G.K.Dey <rsdutta@barc.gov.in>

9.2 STUDY OF THE MARTENSITE TO AUSTENITE TRANSFORMATION IN STEELS BY DILATOMETRY

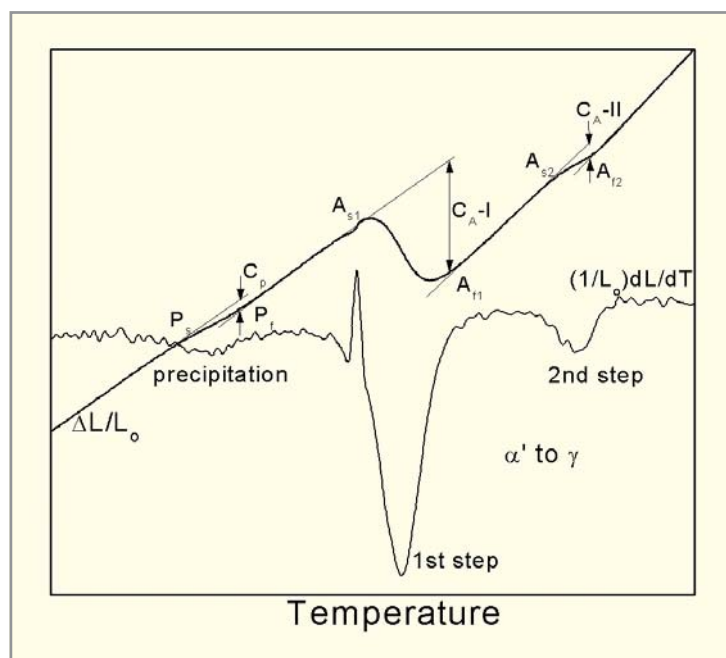
The martensite (α') to austenite (γ) transformation in Fe-rich Fe-Ni steels has considerable practical utility and a good understanding of the transformation mechanisms is required. It was known that the α' to γ transformation splits into two steps in 18 wt% Ni maraging steels at slow heating rates. This heating transformation was studied to ascertain the cause of this splitting. In addition to this, the α' to γ transformation in two stainless precipitation hardenable steels, namely, PH 13-8 Mo steel and 17-4 PH steel, was studied. Both these steels, like 18 wt% Ni maraging steels, are martensitic at room temperature revert to austenite upon heating. Between themselves, they differ mainly in terms of the nature of precipitates that form during aging. Whereas in PH 13-8 Mo steel, nano-sized intermetallic NiAl is known to precipitate at 850 K, pure copper is known to precipitate at about 675 K in 17-4 PH steel. Here, an attempt has been made to re-examine the issue of the mechanism of the α' to γ transformation in these steels using dilatometry.

Experiments were carried out on 18 wt% Ni maraging steel of grade 350 (M350), PH 13-8 Mo and 17-4 PH steels using a computer controlled dilatometer with programmable heating-holding-cooling cycles at ten heating rates ranging from about $0.03^\circ\text{C s}^{-1}$ to about 210°C s^{-1} . The change in length (ΔL) as a function of time was recorded, from which $\Delta L/L_0$ vs. temperature (T) was plotted, L_0 being the original length. A typical plot of $\Delta L/L_0$ vs. T for the PH 13-8 Mo steel, tested at a heating rate of 0.2°C s^{-1} , is shown in Figure. It exhibits two steps in the α' to γ transformation. The precipitate start (P_s), precipitate finish (P_f), austenite start (A_{s1}), and austenite finish (A_{f1}) temperatures for the first step and austenite start (A_{s2}) and austenite finish (A_{f2}) for the second step of the α' to γ are marked on the plot. Tangents to the curves are used to identify the start/finish of transformations and to quantify the extent of contraction undergone due to transformation. C_p is contraction due to precipitation and C_{A1} is the contraction due to the first step and C_{A2} is the contraction due to the second step of the transformation of the aged α' to γ . A clearer demarcation of the two steps of

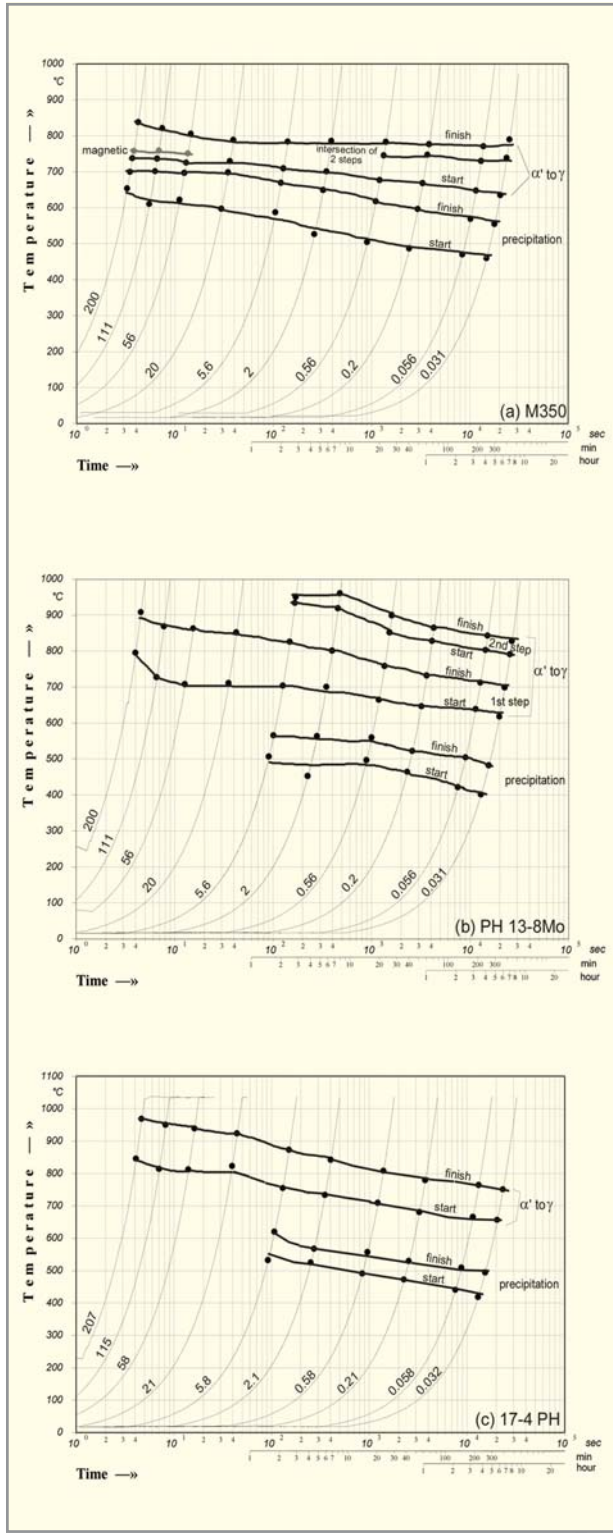
the α' to γ transformation is seen through the derivative $(1/L_0)dL/dT$. A comparison of the results for the three steels is shown in Table.

The effect of the heating rate on the kinetics of precipitation, and austenitization of the initial phases, is better represented in what are generally known as Continuous Heating Transformation (CHT) diagrams, shown in figure for M350, PH 13-8 Mo and 17-4 PH steels.

With the help of the above results and some interrupted / heating rate change tests it was concluded that in M350, the first step occurs through a diffusion process, while the second step occurs through a shear process. In PH 13-8 Mo, the two steps, seen at the lower heating rates, appear to be due to the partitioning of the material, and the transformation in both the steps appear to be controlled by long-range diffusion. In 17-4 PH, the α' to γ transformation occurs via diffusion at low rates and changes over to a shear process at high rates. Precipitation in the three steels occurs through a diffusive mechanism.



Typical plot of $\Delta L/L_0$ vs. T for PH 13-8 Mo steel, tested at a heating rate of 0.2°C s^{-1} , indicating the precipitation and the martensite to austenite transformation. Its derivative, $(1/L_0)dL/dT$ vs. T is also shown.



Continuous Heating Transformation (CHT) diagrams for (a) M350, (b) PH 13-8 Mo, and (c) 17-4 PH steels. Heating rates in °C s⁻¹ are indicated.

M350 Steel	PH 13-8 Mo Steel	17-4 PH Steel
P _s and P _f both increase with increasing heating rate.	P _s and P _f both increase with increasing heating rate.	P _s and P _f both increase with increasing heating rate.
Precipitation observed at all heating rates employed in this investigation.	No precipitation observed at 20°C s ⁻¹ and above.	No precipitation observed at 20°C s ⁻¹ and above.
A ₁ increases with increasing heating rate. A ₁ remains constant with increasing heating rate. A ₁ remains constant with heating rate up to 20°C s ⁻¹ beyond which it increases with heating rate.	A _{s1} , A _{f1} , A _{s2} and A _{f2} all increase with increasing heating rate.	A _s and A _f both increase with the increasing heating rate.
Magnetic transformation is seen to interfere with the α' to γ transformation above 20°C s ⁻¹ .	2 nd step related to the α' to γ transformation not seen at 20°C s ⁻¹ and above.	A single step is seen throughout the whole range of the heating rates employed.
The total contraction of α' to γ transformation changes trend around 20°C/s.	The extents of contraction related to both the steps decrease with the increasing heating rate. The total contraction due to the α' to γ transformation decreases with increasing heating rates.	The total contraction of α' to γ transformation shows a step decrease at heating rates above 20°C/s.

Results for three steels studied

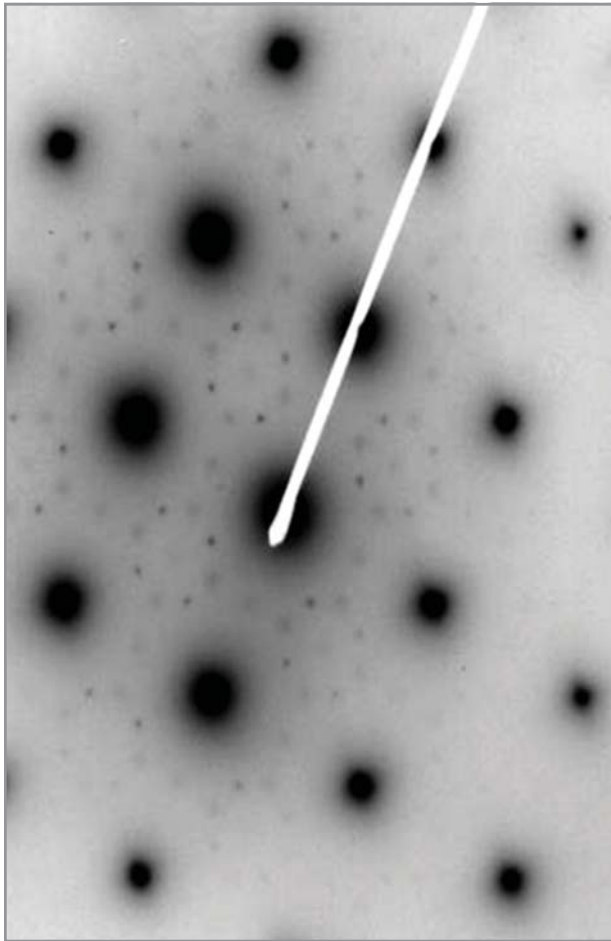
R. Kapoor and I.S. Batra, Metal Science and Engineering, A371 (2004) p. 324-334.

R. Kapoor, Lalit Kumar and I.S. Batra, Materials Science and Engineering, A352 (2003), p. 318-324.

9.3 AGING RESPONSE OF ALLOY 625

Alloy 625 is a Nickel-base alloy that finds applications in the nuclear industry due to its high corrosion resistance, low hydrogen diffusivity in the matrix and good high temperature mechanical properties. Depending on the temperature and duration of aging, a number of ordered phases are known to occur in this alloy that affect strength, ductility and toughness and, also, other mechanical properties in this alloy. Although, there are fcc based and, also, orthorhombic ordered phases that affect strength and ductility of this alloy, precipitation of a Pt₂Mo type ordered phase that forms on aging below 873 K has maximum impact on strength compared to other ordered phases.

Work on the detection of early stages of precipitation, on



Selected Area Diffraction pattern reflecting $\text{Ni}_2(\text{Cr,Mo})$ and γ' from 1200 h (A1200) sample

aging below 873 K, using Acoustic Emission (AE) technique and its effect on the strength of the material was carried out. In this work, Alloy 625 samples were aged at 813 K for 10, 100 and 1200 h. Early stages of precipitation of $\text{Ni}_2(\text{Cr,Mo})$ and γ' have been detected efficiently in 100 h and 1200 h samples and correlated with that of AE results.

To understand the effect of the ordered phases on the structure and properties, Alloy 625 samples were aged at 813 K, 973 K and 1123 K for durations up to 1200 h. Results from these were compared with that of cast and wrought Alloy 625 which had seen 100,000 h of service and with that which had failed during the service after about 24,000 h and, also, with the alloy that had been aged after resolutionizing at 1443 K for 2h. After a comparison of all the microstructures, it was found that formation of

continuous films of carbides and the δ -phase in the grain boundaries makes the alloy very brittle. It was also noticed that from amongst all the ordered phases such as $\text{Ni}_2(\text{Cr,Mo})$, γ' and δ , the former that forms below 873 K has the maximum effect on the room temperature ductility and weldability.

J.Mitra, J.S.Dubey and S.Banerjee, *Scripta Materialia*, 49 (2003) p.1209.

9.4 DIFFUSION IN METALS AND ALLOYS – THERMODYNAMIC INTERDIFFUSION COEFFICIENTS

Conventionally diffusion coefficients are evaluated using concentration gradient as a driving force. But actually chemical potential gradient is the true driving force. Thermodynamic diffusion coefficients have been defined using chemical potential gradient as driving force. Using activity gradient as a driving force, the flux equation can be written as

$$J_i = D_{(i)} N_i (\partial \ln a_i / \partial x)$$

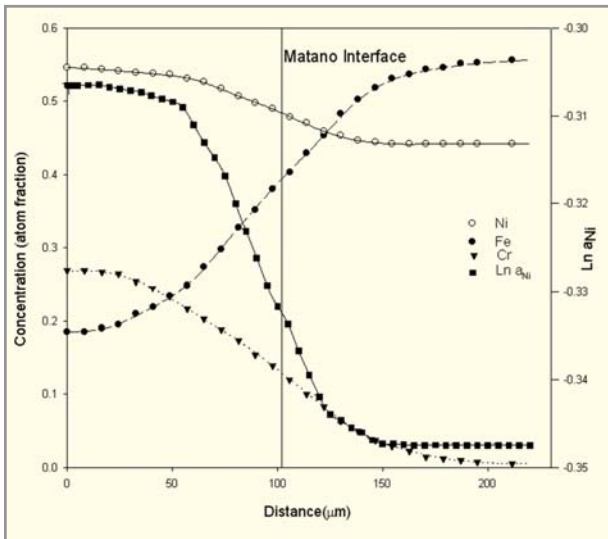
The Boltzmann-Matano equation have been also modified to evaluate chemical diffusion coefficients at composition N^* as

$$D_{(i)} = - 1/2tN^* (\partial x / \partial \ln a_i) (x - x_0) dN$$

Darkens equation also has been modified as

$$D_{(i)} = N_A D_{B(i)} + N_B D_{A(i)}$$

The concept is very useful for evaluation of interdiffusion coefficients for intermetallic compounds where there is very little or no concentration gradient but finite activity gradient. The analysis has been extended to ternary systems and is applied to ternary diffusion in Fe-Ni-Cr alloy system. The typical concentration and activity profile across the diffusion zone is shown in figure.



The four thermodynamic interdiffusion coefficients, $\tilde{D}_{NiNi(\mu)}^{Fe}$, $\tilde{D}_{NiCr(\mu)}^{Fe}$, $\tilde{D}_{CrNi(\mu)}^{Fe}$ and $\tilde{D}_{CrCr(\mu)}^{Fe}$ have been evaluated employing Boltzmann – Matano solution. The composition dependence of these thermodynamic interdiffusion coefficients can be expressed by a relation of the type. $\log \tilde{D}_{(\mu)} = b_1 + b_2 N_{Ni} + b_3 N_{Cr}$. The thermodynamic interdiffusion coefficients for ternary system have been related to the thermodynamic intrinsic diffusion coefficients by extending Darken's analysis for binary system to ternary system.

A. Laik, K. Bhanumurthy and G.B.Kale, J. Nucl. Mater., 305(2002) p.124-133.

A. Laik, K. Bhanumurthy and G.B.Kale, Intermetallics, 12(1) (2004), p.69.

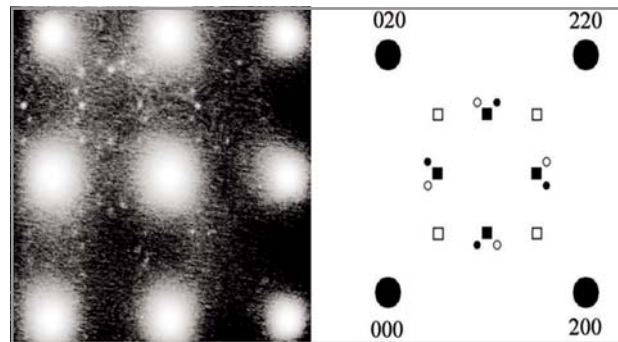
G.B.Kale, K. Bhanumurthy and A. Laik, Trans. Indian. Inst. Metal. 57(1), (2004) p.35.

A.Laik, K. Bhanumurthy and G.B.Kale, J. of Alloys and Comp., 372(1-2), (2004), p.176-179.

9.5 SEQUENCE OF CLUSTERING AND ORDERING IN DILUTE Cu-Ti ALLOYS

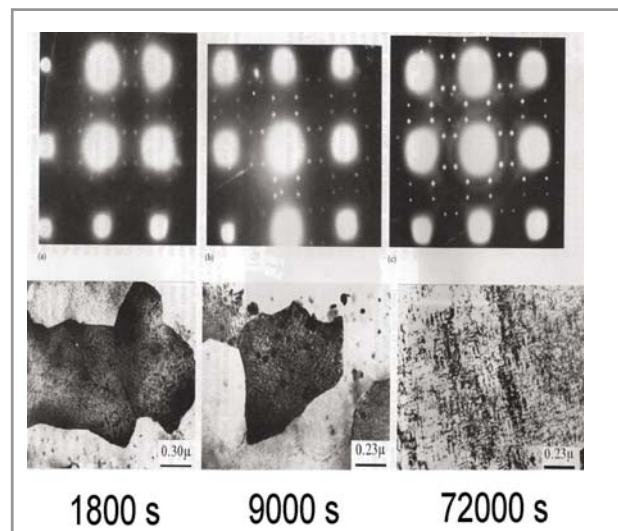
Age hardenable dilute copper-titanium alloys, with yield strength in the hardened condition exceeding 700 MPa, find applications in fabricating high strength springs, electrical contacts, diaphragms, corrosion and wear resistant materials.

The mechanism of their decomposition has, however, been a matter of debate. Whereas Cu-1wt%Ti has been shown to decompose essentially by nucleation and growth while somewhat more concentrated alloys exhibit spinodal decomposition. It was also found that it is impossible to suppress decomposition during quenching in the concentrated side band alloys and, consequently, it is difficult to delineate the sequence in which clustering and ordering occur to form the observed metastable Cu_4Ti precipitates having $D1_a$ structure.



[001] SAD pattern and the corresponding key in the melt-spun Cu-4Ti alloy aged at 673 K for 9000 s (superlattice reflections due to $D1_a$ and N_3M can be seen)

In order to resolve these issues two different approaches were adopted in this work. In the first approach, an attempt was made to suppress the onset of the spinodal reaction in



Evolution of $D1_a$ and the triaxially modulated microstructure aging of melt-spun Cu-4Ti alloy at 723 K

a Cu-4 wt%Ti alloy by spinning it into a thin ribbon directly from the liquid state and, in the second, by addition of a small quantity of a third element to this alloy. Both the approaches were successful in achieving the required suppression. The aging response was studied by the transmission electron microscope with new and interesting results. From both the approaches, spinodal clustering was found to be the first step of the decomposition process. Ordering was found to follow clustering in the titanium enriched regions.

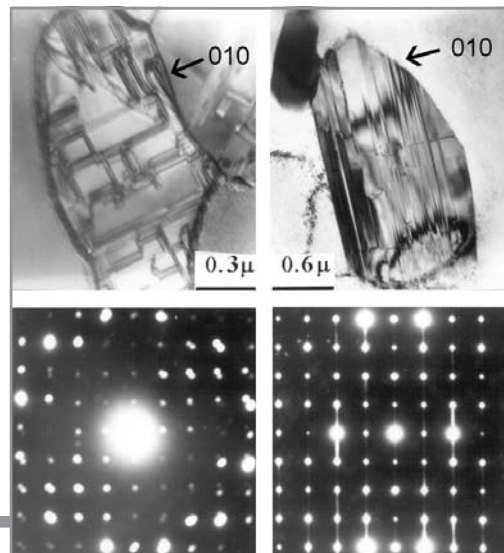
In the case of the melt-spun alloy, formation of hitherto undiscovered transitory special point N_3M phase was observed which disappeared upon prolonged aging giving rise to the metastable Cu_4Ti ($D1_3$). In contrast to this, in the case of the ternary alloy, suppression of the $1\frac{1}{2}0$ spinodal was noticed which was explained on the basis of kinetic and thermodynamic considerations. These results are relevant for other $1\frac{1}{2}0$ alloys as well.

I.S.Batra, G.K.Dey, U.D.Kulkarni and S.Banerjee, *Materials Science and Engineering*; A, 360 (2003), p. 220-227.

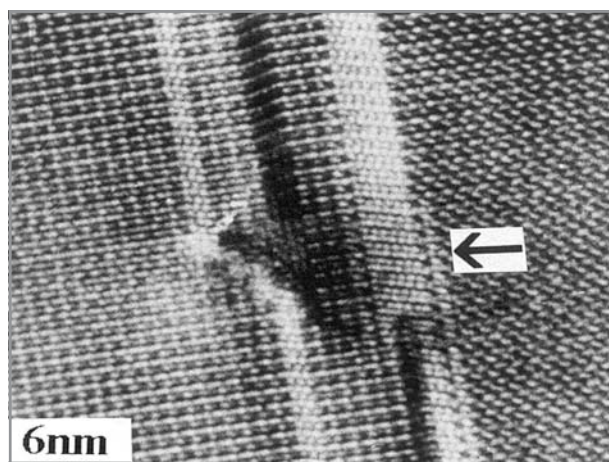
U.D.Kulkarni, G.K.Dey and I.S.Batra, *Metallurgical and Materials Transactions A*, 33 (2002), p.1.

9.6 FORMATION OF SIGMA AND OTHER TOPOLOGICALLY CLOSE PACKED (TCP) PHASES IN NICKEL-MOLYBDENUM-BASE ALLOYS

Ni-base superalloys find application in a number of aggressive environments where high temperature mechanical properties and resistance to oxidation are of paramount importance. Most commercial Ni-base alloys contain a large number of constituents. Although some of them impart high temperature strength and creep resistance to the alloy, they also tend to promote the formation of the Topologically Close Packed (TCP) phases, either singly or in combination with other constituents. The Sigma-phase, which occurs in a number of alloy systems, is a well-known example of a TCP phase. TCP phases, which form in some specific temperature ranges and on prolonged ageing, have a deleterious effect



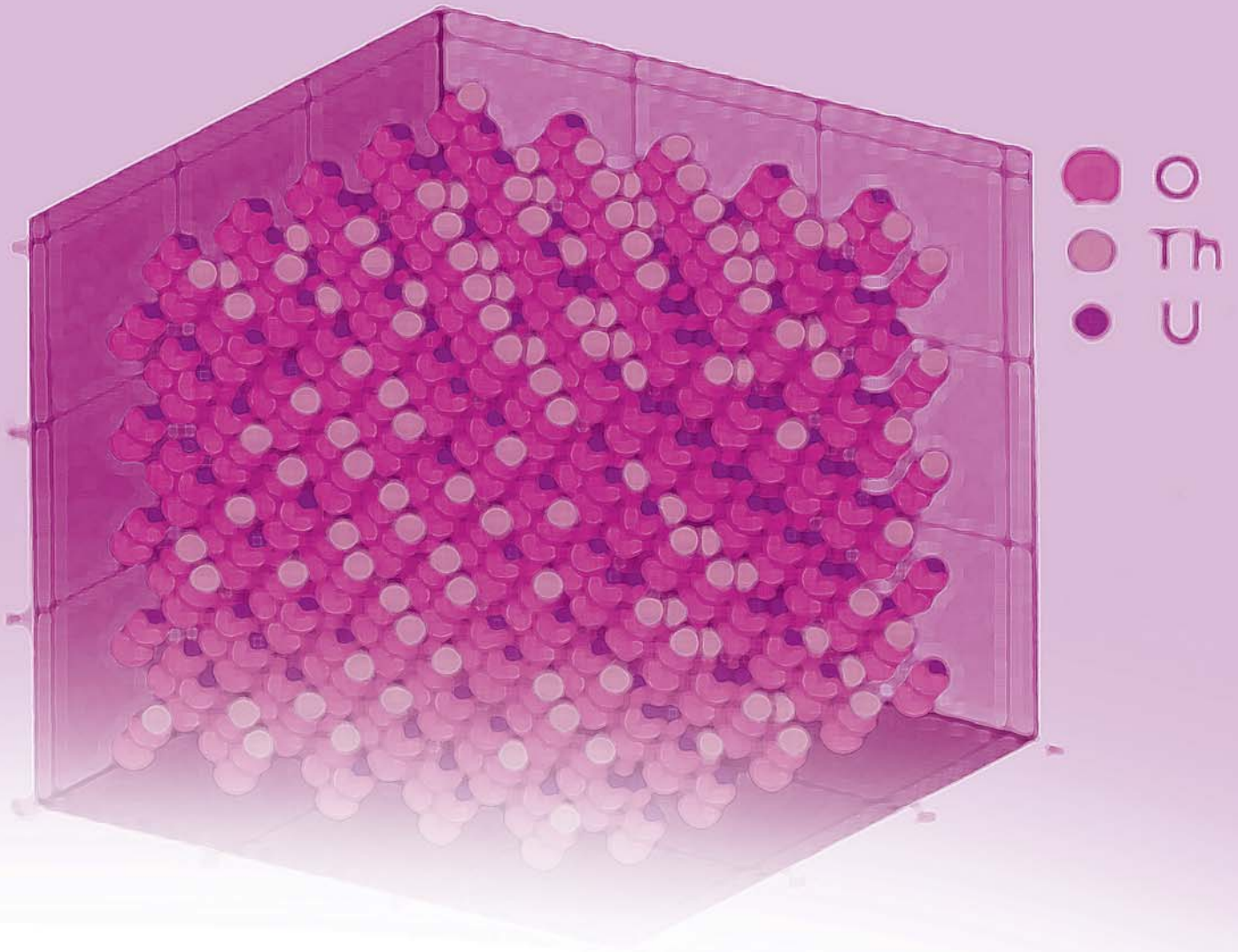
Faulted sigma-phase platelets (upper row) and the corresponding selected area electron diffraction patterns in Ni-25 at%Mo-5at%Al alloy.



High Resolution Transmission Electron Microscopy (HRTEM) Micrograph of a faulted sigma-phase platelet in Ni-25at%Mo-5at%Al alloy

on the mechanical properties of the alloys. TCP phases are generally seen as elongated platelets in the electron micrographs and are often heavily faulted. Their study is of importance, as they tend to cause excessive embrittlement in superalloys.

U. D. Kulkarni and G. K. Dey, *Acta Materialia*, 52, (2004). p.2711-2720.



10. MODELLING AND SIMULATION

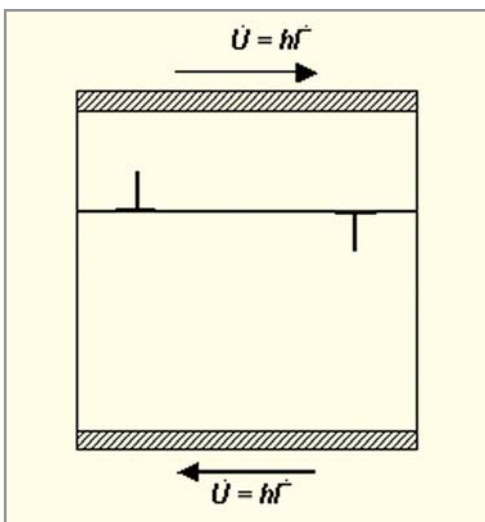
INTRODUCTION

Micromechanisms of processes like precipitation, plastic deformation and fracture in materials have always been of considerable interest to materials scientists. Despite the plethora of modern microscopic and analytical techniques, the early stages of these processes have remained something of an enigma. This is so because the techniques can generally monitor these processes only after a latent period – known as the nucleation or the incubation stage. The atomistic processes involved in the incubation stage are usually not amenable to investigation by the available techniques. In the circumstances, the only option to study the early stages is by means of modelling and simulation. The availability of enhanced computational power in recent years has made it possible to study them, in simulated systems of realistic sizes, without significant loss of accuracy and information. These studies are of utmost importance as they are invaluable aids in designing better materials.

10.1 DISCRETE DISLOCATION PLASTICITY (DDP) MODELLING APPLIED TO IRRADIATED MATERIALS

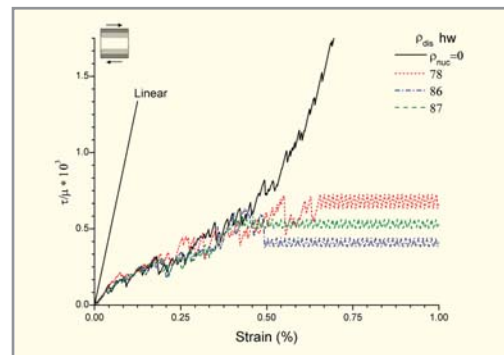
The irradiation of metals by energetic particles causes significant degradation of the mechanical properties - increased yield stress and decreased ductility. Such effects limit the lifetime of pressure vessels in nuclear industry. DDP modelling is being used to demonstrate such effects. Using two-dimensional DDP simulations, an attempt is made to find the plastic flow behavior of aluminum due to irradiation. The irradiation-induced defects are modeled as obstacles where dislocations get pinned during deformation process.

An in-house DDP code is being developed which can be used to determine plastic behavior of materials under different loading conditions: high strain rate, fatigue, irradiation etc. Different dislocation phenomena viz. motion due to interaction of dislocations, annihilation of dislocations, pinning of dislocations at obstacles and creation of new dislocations due to Frank-Reed mechanism are incorporated in the DDP code. Stress-strain curves are generated for aluminum under simple shear deformation. The irradiation effects are modeled here by taking into account an increased number of obstacles. Initially, dislocations corresponding to a dislocation density of $2 \times 10^{10} \text{ cm}^{-2}$ are randomly introduced into unit cell of Al and allowed to relax under fixed displacements on boundary (zero strain).



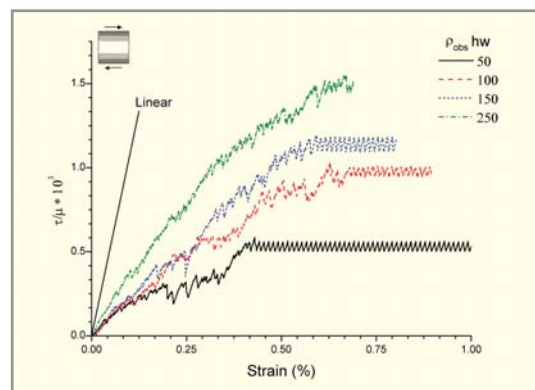
Schematic model of DDP analysis, unit cell of dimension $2h \times 2w$, $h = w = 1 \mu\text{m}$ and μ is the strain rate being imposed

Then nucleation sources and obstacles are introduced randomly into the cell. The material is then sheared in simple shear mode up to 1% of strain in an incremental manner. Currently, the analysis is restricted to pure edge dislocations. The schematic model for DDP analysis is shown in the figure. The DDP simulations are highly computational intensive due to small time increment requirements and for one run of DDP analysis it takes about 10 days on a P-4 Intel machine with 3.0 GHz CPU.



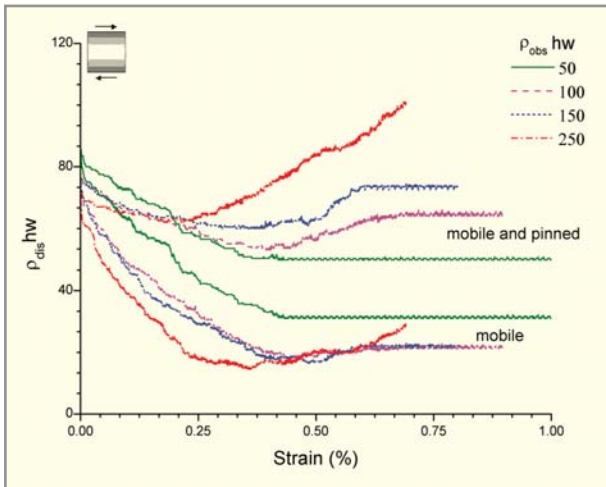
Simple shear response for three different initial dislocation configurations

Simple shear response of aluminum for three different initial dislocation configurations is shown in the above figure, where the response can be seen more or less similar in yielding behavior. τ is the shear stress on boundary and μ is the shear modulus of material under consideration. The curve with $\rho_{mn} = 0$ shows the case with zero source density, and dislocations tend to be removed by annihilation process and response tends to be purely elastic. Effect of obstacle density on simple shear response is presented in the figure below.



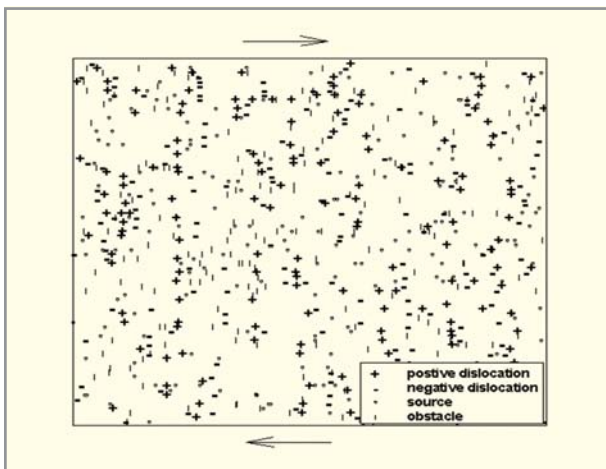
Effect of obstacle density on simple shear response

It can be clearly seen here, the increase in strain hardening due to increased obstacle density. For high obstacle density, the annihilation process is inactive and obstacles prevent motion of dislocations. It is observed that after reaching a maximum, shear stress drops to a steady state value, where slip confines to a particular slip plane and total dislocation density then becomes constant.



Effect of obstacle density on evolution of total and mobile dislocation density

Effect of obstacle density on evolution of total and mobile dislocation density is shown. Dislocation distribution for one of the cases, after shearing up to 0.75% strain is elucidated in the figure.



Distribution of dislocations after shearing up to 0.75% strain

Future work

Presently, DDP modelling is two-dimensional with edge dislocations. This code is to be extended to three-dimensional modelling by taking into consideration the curved dislocation loops with both edge and screw character. Within close distances of dislocation cores, the atomistic descriptions should be accounted in DDP analysis. This requires a coupling between atomistic and the large-scale dislocation length scales. The computational time grows exponential with 3D analysis and parallelization of code is to be done.

P.V.Durgaprasad and B.K.Dutta

<pvd@barc.gov.in>

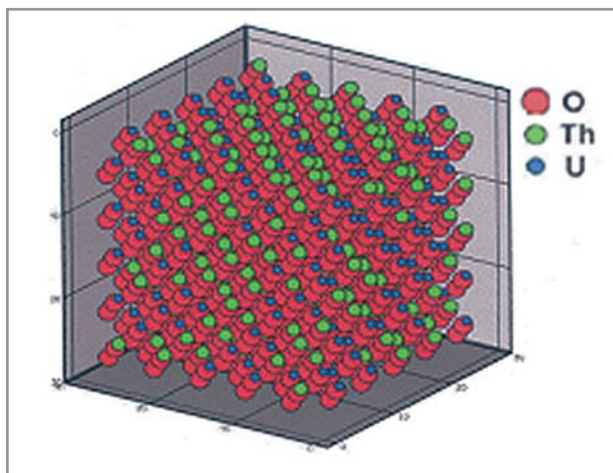
10.2 ATOMISTIC MODELLING OF MATERIALS

In nuclear industries, problems of practical interest are: utilization of the large resources of thorium deposits, providing the structural integrity of safety related components under normal and extreme scenarios, to make use of nano devices, MEMS, development of new materials, etc. Atomistic descriptions of materials help in understanding the role of nano, micro and meso level defects (voids, dislocations, micro cracks, grain boundaries, dislocation interactions etc.) in plasticity of materials so as to support the laboratory experiments.

An In-house code with coupled finite element and atomistic modelling of materials is being developed which can be used to a) determine the thermo-physical properties of materials, b) determine plastic behavior of materials at atomic length scale so as to pass information to higher length scale models such as dislocation dynamics etc. One of the main objectives of atomistic modelling is to determine thermo-physical properties of mixed oxide nuclear fuels (U-Th-Pu) O_2 . Using in-house atomistic code, the elastic constants of ionic materials are being determined. The Catlow's potentials are used for simulations of ionic materials for describing the interacting potentials, viz. Coulombic, short range and Van der Waal interactions. Ewald summation technique is being used to determine long-range nature of Coulombic

Ionic Constants of Ionic Materials						
	C_{11} (GPa)		C_{12} (GPa)		C_{44} (GPa)	
	Literature	Simulation	Literature	Simulation	Literature	Simulation
NaF	108.5	109.4	22.90	30.11	28.99	30.97
NaI	37.61	36.61	7.98	7.65	7.81	8.60
NaCl	57.33	57.69	11.23	13.41	13.31	13.72
KF	75.70	71.41	13.50	14.33	13.36	15.44
KCl	48.32	48.02	5.40	6.45	6.63	6.65
KI	33.80	34.52	2.20	3.45	3.68	3.51
UO2	400.00	481.60	120.00	102.70	68.00	97.60
ThO2		443.10		96.20		93.20

forces. The generated elastic constants for various ionic materials are presented in the Table. The code is also being extended for mixed oxide fuels. An atomistic model for a MOX fuel is shown in the figure.



Atomistic model for MOX fuel

Ongoing and Future work

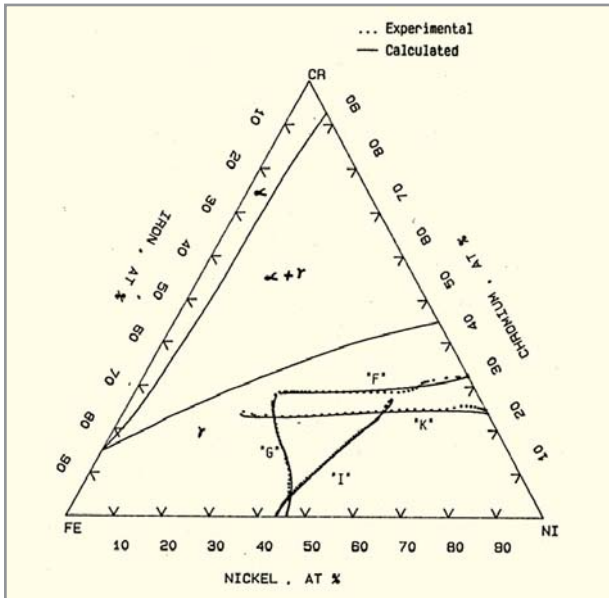
Also the finite temperature calculations using Molecular dynamics simulations are being performed to evaluate specific heat capacities etc. Also the evaluation of other thermo-physical properties like coefficient of thermal expansion, mechanical properties, thermal conductivity etc., will be evaluated.

Amit Pawar, P.V.Durgaprasad and B.K.Dutta
 <apawar@barc.gov.in>

10.3 MODELLING OF DIFFUSION PATHS IN TERNARY SYSTEMS

Diffusion paths in multicomponent system denote the course of flow of diffusing species and are very important in understanding the behaviour of materials during service or heat treatment. Diffusion paths in ternary system are not linear. They may be singly or doubly 'S' shaped. Apart from 'S' shaped diffusion path ternary diffusion may exhibit development of zero flux plane (ZFP) across which flux reversal may take place. Thus it is essential to know the exact nature of diffusion path in a diffusion zone. Determining the diffusion path in a ternary system by experimental means is both tedious and time consuming as it involves making of large number of couples with alloys of different compositions and annealing them at various conditions of temperature and time. The diffusion paths for Fe-Ni-Cr system have been modelled to predict them without carrying out the experiments. Few diffusion couples were made between various Fe-Ni-Cr alloys. The compositions of alloys in diffusion couple were orthogonally transformed to a new set of compositions. Diffusion paths were plotted between orthogonally transformed compositions. Such a diffusion path has two parameters viz. the composition of the point of intersection of diffusion path and linear line joining the end members of diffusion couple and the slope of diffusion path at this point of intersection. These parameters have been correlated with the difference between compositions of end members of diffusion couple. Algorithm has been written to get these parameters from the difference in compositions of end members of diffusion couple and to predict the diffusion path. Figure shows the excellent agreement between the predicted and experimental diffusion paths.

It is now possible to predict diffusion path for any couple made between two Fe-Ni-Cr alloys.



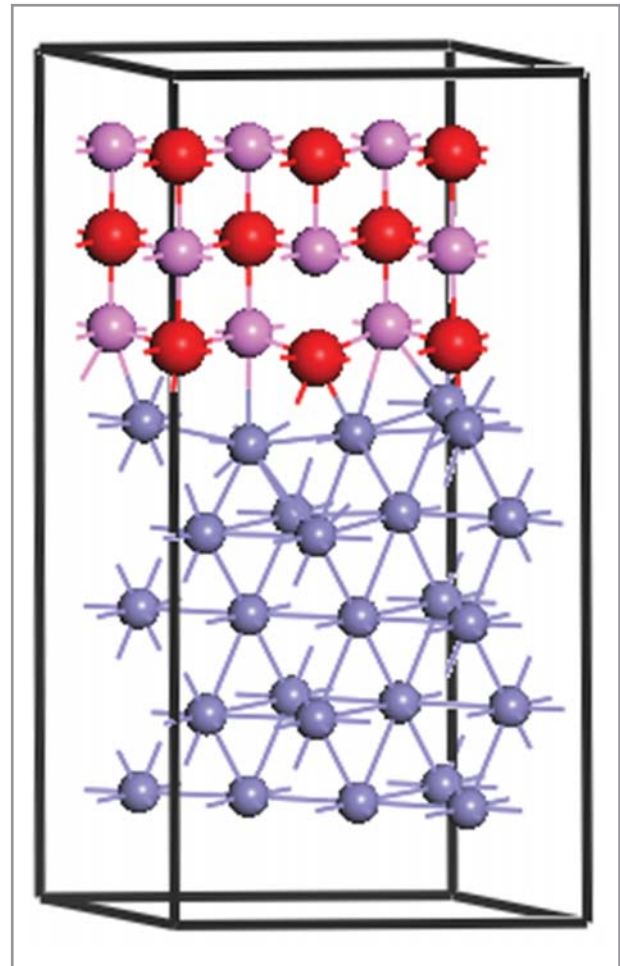
Diffusion paths for couples on the Fe-Ni-Cr isotherm.

G.B.Kale, K.Bhanumurthy, P.S.Gawde and A.Laik, Proc. of Seminar on "Computer Applications in Metallurgy", Sindri, (2002), p. 20-25.

10.4 FIRST-PRINCIPLES CALCULATIONS

■ Investigation of ceramic coatings on steels

In order to search for a suitable alternative (to chromium) protective coatings for ferritic steels, first-principles pseudo-potential-based supercell calculations were performed on a number of transition metal carbides and nitrides (titanium carbide (TiC), zirconium carbide (ZrC), tungsten carbide (WC) and cubic boron nitride (c-BN) and bcc iron (Fe) for their surface energies. Further, suitable Fe/ceramic interface supercell were modelled & computational work was performed to predict the interface structure, bonding and ideal work of adhesion to judge the suitability of the ceramic to act as a coating for steels. The adhesion strength was predicted to decrease in the order $\text{TiC} > \text{ZrC} > \text{WC} > \text{c-BN}$. These interfacial strengths and nature of bonding were compared with that calculated for the Fe/Cr interface.

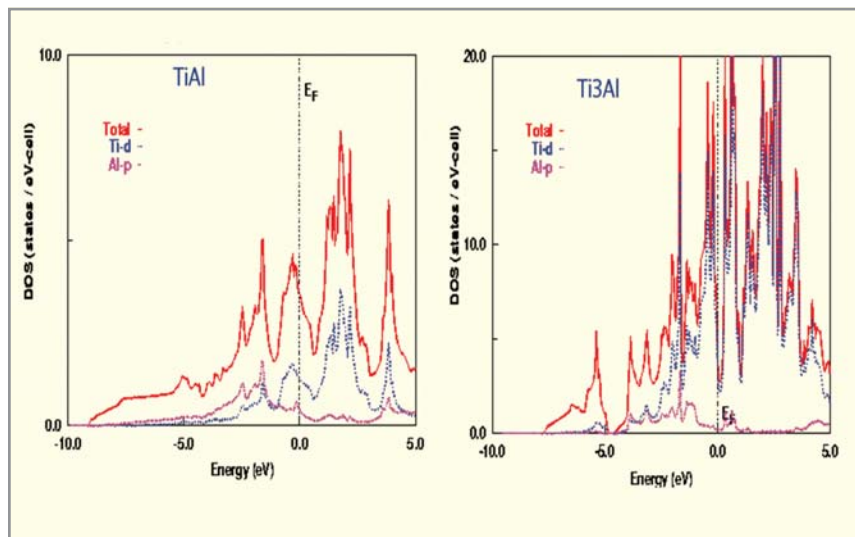


An interface unit cell showing 5 monolayers (ML) of substrate Fe and 3ML of TiC.

A. Arya and Emily A. Carter, *Surface Science*, 560 (2004).

■ Thermodynamic calculations on Ti-based alloys

The stability hierarchy of various stable/metastable binary intermetallic phases of titanium-aluminium (Ti-Al) and titanium-copper (Ti-Cu) alloys across the whole composition range were computed using first-principles DFT-based calculations. This was extended to the phase stability analysis of ternary ordered/disordered titanium-aluminium-niobium (Ti-Al-Nb) alloy phases to study the effect of Nb addition on the cohesive, electronic and mechanical properties of Ti-Al alloys. Further, effective interatomic potentials upto the



Density of states for TiAl and Ti₃Al phases showing higher metallic bonding component for Ti₃Al, imparting it more ductility.

fourth nearest neighbours were extracted using the 'augmented space recursion' method for thermodynamic analysis of Ti₂AlNb alloys to determine the finite temperature phase fields by calculating their free energy as a function of temperature and order parameter.

Ashok Arya <aarya@barc.gov.in>

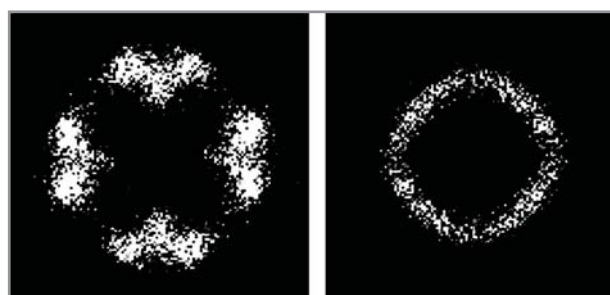
10.5 COMPUTER SIMULATION OF THE EARLY STAGES OF ORDERING TRANSFORMATION IN ALLOYS

There are two distinct types of order in solids. One of these is spatial order that relates to the regular arrangement of atoms that are present in crystalline materials. Ordering in alloys, sometimes referred to as chemical order, is however a term that is used to describe special atomic arrangements characterized by higher than random probabilities of finding unlike atoms (atoms of different elemental species) as nearest neighbours on a crystal lattice. When this form of order extends only over a range of a few atomic diameters the material is said to possess a state of short range order. Study

of the nature of order present in a material is of importance as it has a direct bearing on its properties.

Despite the availability of various advanced experimental techniques like High Resolution Transmission Electron Microscopy (HRTEM), the nature of the early stages of ordering processes in certain alloys continues to be an enigma. In recent years, computer simulation has emerged as an important technique for studying the atomic arrangements in short range ordered states, which prevail in the early stages of ordering in alloys.

Owing to the availability of enhanced computational power, it has now become possible to carry out simulations with systems of realistic sizes. A PC-based menu driven program has been developed for carrying out Monte Carlo simulations of the initial stages of ordering in Ni-Mo and in off stoichiometric g-TiAl alloys. The program also generates computed diffraction patterns of the simulated structures. An excellent match has been observed between the nature of diffuse intensity in the computed and the experimentally observed electron diffraction patterns. Results of the simulation study shed light on the atomistic mechanisms of evolution of ordered phases in these alloys and validate some long-standing theories of ordering.



Computed diffraction patterns for Ni-Mo alloys in the initial stages of ordering showing diffuse intensity arising from the presence of short range order

U. D. Kulkarni, Philosophical Magazine A, 82, (2002), p. 1017-1032.

U. D. Kulkarni, Acta Materialia, 52, (2004) p. 2721-2732.



11. BEAM PROCESSING OF MATERIALS

INTRODUCTION

A strong emphasis on research and development of beam processing of materials has resulted in advanced laser, plasma and electron beam devices for various material processing applications including surface engineering, melting and evaporation of metals and alloys. This includes atmospheric plasma spray system, Microwave ECR Plasma system, Electron Beam melter and welding machine and pulsed solid-state laser system for metallography. Some of the significant contributions are:

- Development of corrosion resistant ceramic-alloy duplex coatings for strategic and specialized nuclear applications
- Development of Plasma Aerosol Generator at Nuclear Aerosol Test Facility (NATF) for metal/ceramic aerosol generation
- Electron Beam processing equipment for welding
- Microwave plasma processing system for deposition of diamond like carbon
- Wire arc plasma torch development for metal deposition

11.1 PLASMA SPRAY COATINGS

One of the major on-going research programmes is the development of metal, alloy and ceramic coatings for Nuclear Fuel Cycle and other advanced applications. A dedicated 40 kW DC Arc Plasma Spray System, developed indigenously, is being regularly used to deposit metals, alloys and ceramics for specialized nuclear applications.

- **Nickel (Ni)-Chromium (Cr)-Aluminium (Al)-Yttrium (Y)-Yttria stabilized zirconia (YSZ) coatings**

The 40 kW atmospheric plasma spray system has been adapted for developing NiCrAlY-yttria stabilized zirconia duplex coatings, which have potential application in high temperature reactors. NiCrAlY-yttria stabilized zirconia has been deposited on inconel substrates. It is observed that the coating characteristics are affected by the input power to the torch. Electron probe microanalysis (EPMA) of the coatings shows that the coating adherence is good and that



Atmospheric Plasma Spray System

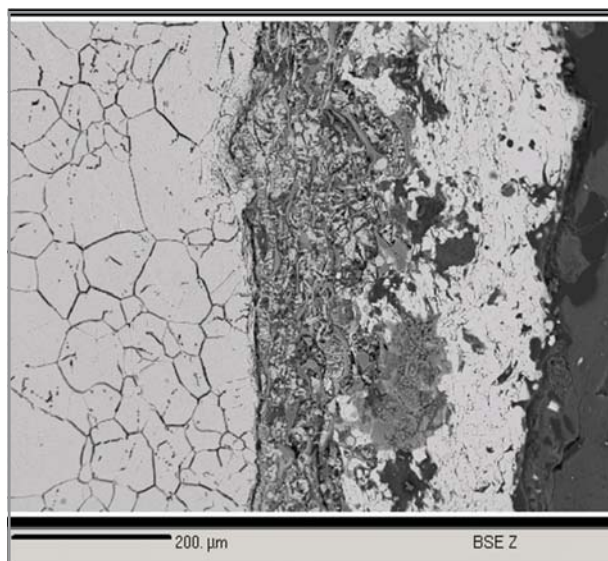


Powder-Laden Plasma Jet

there is negligible oxygen pick-up by the alloy during deposition. The top zirconia layer is also seen to be quite adherent to the bond coat. The elemental profiles for nickel,

zirconium and yttrium indicate that there is no interaction between the ceramic layer and the bond coat.

Theoretical modelling of particle behaviour in a thermal plasma jet is important for process control and coating optimization.



SEM of NiCrAlYYSZ on Inconel substrates

- **Particle Trajectory and Temperature History in the Plasma Jet**

A theoretical model for predicting the in-flight velocity and temperature of particle along the flow direction of plasma spray torch has been developed. The solution of these equations gives the axial velocity, radial velocity and temperature distribution in the plasma region. Results of the modelling studies supplemented by thermo-chemical studies on the stability of aluminium oxide offer useful guidelines in optimizing the spray process. This mathematical model has also been extended to in-flight reaction in the plasma medium.

- **High Power Induction Coupled Plasma Reactor**

A remotely controlled 50 kW RF Induction Plasma Reactor has been developed for materials processing applications.

The reactor consists of a high power triode based oscillator, an induction coupled plasma (ICP) torch, reaction chamber and associated vacuum and remote control instrumentation systems. The reactor would be used for plasma spheroidization work.



4 MHz 50 kW RF Plasma Reactor

Proceedings of DAE-BRNS Workshop on Plasma Surface Engineering, BARC, Mumbai 2004,

Padmanabhan P.V.A., Thiyagarajan T.K., Sreekumar K.P., Satpute R.U., Venkatramani N. and Ramachandran K., *Surface & Coatings Technology*, 168, (2003) p.231,

Satpute R.U., Sreekumar K.P., Thiyagarajan T.K., Kakade M.B., Padmanabhan P.V.A. & Venkatramani N., *Power Beams & Materials Processing*, ed. A.K. Das et.al, Pub. Allied Publishers, ISBN No. 81-7764-353-3, (2002) 369.

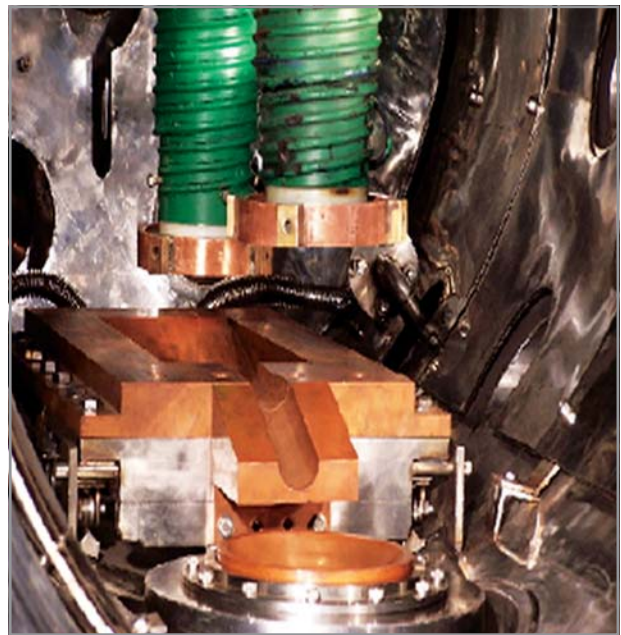
S.Das, S.C.Mishra, P.V.A.Padmanabhan, K.P. Sreekumar and P.V.Ravindran., *Power Beams & Materials Processing*, ed. A.K. Das et.al, Pub. Allied Publishers, Paper No. 4.15, ISBN No. 81-7764-353-3, (2002)

S.C.Mishra, R.Mishra, S.Mishra, S.S.Das, K.P.Sreekumar and P.V.A.Padmanabhan., *Power Beams & Materials Processing*, ed. A.K. Das et.al, Pub. Allied Publishers, Paper No. 4.16, ISBN No. 81-7764-353-3, (2002).

■ Design of Plasma Systems

High Power Plasma Melter:

High power DC arc plasma torches for use in plasma melter have been designed, developed and qualified at 300 kW rating and melting of iron scrap has been carried out at atmospheric pressure. The torches have been mounted on a demonstration twin-torch 450 kW melter for melting reactive alloy scraps. The melter is equipped with appropriate high vacuum system, complex torch handling device and ingot retraction system. 150 mm dia and 300 mm long ingots can be processed in one batch.

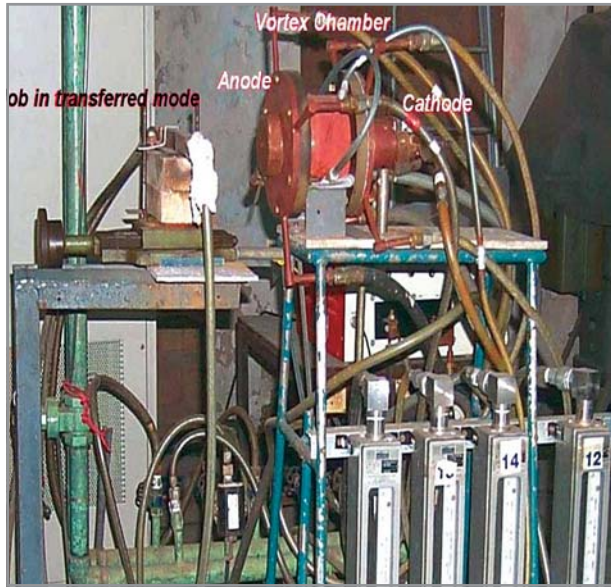


450 kW High power Plasma Melter

Copper Hollow Electrode Plasma Torches :

DC arc hollow copper electrode torches have been developed and operated in both transferred as well as non-transferred arc modes up to 100 kW using air as the plasmagen gas.

The use of air-operated plasma torches in metallurgical applications significantly reduces the processing cost and avoids contamination of the product by tungsten, which is normally used as the cathode. The arc roots were rotated vigorously using magnetic field coils to avoid electrode erosion.



Copper Hollow Electrode DC Arc Plasma Torch Set-up

Under Water Plasma Cutting Torch System for weak alpha active waste:

A 50 kW underwater plasma-cutting facility has been established (Torch and Power Source) for decontamination and dismantling of alpha active waste inside water pool at a depth of 2 meters. Linear cuts up to a meter at 10-30 cm/min and mid-plate puncturing were demonstrated to the user group at Nuclear Recycle Group.

Ghorui S., Tak A.K., Sahasrabudhe S.N., Murty P.S.S. & Das A.K., <sghorui@barc.gov.in>

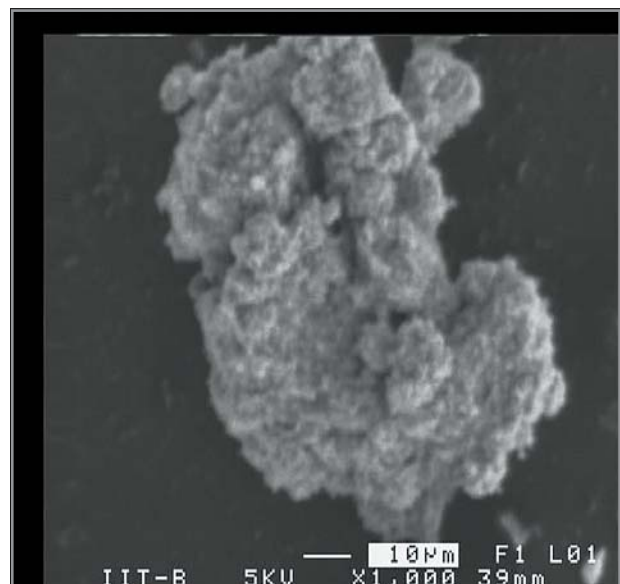
■ **Thermal Plasma Synthesis of nanocrystalline materials**

Ultrafine titanium dioxide powder shows photo catalytic properties and is widely used in water and air purification applications. Nanocrystalline titania has been synthesized by reactive thermal plasma processing using TiH_2 , or titanium metal powder as the starting material. The hydride or the metal was injected into the thermal plasma jet and air was injected downstream. Titanium oxide formed deposits on the reactor walls as nano-sized powder. The process is ideally suited for bulk synthesis of nano-sized ceramic powders.

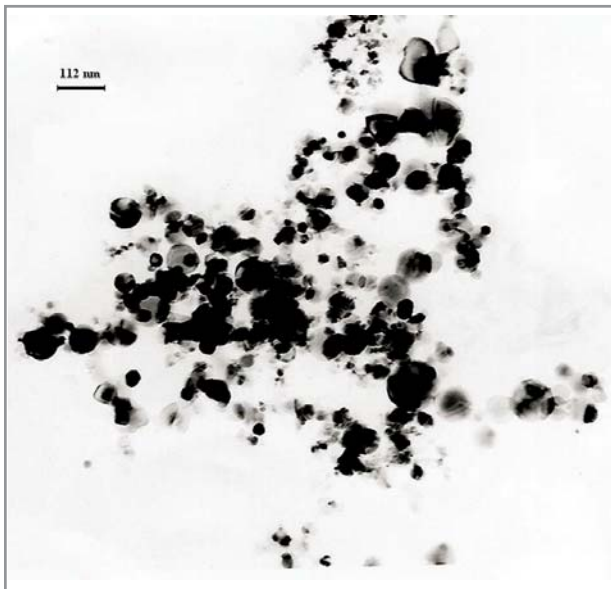


(Top left): Power supply and control console;
(top right) Plasma torch;
(bottom left): SS sheet under water;
(bottom right): Plasma-cut SS sheet

X-ray diffraction of the synthesized powder showed almost complete conversion (>95%) of the feed material to oxide. Metastable anatase phase is formed predominantly. Scanning electron micrograph of a typical sample of the synthesized powder shows clusters of nanocrystallites of TiO_2 . TEM of



SEM photograph showing nanoclusters of titanium oxide



TEM Photograph of nanocrystalline TiO₂

the sample shows well-resolved nano sized particles with more than 70% lying in the range of a few nanometers to 20 nanometers.

P.V.A.Padmanabhan, T.K.Thiyagarajan, K.P.Sreekumar, N.Venkatramani and P.R.Taylor, *Power Beams & Materials Processing*, ed. A.K. Das et.al, Allied Publishers, ISBN No. 81-7764-353-3 (2002) p. 361

P.V.A.Padmanabhan, T.K.Thiyagarajan, K.P.Sreekumar and N. Venkatramani., *Scripta Materialia*, 50 (2004), p. 143-47.

■ **Microwave Electron Cyclotron Resonance (ECR) Plasma Processing facility**

A 2.45 MHz, 1.5 kW large volume (200 mm dia and 200 mm height) ECR plasma system has been developed. The system consists of ECR plasma generation chamber, processing chamber, substrate holder, microwave components, water cooled electromagnets and associated power supplies. The system has been successfully commissioned and stable ECR plasma generation has been obtained.

A RF generator (13.56 MHz, 300W) and Matching network have been integrated with the substrate floated in a microwave ECR plasma.



2.45 GHz 1.5 kW ECR Plasma system

The facility has been used to deposit uniform, hard and scratch-proof Diamond like Carbon (DLC) coatings on 4" diameter silicon substrate with RF self-bias on the substrate. This facility would also be used for various applications like Plasma CVD, nitriding, carbonitriding and deposition of large area coatings of diamond for self-biasing purpose.

Pandey M., Bhattacharya D., Patil D.S., Ramachandran K., Venkatramani N. and Dua A.K., *J. Alloys and Compounds* 386 (2005), p. 296-302.

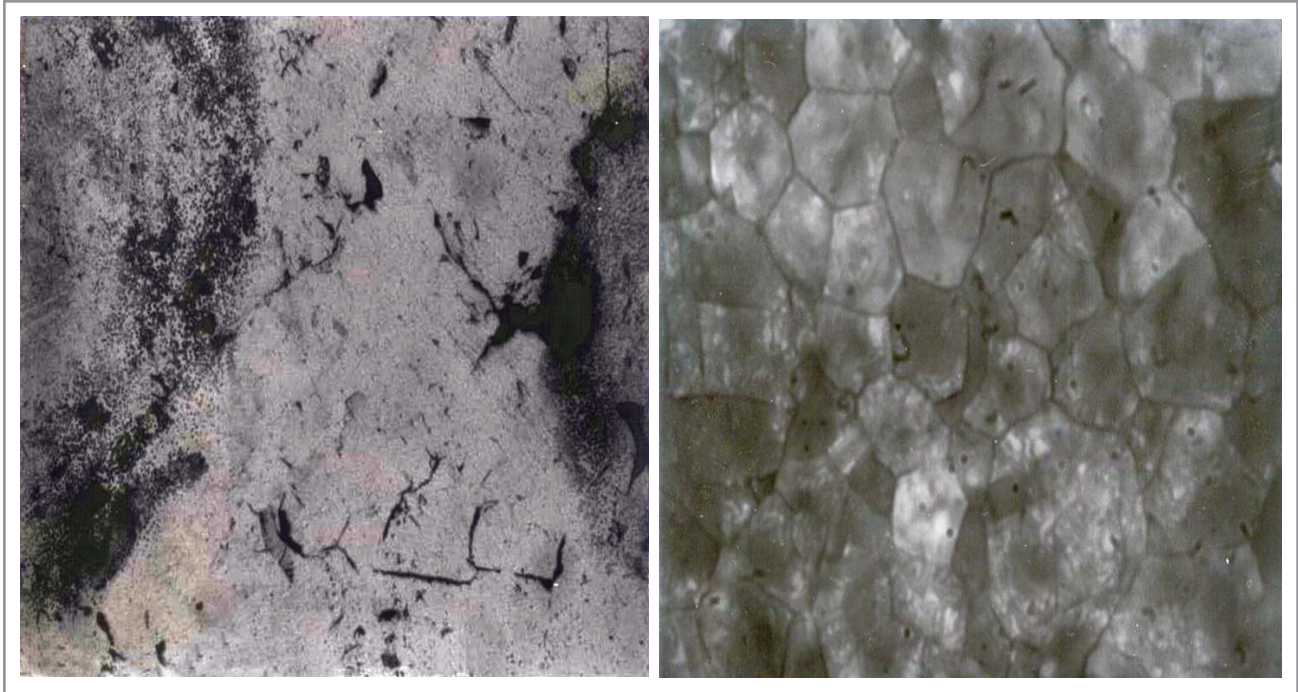
Diamond like Carbon Coatings : AFM and Ellipsometric Studies, M. Pandey, D. Bhattacharya, D. S. Patil, K. Ramachandran and N. Venkatramani, *Surface and Coatings Technol.* 182 (2004), p. 24-34.

Singh S.B., Chand N., Dey R.M. and Patil D.S., *Allied Publishers Pvt. Ltd*, ISBN 81-7764-656-7, p.267-268, 2004

Mukherjee S., Saha T.K., Patil D.S., Sirsat A.N. and Ray A.K., *Allied Publishers Pvt. Ltd*, ISBN 81-7764-656-7, p. 298-299, 2004

Balasubramanian C., Godbole C.P., Rohatgi V.K., Das A.K. and Boraskar S.V., *Nanotechnology*, 15, p. 1-4, 2004.

Bhoraskar S.V. and Das A.K. (Eds), *A manual of Experiments, International Host lab experiments on Synthesis of nanomaterial by thermal plasma*, 17th Nov-1st Dec., 2004, Pune, India, Ebenzer Press, ISBN : 81-8811-3, 2004



Untreated (left) and laser-etched ThO₂ pellets revealing grain structure (right)

11.2 LASER ETCHING OF THORIA PELLETS

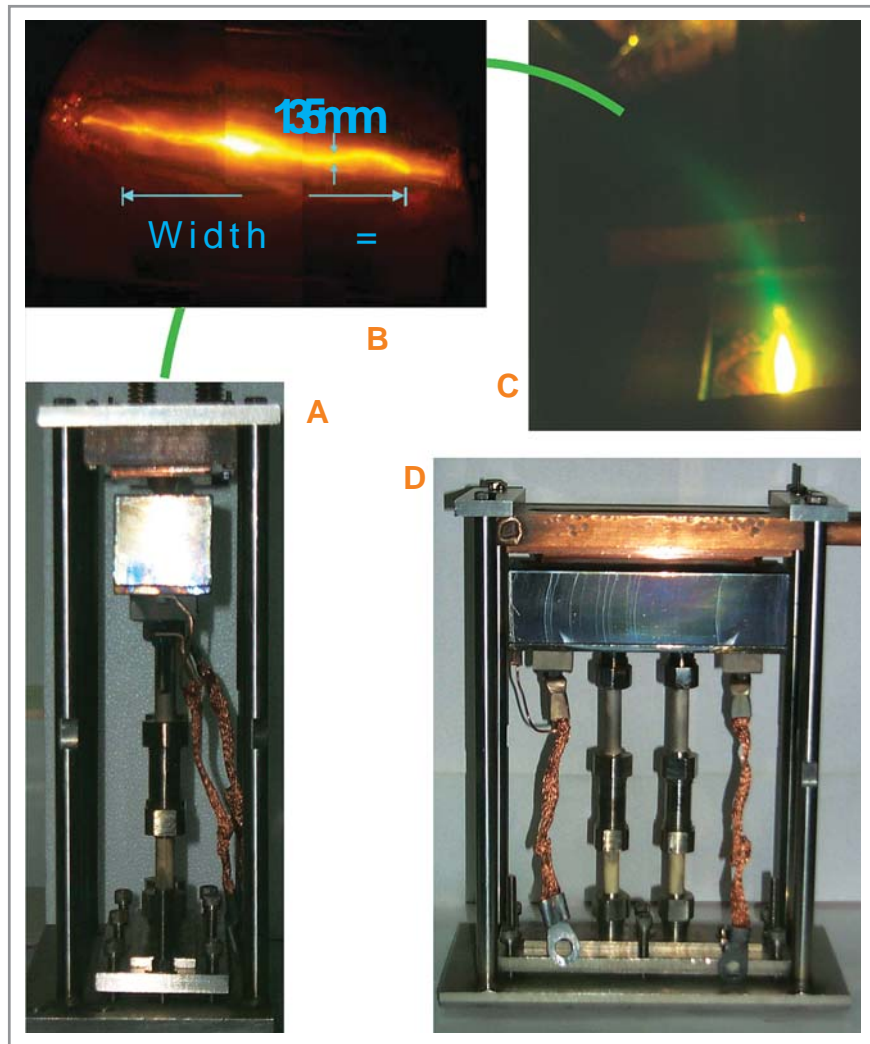
Laser-based surface etching is a potential technique for surface etching of irradiated ThO₂ fuel for metallographic evaluation. A laser-based process generates far lesser volume of active waste in comparison to conventional processes. Preliminary tests on un-irradiated ThO₂ pellets using a pulsed Nd:YAG laser have produced reproducible etching clearly revealing grain structures and well defined grain boundaries (Figure). Details such as, optimum laser parameters leading to laser ablation of surface layers without causing laser induced surface damage via fragmentation, melting and vitrification are being determined.

Sucharitha Sinha, Dasgupta K., Ramadasan E. and Jathar V.P.
<ssinha@barc.gov.in>

11.3 ELECTRON BEAM PROCESSES

■ 100 kW Strip Electron Beam (EB) Gun for Material Processing

A 180° deflection, 130 mm-strip EB gun has been designed, developed and tested for its performance upto 80 kW on copper target placed in a water-cooled copper crucible. This configuration of gun and crucible was found to have many advantages over 270° gun with respect to crucible such as: 1] smaller beam width (<4 mm), 2] focal strip length same as filament length, 3] smaller low intensity tails on either sides of main beam due to AC heating of filament, 4] smaller molten pool resulting in high evaporation rate. The photograph below shows the 180°-bent 130 mm-strip electron gun alongwith molten copper target surface. The green emission by excited copper seen in the photograph can be used to know exact volume of physical overlap of electron beam and atomic beam.



100 kW Strip Electron Beam (EB) Gun

A: Strip Electron Gun in 180° configuration,

B: Electron beam on copper target; Dimension 135 mm x 3.6 mm; Power 56 kW, (the green curve mimics the path of the electron beam),

C: Emission in green spectral region during de-excitation of electron heated copper atoms, which can be used to know physical overlap of electron beam and copper atom beam,

D: Strip Electron Gun in another view showing grid cup, anode, high voltage insulators, electrical connectors and vertical stand

Thakur K.B. and Sahu G.K., *Journal of Physics D* 35 1812-20(2002)

Thakur K.B. and Sahu G.K., *Vacuum, Surface Engineering, Surface Instrumentation & Vacuum Technology*, 75 (2004), p. 283-92

Thakur K.B., Sahu G.K., Gaur S.J., Das R.C., Tak A.K., Patankar R.A., Bhowmick G.K., Manohar K.G., Jagatap B.N. and Venkatramani N., *Vacuum (Surface Engineering, Surface Instrumentation & Vacuum Technology)*, 77 (2005), p. 443-49

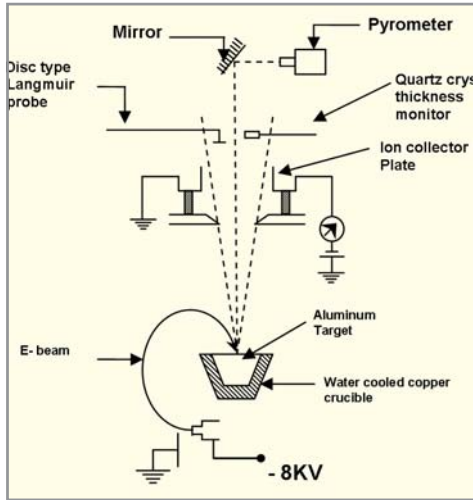
Gaur S.J., Das R.C., Tak A.K., Sahu G.K., Patankar R.A., Bhowmick G.K., Manohar K.G., Thakur K.B. and Jagatap B.N., *BARC Newsletter*, 237, (2003)

“Design Development and Performance of a Strip Electron Gun; A Two Dimensional Source for High Evaporation Rates” by K.B. Thakur and G.K.Sahu; 7th International Conference on ELECTRON BEAM TECHNOLOGIES (EBT’2003) Verna, Bulgaria (1-6 June 2003)

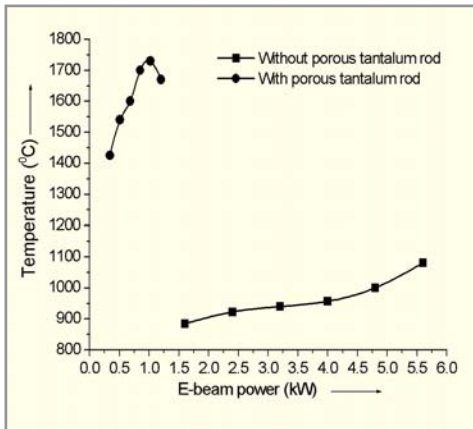
Thakur K.B., Sahu G.K. and Patankar R.A., BARC/2002/R/004

■ **Efficient Electron Beam Evaporation of aluminum with a porous tantalum Rod in Melt Pool**

During electron beam heating significant evaporation occurs at temperatures substantially higher than the melting point. This leads to situations where convective heat transfer in the



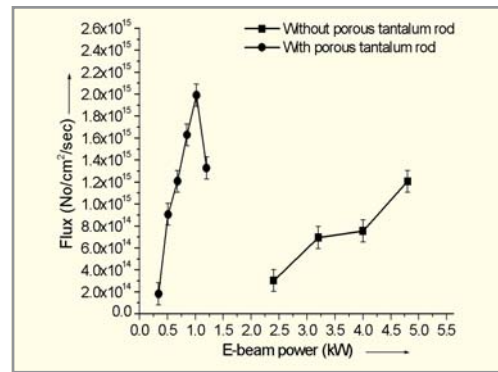
Schematic of the experimental system



Temperature vs. E-beam power

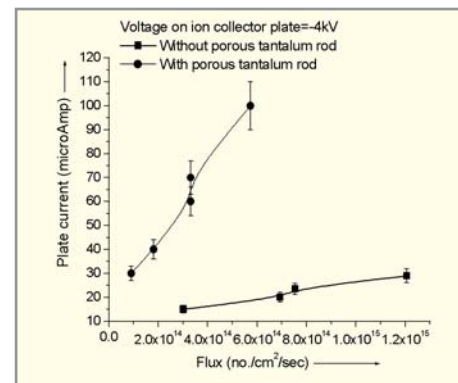
molten pool of target plays an increasingly dominant role with increase in incident e-beam power and puts a clamp on the surface temperature (and consequently the atomic flux). To mitigate this heat drain, a porous tantalum rod (~35% porosity) was placed at the point of e-beam impact point to act as a convection arrestor and the molten aluminum around the porous rod was found to ooze through

the capillaries of the porous rod to emerge as a vapor stream. On measuring the atomic flux and surface temperature at e-beam powers (below a value where tantalum softens),



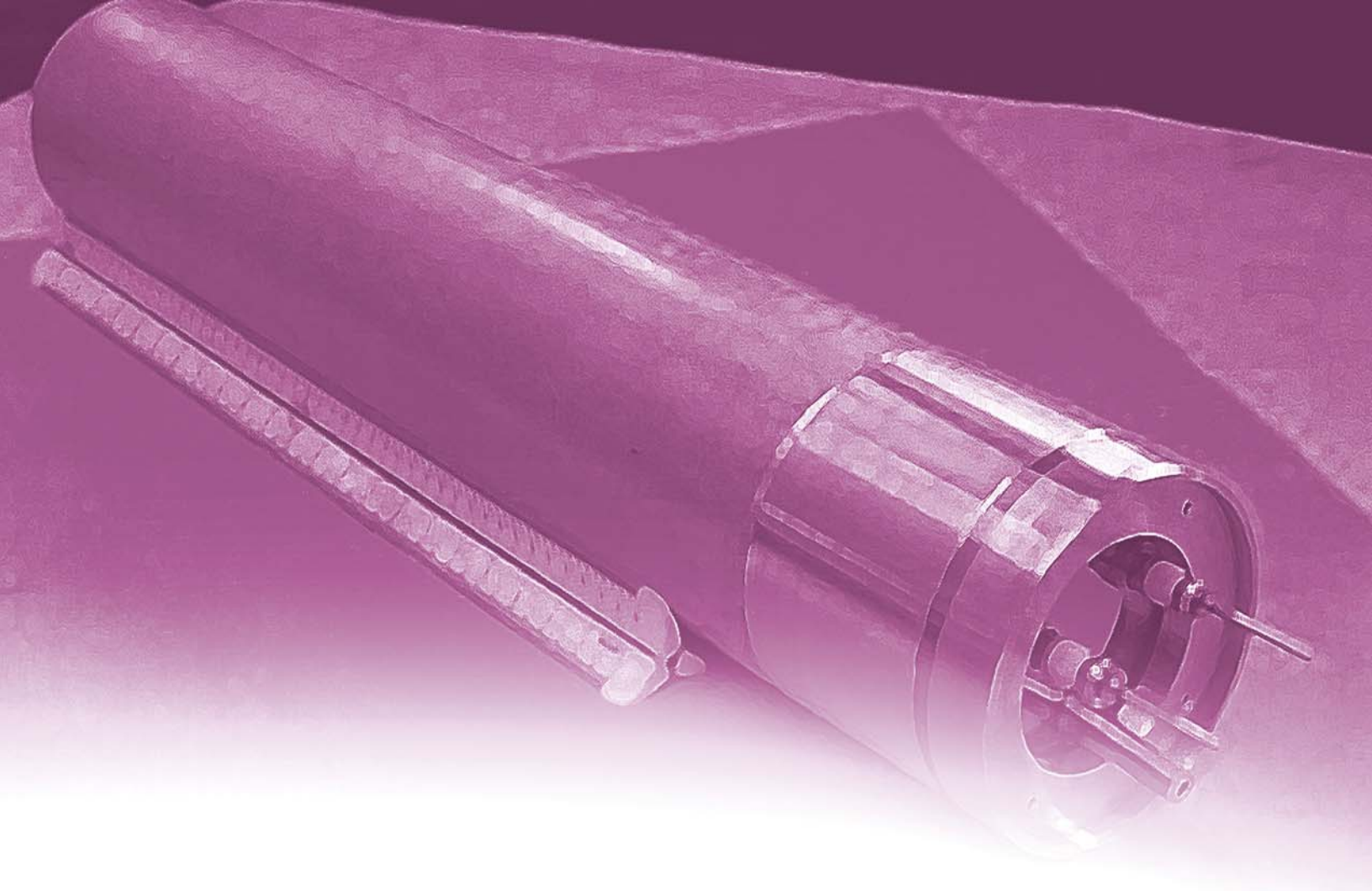
Atomic flux vs. E-beam power

it was found that ~50 % higher temperature was reached with the tantalum rod than without it. Also, the required e-beam power in the case of porous rod was about ~ 1/6th of the e-beam power required without the rod. In this experiment, ion content in the vapor stream was also measured. It was found that the ionization yield in case of porous rod was about five times the yield without the rod.



Estimation of ionization yields due to various processes led to a conclusion that higher ionization in the case of porous rod can be attributed to a higher emission of secondary electrons from the porous rod causing enhanced electron impact ionization.

Dikshit B., Zende G.R., Bhatia M.S. and Suri B.M., J. Phys. D - Appl. Phys., July (2005).



12. ADVANCED TECHNIQUES OF JOINING OF MATERIALS

INTRODUCTION

Modern technologies need the use of materials with diverse physical and chemical properties and these materials need to be joined. These materials cannot be conventionally fusion-welded due to thermal expansion mismatch, development of residual stresses, porosity and formation of undesirable brittle intermetallic phases in the weld zone. Solid state bonding processes can obviate these problems and can provide good joints. The processes are economical, clean and eco-friendly.

The solid state bonding techniques include diffusion bonding, transient liquid phase bonding, friction stir welding, electromagnetic forming.

12.1 SOLID STATE DIFFUSION BONDING

Diffusion bonding is an attractive solid state joining technique where two dissimilar materials are joined under the application of heat and pressure preferably in vacuum environment. Due to micro-deformation of surface asperities and diffusion across the interface, metallic bond forms at the interface of two materials. The temperatures used are well below the melting points of the parent materials and the applied pressure is low to avoid bulk deformation. Interlayers are sometimes used to avoid the formation of brittle intermetallic compounds, to prevent diffusion of undesirable elements and minimise the thermal expansion mismatch.

■ Metal-metal joints

Copper / Stainless Steel

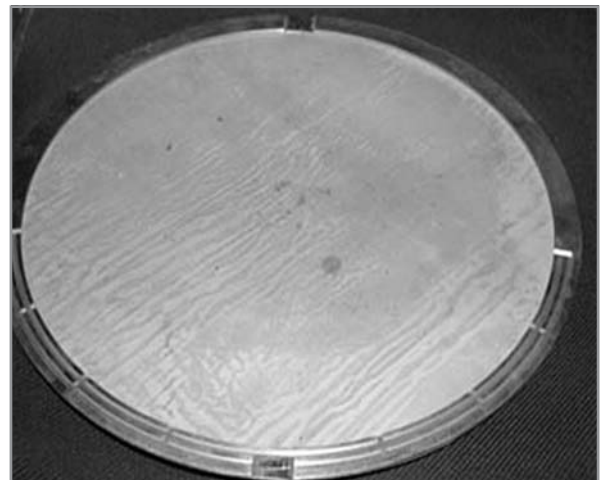
Oxygen Free High Conductivity (OFHC) copper is used for fabricating the tuneable disc for linac accelerator. Stainless steel stud is joined to this tuneable disc to manipulate the air gap between it and resonator cavity. OFHC copper has been joined to stainless steel (AISI 304) using Ni as an interlayer. The bonding has been carried out in the temperature range of 750°–900°C for a duration of 1 hour at the pressure of 10-20 MPa. The strength of bond is higher than 220 MPa and the joint fails at copper side.



Tuneable Disc

Porous Nickel / Stainless Steel

The porous nickel electrode is an important component in a compact water electrolyser for the production of hydrogen. The thin porous nickel mesh is to be joined to support stainless steel. Stainless steel ring was plated with 10-20 μm thick nickel and bonded to nickel mesh at the temperature



Porous Nickel/SS electrode

of 800° C for 1 hour under 10MPa pressure. The strength of joint is superior to parent porous nickel (35 MPa).

Aluminum / Stainless Steel

Joining of SS to Al is required for various applications in DAE programmes:

- Environmental Ion Chambers (CIRUS)
- End Window for Thickness Gauging Ion Chamber
- Cold Neutron Source Assembly (DHRUVA)
- Working Area Ion Chambers 2.5 GeV Electron Accelerator (INDUS II, Indore)

For joining of SS to Al various interlayers were selected and deposited one over another on both the parts. The Choice of interlayer is governed by the following requirements

- Mutual compatibility between the two layers
- No Intermetallic formation
- Similar thermal expansion



Compatible multilayers for diffusion bonding of stainless steel to Aluminium

Detailed study as tabulated below on diffusion bonding of Al to SS was performed by varying the temperature, pressure and duration. The properties obtained under optimum conditions are also highlighted in the table below.

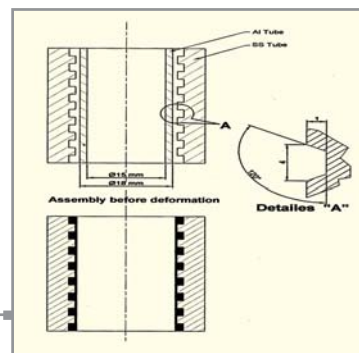
Conditions of Bonding	
Temperature	300 – 500°C
Duration	2 to 4 hours
Pressure	40 to 50 MPa
Properties (Optimum Conditions)	
Bond Strength	185 MPa
Elongation%	23

The joining technology has been successfully used for making cold neutron source and ¹⁰B-lined neutron detector assemblies. Currently it is being utilised for development of working area ion chamber for INDUS II project.



¹⁰B-lined Neutron detector

The tubular products were also joined by similar technique (three interlayers on both the parts) and utilising corrugated design in SS tube and deforming Al tube from inside on SS tube as shown schematically in figure below.



Assembly before and after deformation

Predeformed and Diffusion Bonded tubular products were tested for the followings and found to be successful.

- Thermal cycling between 25– 250°C (500 cycles).
- No cracks along the bonding region at a bending angle of 40° or more.
- EPMA concentration profile was smooth throughout the bonding region indicating non-formation of brittle intermetallics.
- Optical micrographs along the cross section show no pores and voids.

K. Bhanumurthy, D. Joyson derose, G.B. Kale and J. Krishnan, *Materials Science and Technology*, 20(8) (2004), p.1059-1063.

K. Bhanumurthy, G.B. Kale, R.K. Fotedar, A.L. Pappachan, A.K. Grover, *Metallurgical Transactions A* (2006).

Mary Alex, K.R. Prasad, A.L. Pappachan, A.K. Grover, J. Krishnan, D.J. Derose, K. Bhanumurthy and G.B. Kale, *Proc. of BRNS conference on compact nuclear instrumentation and radiation detector*, Jodhpur (2005) p.95.

12.2 CERAMIC - METAL SEALS

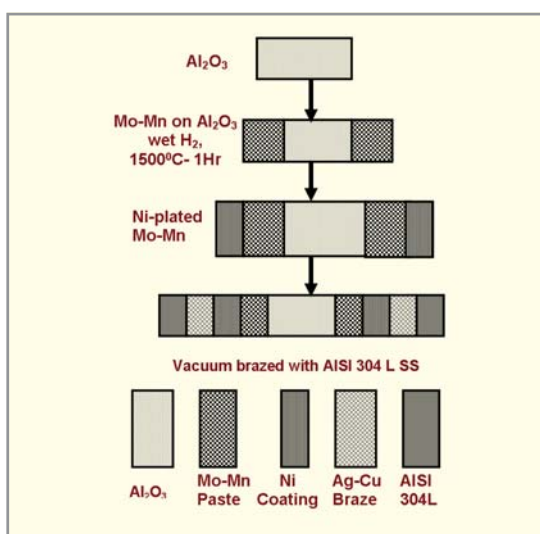
Joining of ceramic component to a metal finds wide applications in electronics and for UHV applications. The advantages of ceramic materials, for example high operating temperatures, good chemical stability low conductivity and high wear resistance can be combined with the better known

properties of metals. The process has been exploited to develop ceramic-to-metal seals which play an important role in manufacturing of various vital components in many DAE requirements.

■ **Moly-Manganese (Mo-Mn) Process**

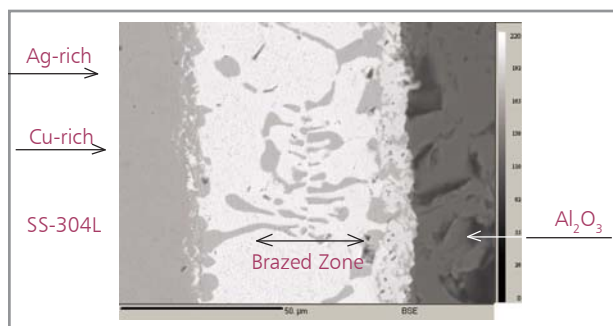
A process based on Mo-Mn has been developed for manufacturing of ceramic to metal seals. The complete flow sheet is outlined below.

A BSE image of SS to alumina brazed zone is shown here.



Schematic diagram showing important stages of brazing SS to Al₂O₃ via Mo-Mn process

There exists good contact between SS/brazed reaction zone/ Al₂O₃. The vacuum brazed seals prepared under optimized conditions (820°C, 20 minutes) gave good joints with helium gas leak rate better than 10⁻⁹ std. cc. s⁻¹.



BSE Image of Al₂O₃/304L brazed with Ag-Cu alloy



Photograph of C/M Seals

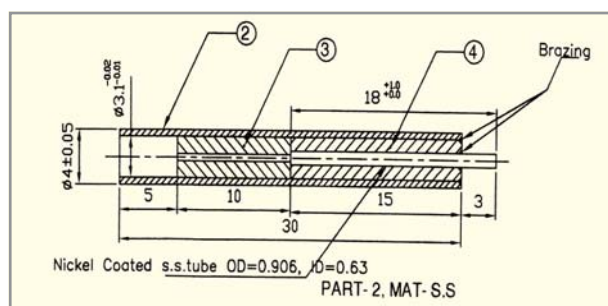
■ **Active Brazing**

Developments of components for sodium leak detector (FBR):

Most structural ceramics e.g. Al₂O₃, ZrO₂ etc. will not be wetted by traditional brazes unless the braze contains an active element such as Ti, V and Zr. Active elements of the braze material reacts with ceramics and forms bonding by the redox reaction.

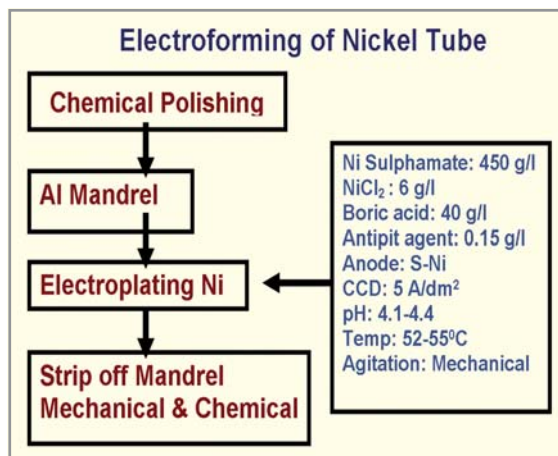


The process of active brazing has been utilized to develop composite Ni/ Al₂O₃/ SS structure required for development of extended spark plug type sodium leak detectors. Titanium activated Ag-ABA braze alloy (solidus Temp. 860°C) has been used for brazing the composite assembly.

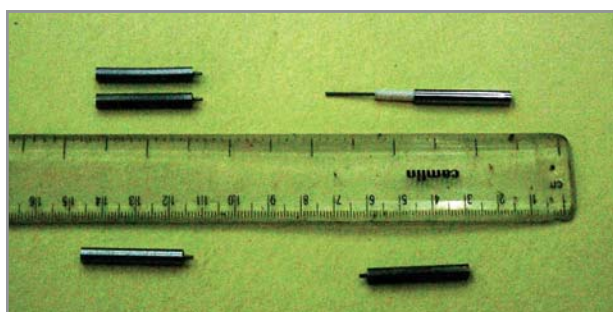


Extended spark plug type sodium leak detector

Nickel tubes required for the application have also been fabricated in-house by electroforming method using nickel sulphamate bath (due to non-availability of tubes of non-standard dimensions).



The brazed structures have been subjected to thermal cycling to qualify for reactor application. The brazed assemblies will be utilized to make sodium leak detector for the FBR project.



Sodium Leak Detector

P.Mishra, P.Sengupta, S. N. Athavale, A. L. Papachan, A.K. Grover, A.K. Suri, G.B. Kale and K. Bhanumurthy, *Metallurgical Transactions A* (2006).

A. Laik, K. Bhanumurthy, A. L. Papachan, S.N. Atahvle, A.K. Grover, G.B. Kale Editor: V.S. Pandit, *Proc. of Indian Particle Accelerator Conference, VECC, Kolkata, 1-5 March* (2005), p.494-495.

■ Lithium zinc silicate glass

Ceramics-Metal seal

Glass-ceramics derived from the base glass of $\text{Li}_2\text{O-ZnO-SiO}_2\text{-Na}_2\text{O}$ and B_2O_3 , etc. can be prepared with a wide range of thermal expansion coefficients (from 50×10^{-7} to $200 \times 10^{-7}/^\circ\text{C}$) by controlling heat treatments LZS glasses containing $\text{Li}_2\text{O-ZnO-SiO}_2\text{-Na}_2\text{O-B}_2\text{O}_3\text{-P}_2\text{O}_5$ were prepared. The seal fabricated with optimal heating schedule and dwell time at melting temperature was found to

withstand a vacuum of 10^{-6} torr with helium leak rate of less than 3×10^{-10} torr litre/sec.



LZS glass-ceramic to metal seal

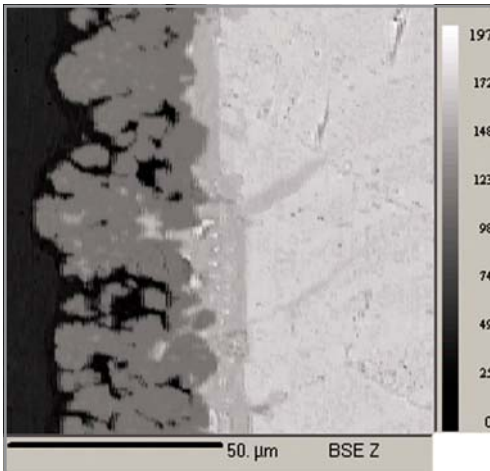
B Indrajit Sharma, Madhumita Goswami, P Sengupta, V K Shrikhande, G B Kale, and G P Kothiyal, *Materials Letters*, 58(2004) p.2423.

G P Kothiyal, B I Sharma, V K Shrikhande, M Goswami, and J V Yakhmi, *Key Engineering Materials*, 280-283(2005) p. 947.

12.3 TRANSIENT LIQUID PHASE BONDING

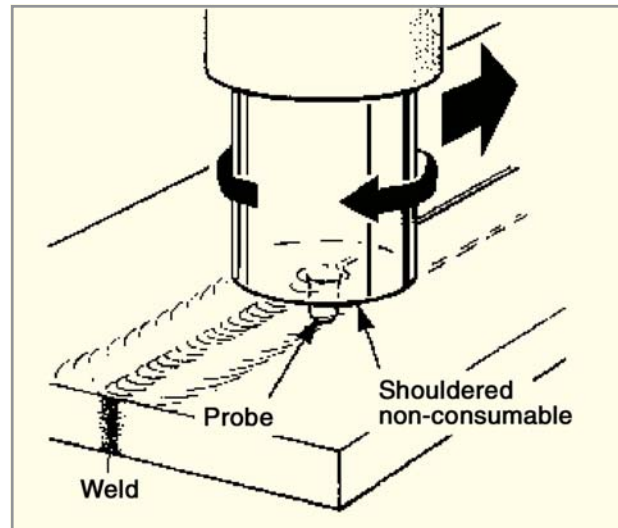
Transient liquid phase (TLP) bonding involves the use of interlayer of low melting point at the interface. The assembly of the materials to be joined is heated above the melting point of interlayer. The constituents of the material diffuse in liquid film formed by melting of the interlayer. The melting point increases with the dissolution of constituents and liquid film solidifies and joining is accomplished. The method is fast and requires small time. Not much surface preparation is required. It is useful for high temperature and hard materials.

Alumina has been bonded to 304 stainless steel by transient liquid phase bonding technique using Zr as interlayer. Good bond can be obtained at 950°C . The reaction zone shows the formation $(\text{ZrFe}_2 + \text{FeCr})$ region, region of eutectic Zr-Fe and $\beta\text{-Zr(Fe)}$ solid solution. The bond strength is around 65 MPa.



Reaction zone between SS and Zr layer

P.S. Gawde, G.B. Kale, P. Sengupta <psgawde@barc.gov.in>



Friction Stir Welding

12.4 EMF (ELECTRO-MAGNETIC FORMING) TECHNIQUE

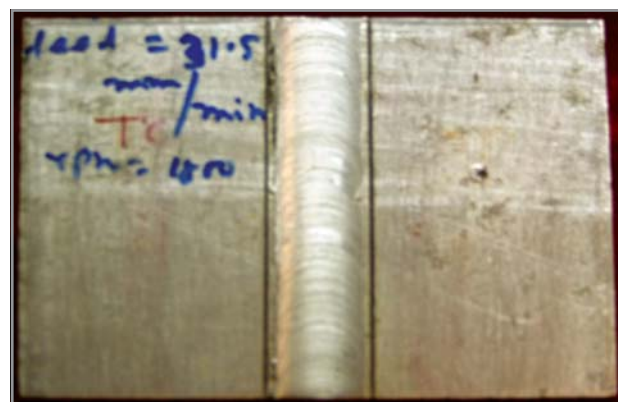
This technique uses electromagnetic energy induced by a large electric current fed by a capacitor bank through a coil. When a coil is placed in a tube and a portion of the tube is surrounded by a thick tube, the tube traverses the space between them at a high speed and collide against the thick tube causing joining/ welding between the two. This technique can be used for high-pressure system where joint has to withstand very high internal pressure. Examples are tube to tubesheet of calendria shell of PHWR, tube to end sheet of heat exchanger, UHV system etc. EMF Joining Technique may prove to be a prospective method of joining.

About fifty test samples were tried for Al to Al joint. The following results were obtained

- Leak rate $< 1 \times 10^{-10}$ std-cc/sec
- Hydro test results no leakage of water at 30 kg/cm²
- Pull out test shows the joint is stronger than the Al tube.

12.5 FRICTION STIR WELDING

Friction stir welding(FSW) is a solid state joining process which uses non-consumable tool to generate frictional heat at the

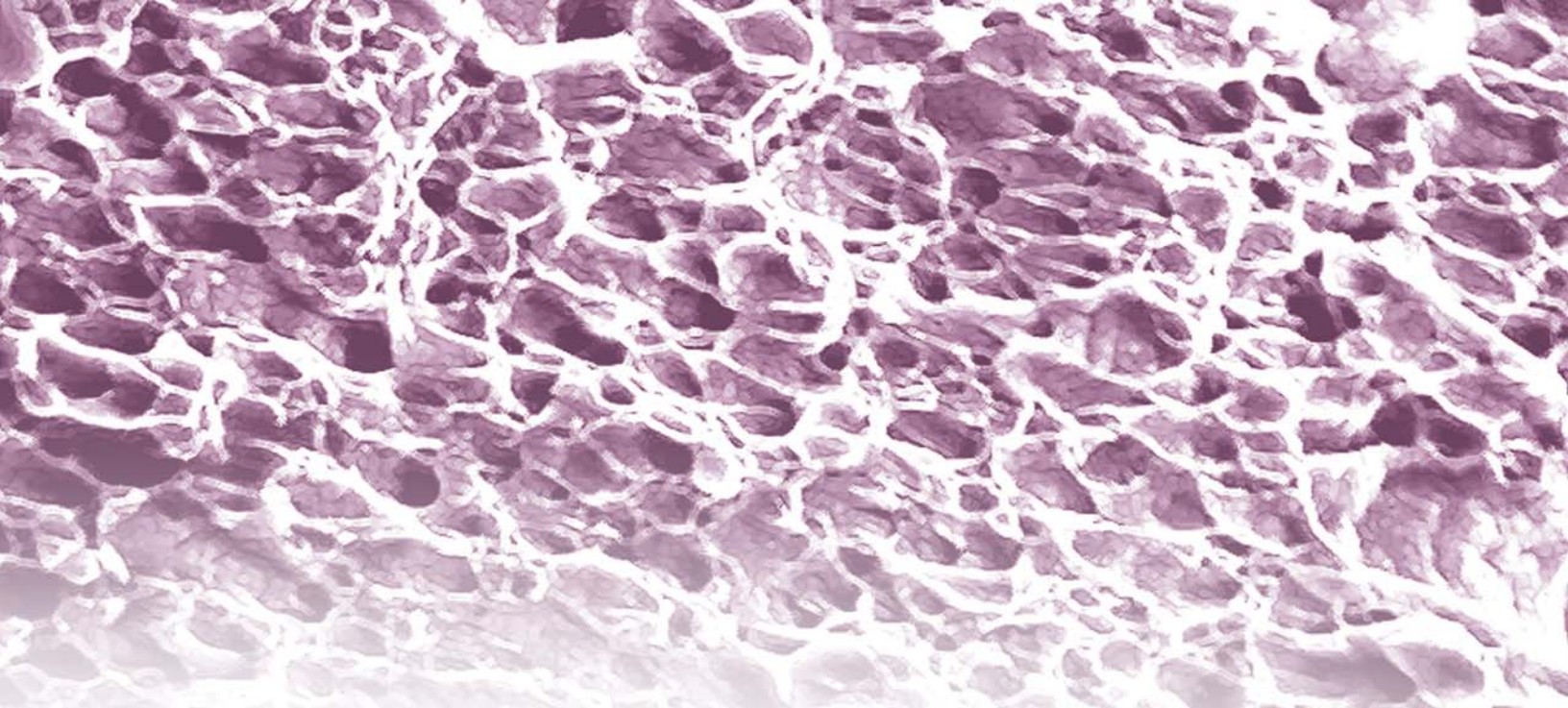


Al -Al Joint made by FSW

point of welding joint. When a high speed rotating tool makes contact at the joint, frictional heat is generated between the wear-resistant welding tool and the material of the work pieces. This causes the latter to soften to the plastic stage without reaching melting point. This allows traversing of the tool along the weld line. The plasticised material is stirred by the leading face of the tool and transported to the trailing face where it leaves a solid state bond between two pieces to be welded.

A trial piece joining aluminium (Al) to Al metal is shown in the figure. Radiography test shows no porosity on the weld.

S.C. Ojha <scojha@barc.gov.in>



13. CORROSION AND COMPATIBILITY STUDIES

INTRODUCTION

Tailoring the properties of structural materials has always been an important aim of research in the field of materials science. Recent work has shown that the corrosion properties of austenitic stainless steels can be tailored by grain boundary engineering. Thermo-mechanical processing of these materials has been shown to improve the resistance to sensitization, intergranular corrosion and intergranular stress corrosion cracking. It has been shown that cold pilgering can be used to improve the corrosion resistance of austenitic stainless steels.

While the degree of sensitization of stainless steels is commonly evaluated by the Electrochemical Potentiokinetic Reactivation (EPR) test, the science behind the test is sought to be established in the current studies. The EPR (single loop and double loop) tests have been developed for alloy 800 and a single loop EPR test has been developed for alloy 600.

It is shown that the fine and uniform distribution of second phase particles in zircalloys are beneficial for resistance against nodular corrosion. A cumulative annealing parameter has been correlated to the nodular corrosion rates and the size and distribution of precipitates in zircalloys. Undesirable features in microstructures may hamper performance during service. A typical case is that of aluminum clad used for the fuel for Dhruva reactor. It has been shown that the FeAl_3 precipitates in the material are the primary reason for blister formation in the fuel clad during storage stage itself.

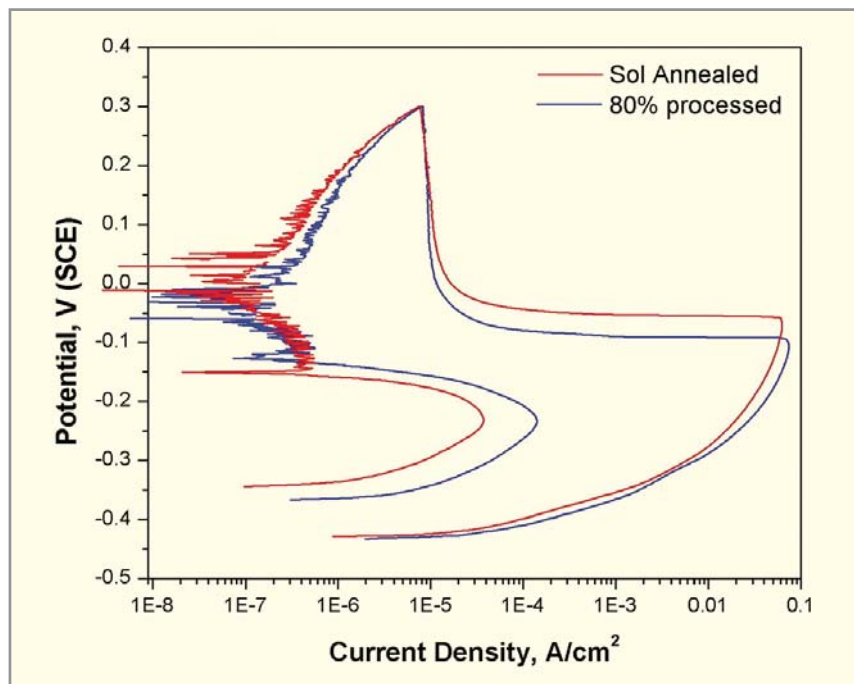
Compatibility of materials with the environment in which it has to perform needs to be established to ensure trouble-free and reliable operation during the entire designed life of the components. This has been done by establishing interaction across the thoria – zircaloy interface. Detailed analyses have shown significant diffusion of thorium (Th) along the grain boundaries and within α -Zr lattice.

Establishing the compatibility of various structural materials in molten Lead-Bismuth Eutectics (LBE) at temperatures upto 500°C is essential for Accelerator Driven Sub-critical System (ADSS). Towards this the compatibility studies of different stainless steels have been done in molten lead- bismuth eutectic at temperatures upto 500°C in static conditions. To test and qualify the structural materials for use in ADSS, thermal buoyancy driven lead bismuth loop (the Material Testing Loop (MTL)) has been fabricated. It will enhance the LBE technology database in support of the spent nuclear fuel transmutation and advanced nuclear reactor applications.

13.1 GRAIN BOUNDARY ENGINEERING TO INCREASE THE RESISTANCE TO CORROSION OF AUSTENITIC STAINLESS STEELS

This process of sensitization in stainless steels is controlled by alloy chemistry, grain size and grain boundary nature. Random boundaries have a high energy and the precipitation of carbides/nitrides is favoured at high energy boundaries. A different method that has been shown in the recent study is that of increasing the fraction of random boundaries ($S > 29$) beyond a threshold fraction to increase the resistance to sensitization. The samples of SS 304 and 316L were cold-rolled to different degrees of reduction in thickness. These samples were subjected to a controlled solution annealing heat-treatment followed by sensitization at 575°C/1h for SS 304 and at 750°C/48h for SS 316L. The susceptibility to intergranular corrosion was also tested according to Practice B, ASTM A262. These results showed that the resistance to sensitization first decreased as the cold work is increased, but above 60% cold working, the resistance to sensitization had increased significantly. The result is confirmed by the degree of sensitization (DOS) measured by the Electrochemical Potentiokinetic Reactivation (EPR) test. These samples were also subjected to susceptibility to IGSCC test according to ASTM G123 in boiling 25% NaCl solution. The 20%, 40% and 60% cold work samples were cracked after 200 hour in the test while no cracking was observed in the 80% cold worked, annealed and sensitized samples.

The fraction of random grain boundaries was measured by Orientation Image Microscopy (OIM) on the cold-worked samples followed by controlled solution annealing. There was increase in the fraction of random boundaries with increase in cold work. For 80% cold-worked and annealed sample the fraction of random boundaries had increased to 77% from 32% in the as-received condition. Thus, increase in fraction of random boundaries by ~80% cold working

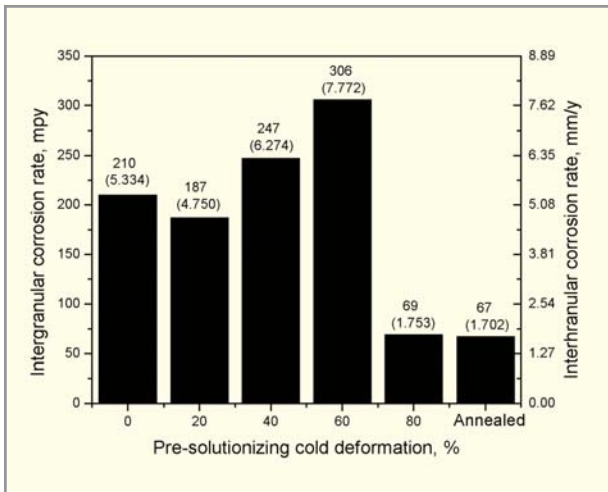


The EPR curves for SS 304 showing comparable degree of sensitization for the annealed and the thermo-mechanically processed sample.

followed by controlled solution annealing improved the resistance to sensitization, IGC and IGSCC. The effect of cold working on formation of martensite and nucleation of strain free grains during solution annealing were also studied in detail. This method of improving the resistance to sensitization has a high potential to be employed for industrial processes such as pilgering of stainless steel tubes. Therefore, a study was carried out in collaboration with NFC, Hyderabad on this aspect.

Different degrees (21%, 54% and 77%) of cold-worked tubes of type 304L stainless steel were provided by NFC. The low level of working was done by cold drawing, while medium and high levels of working were obtained by cold pilgering. Samples of these cold-worked tubes were subjected to a controlled solution annealing followed by sensitization heat-treatment. The microstructure was examined as per Practice A, A262 ASTM. Also, DOS value of these samples was quantitatively measured by EPR test. The results clearly showed lowest value of DOS for 77% cold-work sample.

The susceptibility to intergranular corrosion of the cold worked samples was measured according to ASTM A262 Practice B. The corrosion rates of all the three samples were in a narrow range of 17-20 mpy, indicating very high corrosion resistance, since the material was low carbon grade.



The intergranular corrosion rates of thermo-mechanically processed SS 304 (after sensitization heat treatment) showing comparable corrosion rate with that of the solution annealed material.

D. Wasnik, V. Kain, I. Samajdar, B. Verlinden and P. K. De, *ASM Journal of Materials Engineering and Performance*, 12, (2003), p. 402-407.

D. Wasnik, V. Kain, I. Samajdar, B. Verlinden and P. K. De, *Acta Materialia*, 50, (2002), p. 4587-4601.

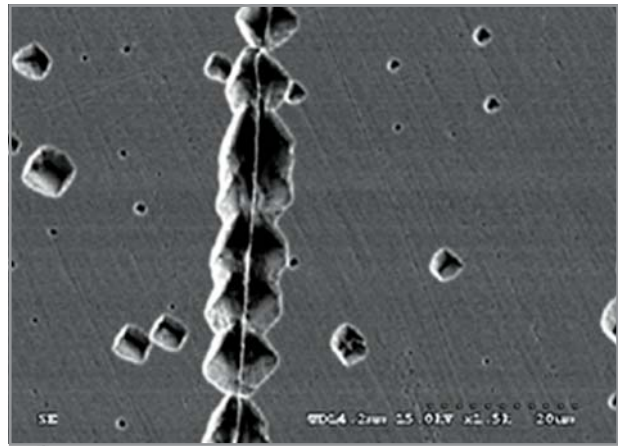
13.2 ELECTROCHEMICAL POTENTIO-KINETIC REACTIVATION (EPR) TEST TECHNIQUE

■ Development of the Test Technique to Evaluate Sensitization in Stainless Steels and Nickel Based Alloys

The Degree Of Sensitization (DOS) of austenitic stainless steels and nickel based alloys is evaluated by the Electrochemical Potentiokinetic Reactivation (EPR) test. Quantification of the degree of sensitization is needed to explain the mechanism of localized corrosion and to predict the crack growth rates in nuclear reactors. A single loop Electrochemical Potentiokinetic Reactivation (EPR) test method has been developed for alloy 600. The test conditions established are given below:

Test parameters of SL-EPR test for alloy 600

Test solution	0.01M H ₂ SO ₄ + 0.0001M KSCN (deaerated)
Temperature	30 ± 1°C
Surface finish	1 μm
Vertex potential	+700 mV (SCE)
Hold time	10 min.
Scan rate	0.5 mV/s



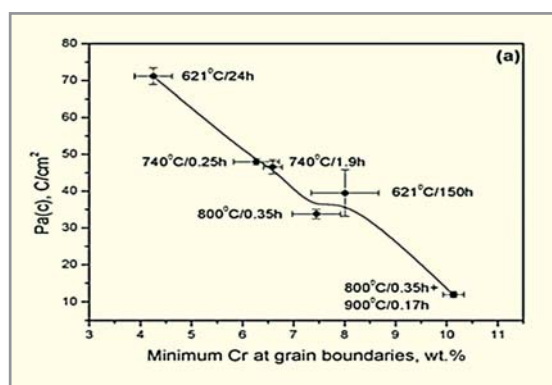
Microstructure of a sensitized Alloy 600 after the EPR test showing undissolved carbides at the grain boundaries and attacked chromium depletion regions.

The developed SL-EPR test is able to distinguish between samples with wide variation in DOS. There was a good correlation between the minimum level of chromium in the depletion regions and the results of the SL-EPR test. The modified Pa parameter was able to give a direct indication of the minimum level of chromium in the depletion regions at the grain boundaries. The carbides did not get attacked during the EPR test and the width of the attacked regions was much larger than the width of chromium depletion regions.

On similar lines, an EPR test technique (single loop as well as a double loop technique) was developed for evaluating the DOS in alloy 800. A number of test solutions based on H₂SO₄ + KSCN composition have been evaluated. It has been shown that dilute test solutions with lower vertex potentials resulted in single loop (SL) and double loop (DL) EPR test

methods that distinguished between different sensitized samples and also between sensitized and desensitized samples of alloy 800. The results produced a good correlation with intergranular corrosion rates as measured by the Huey test.

In a similar study on stainless steels, DOS of austenitic stainless steels (SS 304) was studied in terms of the characteristic parameters of the chromium depletion zones - (i) Coverage - i.e. proportion of the grain boundary length covered by depletion zones, (ii) Width and (iii) Depth- i.e. the minimum level of Cr in the depletion zones. The absolute value of depth was measured by the quantitative potentiostatic electrochemical test. New parameters were developed to express the results of the potentiodynamic, potentiostatic and the EPR tests that reflect the contributions due to coverage and depth or only the depth of Cr depletion zones. It was shown that these new parameters were sensitive in the range of 7.5% - 13.5% Cr in the depletion zones.



A direct correlation of the results from the EPR test with the minimum chromium levels in the depleted regions at sensitized grain boundaries in Alloy 600.

The results of the electrochemical tests (including EPR test) are shown to be sensitive to both coverage and depth of chromium depletion zones.

The results of these test techniques were correlated with the results of the IGC (practice C of A262, ASTM) and IGSCC (G 123 of ASTM) test. Cut-off values of various parameters of these tests were arrived at which screened heats of type 304/304L SS resistant to IGC in nitric acid environments and resistant to IGSCC in hot chloride environments.

P. Ahemadabadi, V. Kain, P. R. Singh and P. K. De, *ASM Journal of Materials Engineering and Performance*, 12, No. 5 (2003), p. 529 – 536.

Vivekanand Kain and Yutaka Watanabe, *Journal of Nuclear Materials*, 302 (2002), p. 49-59.

Vivekanand Kain, R. C. Prasad and P. K. De, *Corrosion – NACE*, 58, (2002), p.15-38.

■ Study of Reactivation Mechanism in AISI 304 Stainless Steel

Electrochemical potentiodynamic reactivation (EPR) is now a frequently used technique for assessing degree of sensitization in steels and nickel alloys. The aim was to get a mechanistic view of process of reactivation with the technique of potentiostatic current-time transients.

SS304 was annealed at 1050°C (1/2 hour) and then sensitized at 650°C for 1 and 5 hours. Electrolyte used are (1) (0.5M-2M) H₂SO₄ + (0.001M-0.01M) KSCN at room temperature (2) 2M H₂SO₄ at 50, 60 & 70°C. Single loop EPR with holding potential of +200mV (2 min) in H₂SO₄ + KSCN solution at a scan rate of 6V/hr and +500mV (2 min) in 2M H₂SO₄ at elevated temperature and scan rate of 10.8V/hr was used to find out the range of reactivation potential. After this step potentiostatic transients were taken at potentials close to the higher end of reactivation potential range i.e. -200, -250 mV in H₂SO₄ at elevated temperature and -130,-140 and -150 mV in H₂SO₄ + KSCN solution.

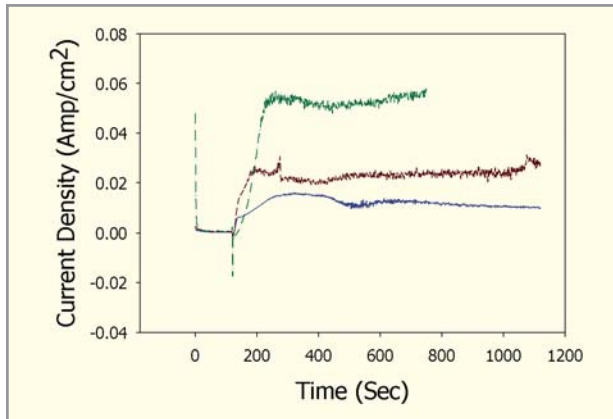
I-t curve showed increase in current with time initially while saturating at longer duration. In all experiments the trend was similar. Initiation time, slope and saturation current depended on steel history and experimental conditions. In sulphuric acid saturation current was higher for higher level of sensitization. In KSCN solution, the saturation current tends to decrease with time and does not directly represent the trend in sensitization level. However short time transients in this media show the trend in level of sensitization.

Reactivation follows a model equivalent (reverse) of three-dimensional circular conical growth and I-t transient fits the equation

$$I = A (1 - \exp(-Bt^3))$$

Where A & B are parametric constants.

It was found that KSCN has two-fold action in EPR; 1) to break film and 2) to react with Fe to form iron thiocyanate complexes. Temperature also facilitates the film break down and increases reactivity of the surface.

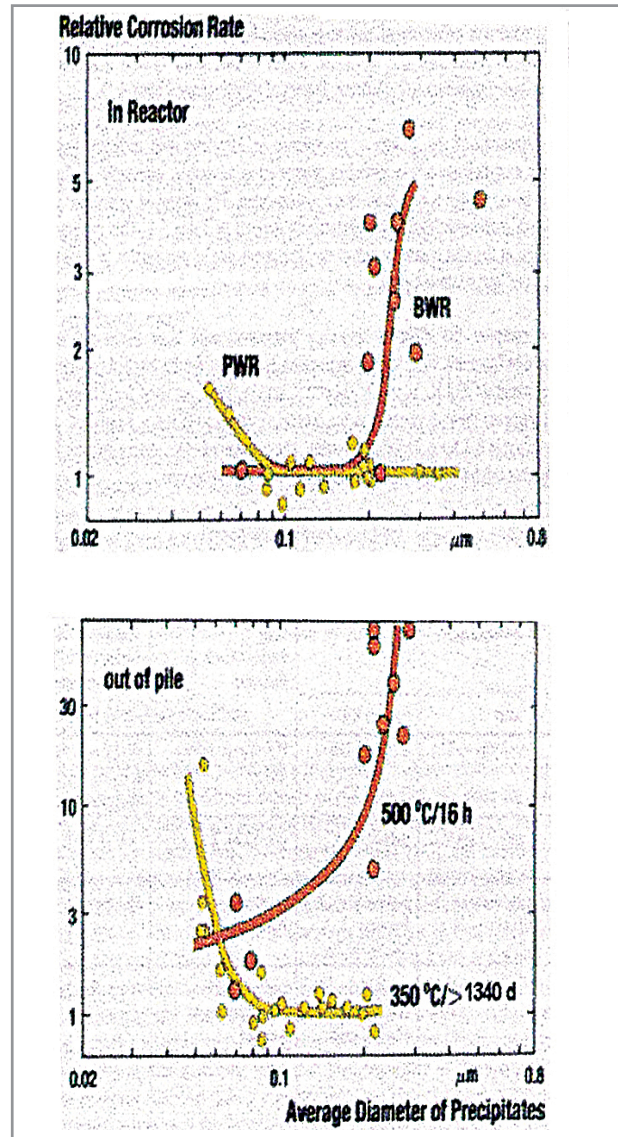


Current – time transients in 2 M H₂SO₄ at 70°C at an applied potential of $-0.25 V_{SCE}$

Geogy J. Abraham and P.R. Singh <gja@barc.gov.in>

13.3 ASSESSING NODULAR CORROSION SUSCEPTIBILITY IN ZIRCONIUM ALLOY CLAD TUBES

Nodular Corrosion is one of the concerns of Zircaloy fuel clad used in Boiling Water Reactor (BWR). Factors affecting nodular corrosion resistance of zircaloys are chemical composition, thermal history after β quenching and the size and distribution of intermetallic precipitates. Precipitates size is controlled by a Cumulative Annealing Parameter (CAP). Higher value of CAP leads to formation of coarse intermetallics that lead to better resistance of uniform corrosion. Lower value of CAP lead to fine intermetallics and improved resistance to nodular corrosion in BWRs and generally favourable in PWRs. There is a small window of precipitates size i.e 0.1-0.2 μm which results in improved resistance to uniform as well as nodular corrosion. NFC follows an optimized fabrication schedule for manufacturing of Zr-2 fuel tubes for BWRs and Zr-4 fuel tubes for pressurized heavy water reactor (PHWR) and it is of interest to determine the Nodular Corrosion Resistance of these tubes.



Correlation of corrosion rate to mean diameter of second phase particle in zircaloy

Accelerated autoclave corrosion tests at 500°C / 24 hrs / 1500 psi steam were carried out to evaluate the susceptibility as well as rank the alloy with respect to susceptibility to nodular corrosion. Weight gain measurements and imaging of oxide nodules on the specimens were used to quantify the degree of corrosion following autoclave testing. The visual appearance rating numbers were given based on the scheme suggested by Schemel. Second phase particles, precipitate size (diameter) and its distribution were estimated. Based on a volumetric statistical analysis, mean particle size and

spacing were calculated. Based on above investigation the following conclusions were drawn:

- **Indigenously produced Zircaloy-2 and Zircaloy-4 clad tubes show nodular corrosion susceptibility. Zircaloy-4 shows poorer resistance to nodular corrosion than Zircaloy-2.**
- **The value of CAP calculated from the flow sheet for indigenously produced BWR fuel tube is around 104.1×10^{-18} hr, which is much higher than the recommended limit (less than 2×10^{-18} hr)**
- **There is a variation of second phase particle size distribution in the tube.**
- **Fine and uniform distribution of second phase particles increases the resistance to nodular corrosion whereas non uniform distribution of second phase particles and higher spacing between the particles lead to higher susceptibility to nodular corrosion.**

Gargi Choudhuri, R. Ramanathan, K. R. Gurumurthy and B. K. Shah
<gargi@barc.gov.in>

13.4 THERMAL BUOYANCY DRIVEN LEAD - BISMUTH EUTECTIC LOOP

Lead - bismuth eutectic (LBE) has been proposed as spallation target and coolant in Accelerator Driven Subcritical Systems (ADSS). The operative temperature range will be

350°C- 500°C. The range of temperature will be much higher (up to 1000°C) in Compact High Temperature Reactor (CHTR) where it will be used as primary coolant. Thus material compatibility of the structural material will be a key issue in the success of target development for the ADSS programme.

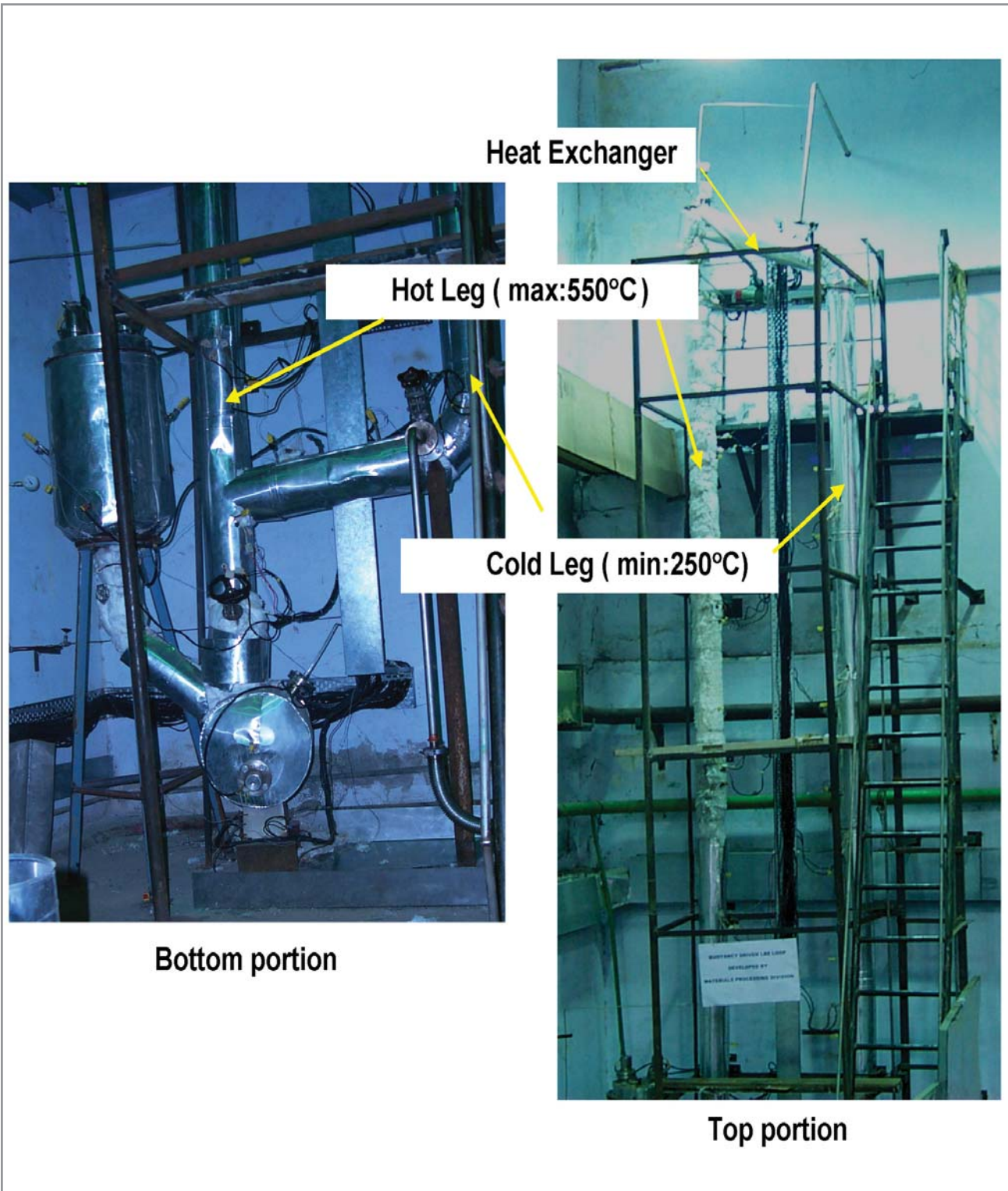
Objectives

Material Testing Loop (MTL) is a facility designed to test the corrosion behavior of candidate materials and related control systems, and performance of component selection and safety procedures. The near term objective of the MTL is to support the engineering design and development efforts for ADSS. The longer-term objective is to enhance the LBE technology database in support of the spent nuclear fuel transmutation and advanced nuclear reactor applications.

The natural convection potential is a key to the operation of liquid lead-bismuth loop. Under natural convection conditions, the buoyancy pressure drop drives the flow. The temperature difference between the inlet and the outlet produces the coolant density change. The higher the temperature difference ΔT , greater will be the fluid flow.

The loop consists of 1 inch. schedule 40 pipe (26.6 mm ID) welded together to measure 15 m in length.

The 6 m vertical section standing above the Dump tank called hot leg is operated at 400, 450 and 500°C. A heat exchanger 1m in length connects the hot leg to a cold leg which measures 5 m in length. Another 1m pipe also called hot leg connects the main hot leg to cold leg. There are two bellow sealed globe valves and three needle valves. One of the globe valves connects loop to the dump tank and opens only when the loop needs to be filled up or drained. This valve also serves as a safety mechanism. The other one permits to bleed the liquid metal for chemical analysis. The needle valves are located on the expansion and dump tanks. They are used for gas pressurization. ASME standard $\frac{1}{2}$ inch tensile specimens and 10x10 mm charpy specimens are placed at test locations. There are also 15 heaters, each segment of the heater in the hot leg is designed for 3 kW power and the cold leg for 1 kW power. The power in each heater is modulated through PID and PLC controllers.



The electrical, mechanical and SCADA of the loop have been tested. The Loop was tested with gas at 500°C for a number of hours.

Bottom and Top view of the Thermo-buoyancy driven Lead- bismuth eutectic Loop

■ Briefcase Type Thermo-Convection LBE Loop

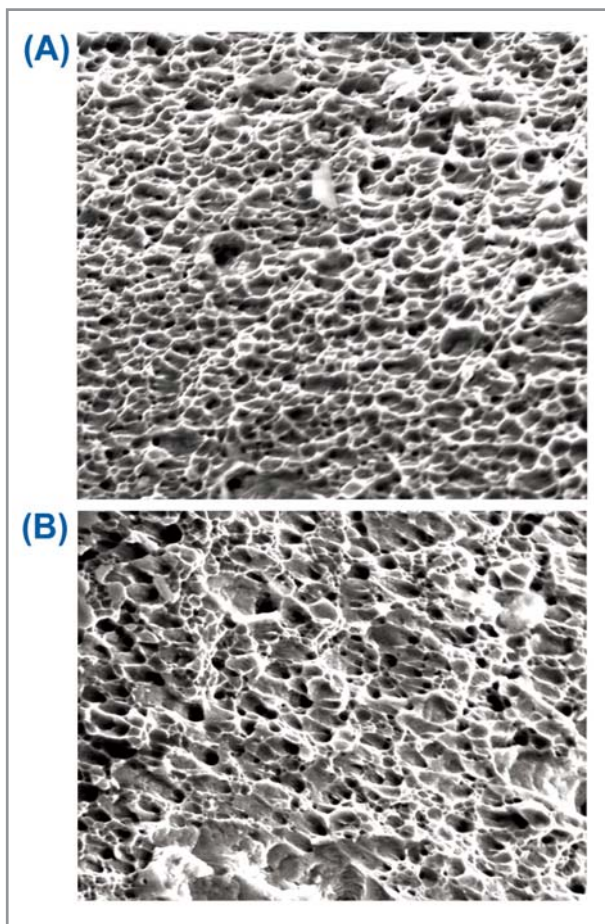
A small briefcase type loop which is a replica of the thermo-buoyancy loop has been set up. It is made up of stainless steel 316L. Each arm of this loop including hot and cold leg is one meter long and 12.5 mm ID. Temperature difference of 100°C or more between hot and cold leg has been achieved. This loop is under operation for more than 1500 hrs without any corrosion of loop even at highest temperature of about 500°C.



Briefcase Type Thermo-Convection LBE

■ Material Compatibility in Lead-Bismuth Eutectic (Static)

As a precursor to dynamic corrosion study, static experiments were carried out in the eutectic at 500°C under active oxygen control in the gas phase. The LBE has been prepared by repeated melting in vacuum using high purity lead and bismuth metals. In the first experiment, only SS 316L tensile



SEM fractographs of stainless steel 316L (A) as received and (B) exposed to Pb-Bi eutectic at 500°C for 100hr

test specimens were exposed for 100 hr and after that other alloys such as 316LN, 9Cr-1Mo and air oxidized SS316 were too exposed at 500°C for 500 hrs. The weight gain was nominal and ranged between 0.02 – 0.05 mg.cm⁻² which showed negligible attack by the molten alloy. The tensile strength on exposure for 100 hrs reduced marginally from 80 kg.mm⁻² to 77.6 kg.mm⁻².

The mode of fracture was similar, both showed regions of dimpled surfaces except the dimples were of uniform size in the case of unexposed sample and varying in size for the sample exposed to molten LBE.

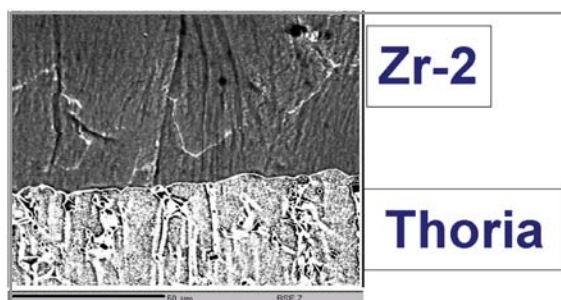
XPS analysis of SS 316L and 9Cr-1Mo exposed for 500 hr at 500°C revealed the presence of iron, chromium, lead and bismuth while molybdenum was not present. Binding

energies showed the film to be consisting of Fe_2O_3 and Cr_2O_3 . While lead was in the form of Pb_3O_4 , bismuth was as Bi_2O_3 .

R.K.Fotedar, C.Das, S.V.Phadnis, A.K.Grover and A.K.Suri
<fotedar@barc.gov.in>

13.5 COMPATIBILITY STUDIES BETWEEN THORIA AND ZIRCALOY-2

It is being proposed that thoria/thoria-based-pellets will be used in future at different stages of nuclear power generation. Zircaloy-2 is the potential cladding material for such pellets. Thus understanding the mode of interaction between Zircaloy-2 and thoria is very important.



Interface between the Zircaloy-2 and thoria.

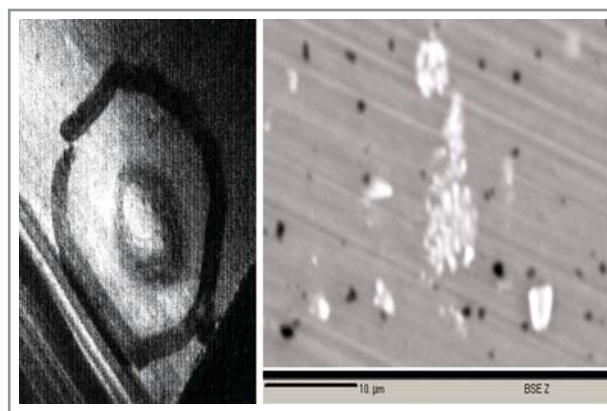
Compatibility studies between thoria, the fuel in AHWR, and cladding material zircaloy-2 were carried out in the temperature range of 1373 K to 1523 K and were studied with EPMA. BSE images and X-ray analyses identified good contact between the two materials in all the couples. No intermediate phase was found to decorate the interfaces. On the other hand, qualitative and quantitative analyses showed significant diffusion of Th along the grain boundaries and within α -Zr lattice. Interdiffusion coefficients estimated from the experiments indicated slow elemental exchange. Thorium diffuses in zircaloy-2 via lattice diffusion as well as through grain boundary diffusion. The kinetics of diffusion has been established.

P. Sengupta, P.S.Gawde, K. Bhanumurthy and G.B.Kale, *Journal of Nucl. Mater.*, 325 (2004), p.180.

P. Sengupta, P.S.Gawde, K. Bhanumurthy and G.B.Kale, *Proc. "Zirconium 2002 (ZIRC02)"*, Mumbai, p. 436

13.6 METALLURGICAL INVESTIGATION OF ALUMINIUM CLAD OF DHRUVA FUEL

A metallurgical investigation was carried out on 1S aluminium Dhruva clad material to determine the root cause of the blisters formed in unirradiated fuel pins during storage. The presence of inhomogeneous distribution of FeAl_3 precipitates of varying size was found to be responsible for such blister formation.



Blisters formed on the aluminum clad tubes and the precipitates in the material.

The specific electrical resistivity values have also been correlated with the microstructure of the fuel clad tubes. The study shows that the specific resistivity varies with the volume fraction, size and distribution of FeAl_3 precipitates. Non-uniform distribution of these precipitates/clusters shows higher resistivity values. Large size FeAl_3 particles, if present on the edges, affect the quality of the welding occurring during hot extrusion of aluminium tubes by the port die hole technique. The present correlation study can be used as a basis for quality control at the manufacturing site during various stages of processing. Since resistivity measurement is simple, least expensive and can be used in plants to monitor and maintain the required quality of the tubes.

P.K.De, A. Laik, G.B.Kale, I.S.Batra, R.Kumar and R.P.Singh, B.A.R.C. Internal Report No. BARC/2003/1/10



14. MATERIAL ISSUES IN WASTE MANAGEMENT

INTRODUCTION

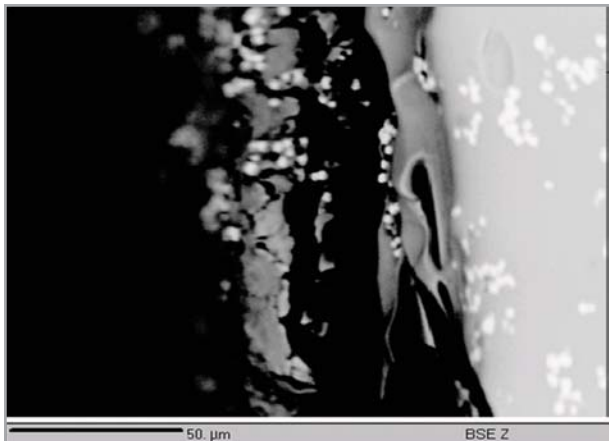
Management of waste in any industry is the key issue in its successful operation. It is of immense importance in case of nuclear and toxic industries as the waste is very harmful to the environment and human-beings in particular. Disposal of radioactive waste involves (i) immobilization of waste oxides in suitable stable and inert glass in canisters⁰ and (ii) disposing of canisters in suitable deep geological repositories. The materials problems in waste disposal are being studied. Presently compatibility studies between glass and canister materials have been taken up.

Toxic waste is generated in beryllium metal plant. Beryllium is highly toxic and environment is kept free by trapping pollutant particulates. These particulate filters contain toxic materials and are to be disposed off in a safe manner. The highlights of these activities are outlined in this chapter.

14.1 NUCLEAR WASTE

■ Microstructural characterization of borosilicate glass for nuclear waste immobilization

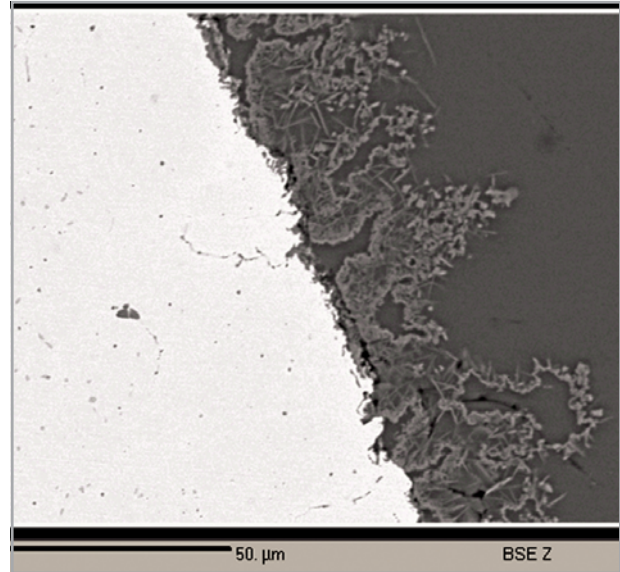
Borosilicate glass has been developed for high level liquid nuclear waste immobilization. The glass was microstructurally characterized employing electron probe microanalyser. The glass was found to be homogeneous with respect to all the elements. The upper limit of homogeneous waste containment in glass matrix was found to be 20% of waste. Chemical durability was studied by leaching the glass samples with hot water. It showed the development of three different reaction layers, formation of precipitates. and diffusion of boron (B), sodium (Na) from glass.



Reaction layer of leached glass

■ Compatibility studies between borosilicate glass and structural materials

Compatibility of borosilicate glass has been studied with melter pot Inconel 690 and canister materials viz stainless steel, Inconel 625. Results show the depletion of chromium from Inconel and development of Cr rich phase at glass/Inconel interface. Boron also diffuses in to Inconel and forms B-rich precipitate at the grain boundaries.



Interaction between Inconel and Glass

Pranesh Sengupta and G.B.Kale, *International Geoscience Journal*, 7(4S), (2004), p.1384-1386.

C.P Kaushik, R.K.Mishra, V.G.Katarni, Vidya Thorat, N Soudamini, P.D.Ozarde, Kanwar Raj P.Sengupta, P.K.De and G.B.Kale, *BARC Report BARC/2004/E/019*. p.1-29

Pranesh Sengupta, and G.B., Kale, *Proceedings of NUCAR (2005) Amritsar*, p.177-178.

14.2 TOXIC WASTE

■ Bag Filter for Dry Collection of Ammonium Fluoride

The existing wet scrubber unit in production of BeO/Be has been replaced with more efficient dry collection system. A plant scale bag filter system was designed, fabricated and installed in a non-toxic area for conducting trials before adopting the system in to the beryllium process line.

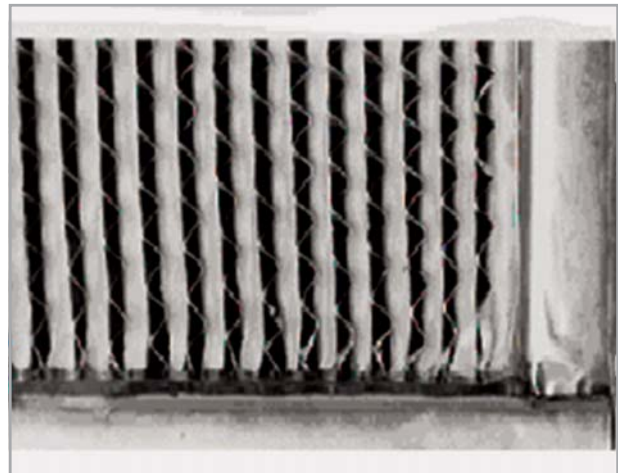
This bag filter unit contains 40 numbers of 150 mm dia, 2440 mm long PTFE laminated filter bags with polypropelene felt as a back-up filter media. This teflon lamination prevents penetration of fine powder into the filter media and also helps in easing the unloading of the collected powder cake from the bag surface. These bags are hung on a tube plate

and are enclosed in a chamber, divided into two sections and separated by an air distribution module. For continuous operation a pulsejet cleaning system was integrated with the unit, to unload the powder cake from the bag surface. For online filter cleaning compressed air at 4.5 kg/cm² is pulsed through the bags with the help of solenoid operated valves, ventury and a timer.

This dry collection system consists of the following :

1. An induction furnace with graphite crucible for sublimation of NH₄F
2. A containment enclosure
3. A centrifugal exhaust blower of 1700 m³/hr capacity at 300 mm water guage
4. Necessary interconnecting pipes

The bag filter unit showed an efficiency of 85% for 0.3-micron aerosol. The unit is being incorporated in the beryllium process line.

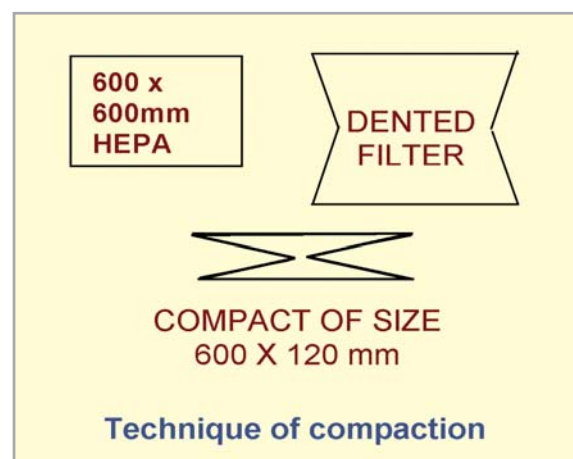


Magnified view indicating the aluminium foil layer on the inside surfaces of the frame

testing. In this design the filter medium can be compacted to reduce the final waste volume to <10% of the original volume. The compact forms a composite and does hardly need further concretisation for fixing the pollutant.

■ **Technique of compaction of contaminated HEPA filters of standard design, for efficient disposal.**

The technique of compacting the contaminated filters to form compacts of size nearly of one-fifth of original volume in a predictable geometry has been developed. As per this concept, the side faces of the filter are dented, and then pressed from the top as shown in the sketch below:



S. Narasimhan <narasimhan_pai@rediffmail.com>

■ **New design of HEPA filter for use in waste management**

HEPA filter is used in ventilation systems in special metal plants. A new design of construction of HEPA filter has been developed. In the new design, an aluminium foil (or any other suitable material) layer is given in between the frame and the filter medium. This design helps in separating out the filter pack from the frame by unscrewing the screws/nuts & bolts of the filter frame.

Figure shows the magnified view indicating the aluminium foil layer on the inside surfaces of the frame.

Full size (600 mm x 600 mm x 300 mm) filters with Al-foil have been made and found to be satisfactory after standard

The following are the merits of this technique:

1. The filters can be compacted along with the packaging of corrugated box and polyethene bag for operational safety.
2. The compaction process is smooth and produces the compacts of predictable shape.
3. The compaction process produces minimum release of contamination,

Wattal. P. K, Saha. S, Singh. A. K, Sengar. P. B. S, Surendranath. M. V, Gupta. S, Kulkarni. P and Nagbhushan S.V., Proc. Edited by Gandhi, K. G. and Ramachandran, S., Ebenezer Printing House, Mumbai, Feb. (2003) pp.141-150

P.H. Thygaraju, B.P. Sharma, Proc.of MEEMA – September (2003) Powder Metallurgy Association of India and Magnetics Society of India.

15. TECHNOLOGY TRANSFERS & PATENTS

15.1 TECHNOLOGY TRANSFERS

1. "Production of nano-size ceria powder for optical polishing application". Technology transferred to Indian Rare Earths Ltd (IRE) (Powder Metallurgy Division)
2. "Ultrafine grinding of graphite". Technology transferred to M/s Graphite India Ltd., Bangalore, (Powder Metallurgy Division).
3. "Triode sputter ion pumps". Technology transferred to M/s Technovac Corporation, Pune, and M/s. Kamal Engineering Works, Goregaon (East), Mumbai (Mechanical Design and Prototype Development Section, Physics Group)
4. MOU between BARC and HWB for Scale up of process for synthesis of Di - (nonylphenyl) phosphoric acid [DNPPA], an extractant relevant to the front end of nuclear fuel cycle. Signed on 15/04/2005. (Hydrometallurgy Section, Materials Group)
5. MOU between BARC and HWB for Scale up of process for synthesis of Tri-alkyl Phosphine Oxide (TAPO), an extractant relevant to the Front/Back end of nuclear fuel cycle. Signed on 15/04/2005. (Hydrometallurgy Section, Materials Group)

15.2 PATENTS

1. "A batch reactor for gel combustion reaction" Patent Application No. 708/MUM/2003, 10.07.03 (Powder Metallurgy Division)
2. "Process for the preparation of ceria nano powder suitable for optical polishing" Patent Application No. 707/MUM/2003, 10.07.03. (Powder Metallurgy Division)
3. "A process for the manufacture of novel composites of austenitic stainless steel and either commercially pure aluminium or any Al base alloy of 6 series" Patent Application No. 643/Mum/2002 (Materials Processing Division, Materials Science Division, Centre for Design & Manufacture)
4. "Process for the synthesis of liquid Tri-alkyl Phosphine Oxide (TAPO) used as metal extractant in nuclear and non-nuclear hydrometallurgical industries." Dated 03/01/2005. (Materials Processing Division, Materials Group)
5. "Process for the synthesis of Tri-octyl Phosphine Oxide (TOPO) used as metal extractant in nuclear and non-nuclear hydrometallurgical industries." Dated 09/07/2005. (Hydrometallurgy Section, Materials Group).